Vibrational dynamics of liquids and solids investigated by picosecond light pulses

A. Laubereau and W. Kaiser

Physik Department, Technische Universität München, München, Federal Republic of Germany

With well-defined coherent light pulses of several 10^{-12} sec duration we are in a position to investigate a variety of ultrafast vibrational processes in liquids and solids. Several new experimental techniques have been devised to study directly the dynamics of different vibrational modes and molecules in the electronic ground state. A first light pulse excites the vibrational system via stimulated Raman scattering or by resonant infrared absorption. A second interrogating pulse allows one to determine the instantaneous state of the excited system. Using a coherent probing technique one can measure the dephasing time of homogeneously broadened vibrational transitions and a collective beating of multiple isotope levels. In addition, one can investigate inhomogeneously broadened vibrational modes and observe the dephasing time of a small molecular subgroup. Different information is obtained when the coherent anti-Stokes Raman scattering of the probe pulse is measured. The population lifetime of known vibrational modes can be investigated and evidence for inter- and intra-molecular interactions is obtained. In a third probing technique, the vibrationally excited jolecules are promoted to the first electronic state by a second pulse and the fluorescence is measured. In this way it is possible to see the very rapid change of population of the primary excited vibrational mode. The article gives a detailed theoretical treatment of different excitation and probing processes. Several experimental techniques successfully applied in the authors investigations are outlined and a variety of results is presented and discussed. New information, not available from other experimental methods, is obtained.

CONTENTS

I. INTRODUCTION

During the past decade, vibrational relaxation and energy transfer processes have received increasing attention. In gases, detailed studies were made on energy decay routes, energy exchange rates, and the distribution of energy over various modes of a polyatomic molecule (for reviews see Moore, 1971; Weitz and Flynn, 1974). Strong impetus for these investigations came from the rapidly expanding area of laser-initiated chemical reactions and especially from the recent interest in laser isotope separation (see, for example, Letokhov and Moore, 1976; Berry, 1975).

For the gaseous state one has a wide scope of experimental techniques at one's disposal. Investigations using ultrasonic or shock tube techniques, inelastic scattering experiments, and a variety of spectroscopic methods have produced an extensive literature (for recent reviews see Ormonde, 1975; Amme, 1975; Clarke and McChesney, 1976; Brewer, 1975). Investigations where molecules are trapped in rare-gas matrices have provided a variety of information on vibrational relaxation at very low temperatures (for a review see F. Legay, 1977). It is most fortunate for the study of gases and of molecules in solid matrices that the relevant time constants are in general longer than 10^{-9} sec, allowing the application of standard electronic techniques.

In liquids and solids at room temperature vibrational processes are very rapid. Time constants of the order of 10^{-12} sec are common, requiring new experimental tools for quantitative investigations. In fact, the study of the dynamics of very fast vibrational phenomena was made possible by recent progress in the generation of ultrashort coherent light pulses and recent advances in the understanding of nonlinear optical processes.

In liquids at room temperature our knowledge of vibrational relaxation processes is rather scanty. Ultrasonic waves interact predominantly with the lower vibrational modes and do not provide specific relaxation values of the (many) higher normal modes of polyatomic molecules (Herzfeld and Litovitz, 1959; Sette, 1968). Linewidth measurements of infrared and Raman bands are the main source of "vibrational" relaxation times. In general, linewidth data are difficult to interpret, because a number of physical processes contribute to the observed line shape. Line broadening factors are phase relaxation, energy relaxation, rotational motion, isotope splitting, and inhomogeneous broadening due to a distribution of vibrational frequencies. Under certain assumptions it is possible to separate the rotational contribution. The rest, which is frequently called the intrinsic vibrational part of the band contour, contains the other line broadening factors. At present, it is not possible to isolate the different contributions by standard spectroscopic methods. For instance, the important question concerning the population lifetime of an excited vibrational state was unknown up to very recently for any vibrational mode in the liquid state. Similarly, the inhomogeneous contribution of a spectroscopic line is unknown in most cases and, as a result, the dynamic vibrational time constants are obscured by the molecular frequency distribution.

In this paper we are primarily interested in vibrational modes in the electronic ground state. We first discuss new methods of studying the dynamic behavior of molecular vibrations in liquids and of optical phonons in solids. A variety of experimental results is presented in the second part of this report.

Figure 1 outlines schematically the experimental methods used and the results obtained. The excitation of molecules or lattice vibrations is achieved by an intense laser pulse via stimulated Raman scattering or directly by a resonantly absorbed infrared pulse. After the passage of the first pulse the excitation process rapidly terminates and free relaxation of the excited mode occurs.

A second weak probe pulse properly delayed with respect to the first pulse monitors the instantaneous state of the vibrationally excited system. Three types of probing methods were used in order to obtain the dynamical information listed on the right side of Fig. 1:

(i) Coherent probe scattering results from the interaction of the probe pulse with the coherently excited system. For molecular modes with essentially one vibrational frequency the dephasing time of the excited mode is deduced from the loss of phase correlation within the excited volume, i.e., from the decay of the probing signal. The situation is more complex for molecular vibrations with different neighboring frequencies (e.g., several isotope components) or with a

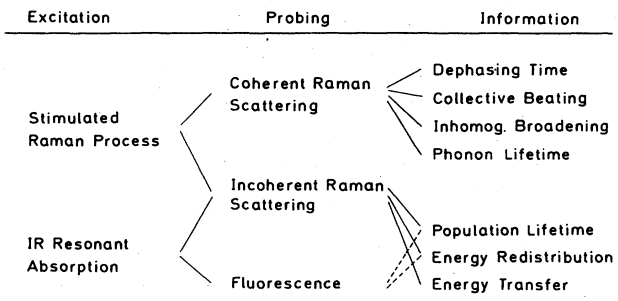

FIG. 1. Short outline of the paper. Two excitation processes allow us to excite a specific vibrational mode. Three different probing techniques provide time-resolved data on a variety of subjects listed on the right.

distribution of vibrational frequencies (inhomogeneous band). Investigations under different wave-vector geometries give strong indications of k-vector conservation of the collective vibrational excitation in the condensed phase. These observations have led to the study of the phase relaxation time when the vibrational band is inhomogeneously broadened. We have developed a selective k-vector geometry to isolate one frequency component or a limited number of molecules with a small frequency spread. With a less selective k-matching geometry of the probe pulse we observe a collective beating of neighboring frequency components. Finally, with coherent probe scattering we have studied the lifetime of optical phonons in three well-known crystals.

(ii) Spontaneous anti-Stokes probe scattering, an incoherent scattering process, allows us to study directly the momentary degree of occupation of a vibrational energy state. Using this technique it was possible, for the first time, to observe population lifetimes, energy transfer, and energy redistribution in the liquid state. Time constants between 1.0 and approximately 100 psec were measured for different dynamical processes in a number of polyatomic molecules.

(iii) We have developed a fluorescence technique where a first infrared pulse excites a vibrational mode and a second delayed probe pulse promotes the molecules close to the bottom of the fluorescent first singlet state. The degree of fluorescence is a direct measure of the occupation of certain vibrational quantum states. This technique is found to be especially useful for the investigation of highly diluted systems.

In Sec. II we discuss our excitation processes. In particular, we present a detailed theory of the stimulated Raman process as far as relevant to this paper. Special emphasis is given to the various forms of material excitation. Rotational motion and a distribution of vibrational frequencies is included in the general equations. We begin with vibrational modes with homogeneously broadened Raman lines (II.B and II.C). The more complicated inhomogeneously broadened Raman bands are treated next (II.D) and the possibility of observing the homogeneous part is investigated. In Sec. II.E the excitation of well-defined vibrational modes by direct resonant infrared absorption is discussed. Sec. III gives a theoretical description of the different probing techniques. For coherent Raman probe scattering (III.A), the understanding of the k-vector situation is essential. It will be apparent that the physical process one observes depends upon the probing geometry. Incoherent Raman scattering (III.B) and fluorescence probing (III.C), on the other hand, give direct information of the degree of occupation of various vibrational quantum states.

Experimental remarks on the generation of ultrashort laser pulses are made in Sec. IV.A, together with a short description of the production of infrared pulses (IV.B). We stress the importance of working with high quality, single-picosecond pulses for quantitative investigations. Three experimental systems to collect various dynamic data are outlined in Secs. IV.C and IV.D.

In Sec. V we present our experimental results on dephasing processes in liquids. First, the dephasing time of homogeneously broadened Raman lines is measured and compared with the spontaneous Raman linewidth. Second, neighboring discrete Raman lines are investigated and the dephasing time of one component is determined even for the case of broadly overlapping bands. In addition, a collective beating phenomenon is observed under special experimental conditions. Third, inhomogeneously broadened Raman lines with a continuous distribution of components are studied. It is possible to measure the dephasing time of a molecular subgroup and obtain evidence of inhomogeneous broadening.

Our results on the energy (population) lifetime of vibrational quantum states are discussed in Sec. VI and decay routes are found in several cases. Clear evidence is presented for rapid energy transfer between vibrational states of different molecules in liquid mixtures. Distribution of vibrational energy between various quantum states is observed in several molecules. In Sec. VII, experimental results on vibrational relaxation times of diamond, $CaCO_3$, and GaP are described. The paper concludes (Sec. VIII) with remarks concerning the potential of the investigations presented in this paper. It should be emphasized that some of the techniques discussed here provide new information not obtained by previous experimental methods.

II. THEORY OF THE EXCITATION PROCESSES

For time-resolved investigations of dynamical processes we prepare a nonequilibrium initial state of the physical system. In this section, two methods for the excitation of well-defined vibrational modes of polyatomic molecules are studied. Sections II.A–II.D are devoted to the stimulated Raman process under different physical conditions. Resonant infrared absorption is discussed as an ultrafast pumping process in Sec. II.E.

Stimulated Raman scattering is well suited for the study of vibrational excitation of normal modes in condensed matter. Several important factors are briefly discussed here:

(i) The Raman interaction is nonresonant. The frequency of the excitation pulse may vary over a large frequency range from the near-infrared to the uv in transparent media. This fact has opened the possibility of studying a variety of vibrational modes of different molecules with a single solid-state laser system. Furthermore, the stimulated Raman excitation is selective. Only one normal mode, the vibration with the largest scattering cross section, is strongly excited.

(ii) The stimulated process excites the vibrational system coherently; i.e., the molecules oscillate in unison within the excited volume.

(iii) Stimulated Raman excitation and Raman probing are weakly influenced by the rotational motion of the molecules. We obtain detailed information of the dynamic properties of the vibrational modes.

(iv) A quantitative theory of the stimulated Raman process is available. The treatment is considerably facilitated if we restrict our investigations to small conversions ($\sim 10^{-2}$) of laser into Stokes light. Under this condition, the generation of higher-order Stokes or

anti-Stokes frequencies is negligible. In addition, higher excited vibrational states may be neglected since the first excited vibrational level, $v=1$, has a small occupation number of $\lesssim 10^{-2}$.

(v) Unfortunately, stimulated Raman scattering is a highly nonlinear process. For an exponential gain of $\exp 25 \simeq 10^{11}$ one needs concentrated molecular systems, amplification lengths of the order of centimeters, and high peak intensities of the excitation pulse of 10^9–10^{10} W/cm^2. These factors limit the applicability of stimulated Raman scattering. In particular, the high intensity level necessitates an understanding of competing nonlinear processes such as stimulated four-photon parametric amplification, self-phase modulation, or self-focusing of the laser beam. Carefully chosen experimental conditions are required for a quantitative comparison between theory and experiment.

With ultrafast infrared pulses the direct excitation of vibrational modes is straightforward. Several salient features of this pumping process should be mentioned:

(i) Various vibrational states of the same polyatomic molecule can be excited by tunable ir pulses. We note the different selection rules for ir absorption and Raman scattering. The absorption process is complementary to the Raman interaction for a variety of molecular vibrations.

(ii) The resonant coupling to a dipole transition is stronger than the Raman interaction by several orders of magnitude. As a result, highly diluted specimens may be optically excited. In addition, it is possible to concentrate the molecular excitation in a small interaction volume (depending upon the absorption cross section of the transition).

(iii) The ir absorption represents a linear process over a wide intensity range. The produced excitation is proportional to the incident intensity. This fact is advantageous compared to the highly nonlinear stimulated Raman process.

(iv) Bandwidth-limited ir pulses allow the coherent excitation of vibrational states. The transmission of the medium does not follow Beer's law for sufficiently short pulses.

A. Transient stimulated Raman scattering (general)

In recent years, an extensive literature has accumulated on the stimulated Raman process. (For reviews see Bloembergen, 1967; Kaiser and Maier, 1972; Schubert and Wilhelmi, 1974; Grasyuk, 1974; Wang, 1975; Shen, 1975.) Transient stimulated Raman scattering has been treated theoretically by Akhmanov (1969), Carman *et al.* (1970), Kroll and Kelley (1971), Streudel (1972), and Akhmanov *et al.* (1971, 1972, 1974). The present investigation extends previous publications in various respects:

(a) Our interest is focused on the vibrational excitation produced in the stimulated process. The time dependence of the coherent and incoherent material excitation is discussed in detail.

(b) Rotational motion of the molecules in the liquid is included in our calculations. Molecular rotation enters the theory via the anisotropy of the Raman scattering tensor. This point has not been considered in previous work on transient stimulated Raman scattering.

(c) More complicated vibrational systems consisting of vibrational modes with several isotope components or normal modes with a distribution of vibrational frequencies (inhomogeneous lines) are investigated. We obtain results not discussed previously.

(d) Numerical calculations are presented which illustrate the potential of the stimulated excitation technique. The graphs should serve as a guide for practical cases where stimulated Raman scattering is applied to the study of vibrational relaxation, especially in liquids.

1. Light fields

Our theoretical approach is semiclassical, treating the vibrational system quantum mechanically and the light fields classically. The latter point appears to be well justified by the high light intensities, i.e., by the large number of photons involved in the scattering process. The total electric field E consists of an incident laser field and a generated Stokes field. The propagation of the light pulses through the sample and the interaction with the vibrating molecules are described by Maxwell's equations which lead to the wave equation

$$\Delta \mathbf{E} - \frac{1}{c^2}\frac{\partial^2}{\partial t^2}(\mu^2 \mathbf{E}) = \frac{4\pi}{c^2}\frac{\partial^2}{\partial t^2}\mathbf{P}^{\mathrm{NL}}. \tag{1}$$

μ denotes the refractive index of the medium under investigation. The nonlinear polarization $\mathbf{P}^{\mathrm{NL}}$ in Eq. (1) accounts for the coupling between the light fields and a molecular vibrational mode. $\mathbf{P}^{\mathrm{NL}}$ represents the macroscopic change of polarization connected with the coherent material excitation of the stimulated Raman process (see Sec. II.A.3). The local field correction required for condensed phases is contained in the nonlinear polarization $\mathbf{P}^{\mathrm{NL}}$ (Levenson and Bloembergen, 1974). Linear losses are omitted in Eq. (1); i.e., transparency of the medium is assumed.

In the following calculations we make the usual assumptions that the total light field consists of plane waves of different frequencies and time-dependent amplitudes. Stimulated light scattering occurs in the forward direction in our investigations. The short duration of the pulses considered here ($\sim 10^{-12}$ sec) and the resulting short interaction length for stimulated backward scattering makes this process negligible. Linear polarization of the incident light field is assumed with the E vector pointing in the z direction. We choose the x axis as propagation direction and write the electric field in the form:

$$\begin{aligned}\mathbf{E}(x,t) = \tfrac{1}{2}\mathbf{e}_z[&E_L \exp(ik_L x - i\omega_L t) \\ &+ E_{Sz}\exp(ik_S x - i\omega_S t)] \\ &+ \tfrac{1}{2}\mathbf{e}_y E_{Sy}\exp(ik_S x - i\omega_S t) + \text{c.c.}\end{aligned} \tag{2}$$

where $\mathbf{e}_y$ and $\mathbf{e}_z$ denote unit vectors in the y and z direction. The subscripts L and S refer to the incident laser field and the generated Stokes field, respectively. Higher-order Stokes and anti-Stokes components are omitted in Eq. (2); this simplification is justified since we restrict our calculations and experiments to small conversion of laser to first Stokes radiation.

2. Molecular system

The interaction between the electromagnetic field and the normal vibrational mode of interest is described by the polarizability tensor (α_{hi}), which depends on the vibrational coordinate q of the oscillating molecule (Placzek, 1934). Expanding α_{hi} in terms of the local coordinate q to first order, we obtain the relation

$$\alpha_{hi} = \alpha_{hi}^{0} + \left(\frac{\partial \alpha}{\partial q}\right)_{hi} q \,. \tag{3}$$

The second term, which produces Raman scattering, is important here. The subscripts h, i refer to a coordinate system (X, Y, Z) which is fixed to the symmetry axes of the individual molecules. Vibrational dynamics enter the calculation via the vibrational coordinate q. With the help of Eq. (3) we write the Hamiltonian of the molecular system:

$$H = H^{0} - \tfrac{1}{2} q \sum_{h,i} \left(\frac{\partial \alpha}{\partial q}\right)_{hi} E_h E_i \,. \tag{4}$$

H^0 refers to the undisturbed system. q now denotes the operator of the vibrational coordinate. Only the ground and the first excited vibrational state $(v = 1)$ of the electronic ground state are involved in our investigations. Transitions between higher vibrational states can be neglected on account of the anharmonic frequency shifts and the small population of the excited levels. Two-level systems appear to be a good approximation in the following treatment.

It has been discussed previously (Giordmaine and Kaiser, 1966; Maier, Kaiser, and Giordmaine, 1969) that the molecular motion under the effect of the external electromagnetic field is characterized by two quantities: the expectation value of the displacement operator $\langle q \rangle$ and the probability n of finding the molecule in the upper vibrational state. The equations of motion for the Raman interaction of Eq. (4) are derived in Appendix A. It is shown that a close analogy exists with the electric dipole transition of a two-level system. One arrives at the following differential equations for the dynamic variables $\langle q \rangle$ and n:

$$\frac{\partial^2}{\partial t^2}\langle q \rangle + \frac{2}{T_2}\frac{\partial}{\partial t}\langle q \rangle + \omega_0^2 \langle q \rangle = \frac{1}{m} F(t)[1 - 2(n + \bar{n})] \tag{5}$$

and

$$\frac{\partial}{\partial t} n + \frac{1}{T_1} n = \frac{1}{h\omega_0} F(t) \frac{\partial}{\partial t}\langle q \rangle \,. \tag{6}$$

n represents the occupation number in excess of the thermal equilibrium value $\bar{n}$. m and ω_0 are the reduced mass and the frequency of the vibrational mode, respectively. F denotes the effective force exerted by the electromagnetic field on the vibrating molecules:

$$F = \frac{1}{2} \sum_{h,i} \left(\frac{\partial \alpha}{\partial q}\right)_{hi} E_h E_i \,. \tag{7}$$

The effective force introduced by Eq. (7) refers to a system of weakly coupled molecules. A possible contribution by neighboring molecules is neglected at this point. We shall return to this problem in Sec. III.A.

Two time constants T_2 and T_1 are introduced in Eqs. (5) and (6) in analogy to the Bloch equations for a two-level spin system (see Appendix A and Slichter, 1963). They are of special importance in this paper. T_2 denotes the dephasing time of the vibrational amplitude, and T_1 represents the population lifetime (energy relaxation time) of the first excited state of the specific vibrational mode of interest.[1] Equations (5) and (6) indicate that the coherent vibrational excitation and the excited-state population decay exponentially after the excitation process has terminated.

It is interesting to see from Eq. (5) that the expectation value $\langle q \rangle$ of the vibrational coordinate behaves similarly to an amplitude of a classical oscillator. For a classical interpretation of the relaxation time T_2 in Eq. (5) one should consider an ensemble of oscillators instead of a single vibrational system. $\langle q \rangle$ may then be visualized as the ensemble average of the vibrational coordinate q, where q contains the phase and amplitude of the individual molecules. $\langle q \rangle$ is a measure of the coherent excitation of the molecules and will be called the coherent amplitude in the following.

It should be noted that Eq. (5) assumes a single resonance frequency for all molecules; i.e., a homogeneously broadened line is considered. Below, we will extend our treatment to vibrational systems with a distribution of frequencies (inhomogeneously broadened vibrational band). We shall replace Eqs. (5) and (6) by corresponding sets of differential equations for the vibrational amplitudes $\langle q_j \rangle$ and excess occupation numbers n_j. The various components j differ slightly from each other by their resonance frequencies ω_j.

3. Nonlinear polarization

In the simplest case, the nonlinear polarization P^{NL} entering Eq. (1) has the form: $P^{NL} = N(\partial\alpha/\partial q)qE$. Here, we wish to treat a more general situation considering specifically rotational motion and normal modes with a distribution of vibrational frequencies. For briefness we confine ourselves to molecules of rotational symmetry with the symmetry axis pointing in the Z direction. The polarizability tensor has the form (Wilson *et al.*, 1975)

$$\left\{\left(\frac{\partial \alpha}{\partial q}\right)_{hi}\right\} = a + \begin{Vmatrix} -\gamma/3 & 0 & 0 \\ 0 & -\gamma/3 & 0 \\ 0 & 0 & 2\gamma/3 \end{Vmatrix} , \tag{8}$$

where $h, i = X, Y, Z$. The isotropic contribution is denoted by the letter a; γ represents the anisotropy of the scattering tensor. As shown in Appendix B, the Raman polarizabilities a and γ may be obtained from spontaneous scattering data. The external field produces a dipole moment in the individual molecules which depends

[1] We note for comparison with our previous publications: $\tau = T_2/2$ and $\tau' = T_1$. While τ is the experimentally observed decay time (of the intensity), T_2 is the currently used time constant of the coherent amplitude of the two-level system. For a homogeneously broadened line, T_2 denotes the relaxation time defined by the vibrational correlation function.

on the molecular orientation. We introduce the angles $\theta_{ij}(i=2,3)$ of the symmetry axis of a molecule with respect to the laboratory frame. The subscript j labels the molecules according to their resonance frequencies ω_j. In order to calculate the components of the dipole moment of one molecule we have to transform the electric field into the molecular system, calculate the interaction with the polarizability tensor, and transform back to the laboratory frame. Averages over the orientational distribution have to be carried out similarly to calculations of the spontaneous Raman process (see, for example, Brandmüller and Moser, 1962; Koningstein, 1972). The total polarization P^{NL} is subsequently found by the linear superposition of the induced dipole moments of all molecules:

$$P_y^{\mathrm{NL}} = E_y N \sum_j f_j \langle\langle q_j\rangle [a+\gamma(\cos^2\theta_{2j}-\tfrac{1}{3})]\rangle_{\mathrm{or}} + \tfrac{1}{2}\gamma E_z N \sum_j f_j \langle\langle q_j\rangle \cos\theta_{2j}\cos\theta_{3j}\rangle_{\mathrm{or}} , \tag{9}$$

$$P_z^{\mathrm{NL}} = \tfrac{1}{2}\gamma E_y N \sum_j f_j \langle\langle q_j\rangle \cos\theta_{2j}\cos\theta_{3j}\rangle_{\mathrm{or}} + E_z N \sum_j f_j \langle\langle q_j\rangle [a+\gamma(\cos^2\theta_{3j}-\tfrac{1}{3})]\rangle_{\mathrm{or}} . \tag{10}$$

Averages with respect to molecular orientations are indicated by $\langle\rangle_{\mathrm{or}}$. Nf_j denotes the number density of component j of the inhomogeneous vibrational distribution ($\sum f_j = 1$). The constants a and γ refer to the liquid state and contain a local field correction for condensed phases (see Appendix B).

Two points should be noted concerning the derivation of Eqs. (9) and (10): (i) Molecular rotation is treated purely classically. This approach holds for liquids with rapidly interacting molecules (Frenkel, 1955; Bratos *et al.*, 1970, 1971). (ii) Spatial homogeneity is assumed; all molecules of the orientational and vibrational subsystems are present with constant number densities in volume elements small compared to the wavelength of the optical pulses. This assumption is well justified by the large number density of liquids.

4. Set of differential equations

Equations (1), (9), and (10), supplemented by the material equations (5), (6), and (7), represent the theoretical description of stimulated Raman scattering. We will solve these equations for the transient case with the help of Eq. (2) and a similar ansatz for the coherent vibrational amplitude $\langle q_j\rangle$:

$$\langle q_j\rangle = i/2 Q_j(x,t)\exp(ik_j x - i\omega_j t) + \mathrm{c.c.} \tag{11}$$

The wave vector k_j represents the phase relation between the molecules of the component j at different points x in the sample. After some algebraic manipulation we arrive at the following set of equations:

$$\left(\frac{\partial}{\partial x}+\frac{1}{v}\frac{\partial}{\partial t}\right) E_{Sz} = \kappa_1 E_L \sum_j f_j \langle Q_j^* s_{1j}\rangle_{\mathrm{or}} \exp(-i\Delta\omega_j t) , \tag{12a}$$

$$\left(\frac{\partial}{\partial x}+\frac{1}{v}\frac{\partial}{\partial t}\right) E_{Sy} = \kappa_1 E_L \sum_j f_j \langle Q_j^* s_{2j}\rangle_{\mathrm{or}} \exp(-i\Delta\omega_j t) , \tag{12b}$$

$$\left(\frac{\partial}{\partial t}+\frac{1}{T_2}\right) Q_j = \kappa_2 E_L (E_{Sz}^* s_{1j} + E_{Sy}^* s_{2j})\exp(-i\Delta\omega_j t) , \tag{13}$$

$$\left(\frac{\partial}{\partial t}+\frac{1}{T_1}\right) n_j = \frac{a}{8\hbar} E_L (E_{Sz}^* \langle Q_j^* s_{1j}\rangle_{\mathrm{or}} + E_{Sy}^* \langle Q_j^* s_{2j}\rangle_{\mathrm{or}})\exp(-i\Delta\omega_j t) + \mathrm{c.c.} \tag{14}$$

The following abbreviations were used:

$$\kappa_1 = \frac{\pi\omega_S^2}{c^2 k_S} aN , \quad \kappa_2 = \frac{a(1-2\bar{n})}{4m(\omega_L-\omega_S)} , \tag{15}$$

$$s_{1j}(t) = 1 + (\gamma/a)(\cos^2\theta_{3j}(t) - \tfrac{1}{3}) , \quad s_{2j}(t) = (\gamma/a)\cos\theta_{2j}(t)\cos\theta_{3j}(t) , \tag{16}$$

$$\omega_L - \omega_S - \omega_j = \Delta\omega_j , \tag{17a}$$

$$k_L - k_S - k_j = 0 . \tag{17b}$$

v denotes the group velocity of the Stokes pulse. The sum over the right-hand side of Eqs. (12a) and (12b) has to be carried out over all components j of the molecular distribution. $\Delta\omega_j$ denotes the frequency mismatch between the force F (at the frequency difference $\omega_L - \omega_S$ of the light fields) driving the vibrational component j and the resonance frequency ω_j. Equation (17b) represents the k-matching condition of the stimulated excitation process. We assume in Eqs. (13)–(15) that the components j have equal values of the following parameters: time constants T_1 and T_2, reduced mass m, and Raman polarizabilities a and γ.

Several approximations were used in deriving Eqs. (12)–(17): (i) Depletion of the incident laser pulse is not considered; our calculations are restricted to a small conversion of laser into Stokes light. (ii) Second-order derivatives of E_S and Q_j are neglected. This assumption corresponds to the "rotating frame approximation," which holds for picosecond pulses and for the high frequencies of the molecular vibrations ($\omega_j \sim 10^{14}$ sec^{-1}) (see, for example, Sargent *et al.*, 1974). (iii) Since the excess population of the upper vibrational state is small ($n_j \ll 1$) we omitted this term in κ_2. (iv) Group velocity dispersion is neglected; i.e., our calculations are limited to values of the sample length of several centimeters in condensed matter. The conditions (i)–(iv) are well fulfilled in our experiments described below. Solutions of Eqs. (12)–(17) will be derived for specific physical situations in Secs. II.B–II.D.

5. Discussion of the time constants

In the preceding sections two different aspects of the vibrational motion were discussed. The coherent vibrational amplitude $\langle q_j\rangle$, which is sensitive to the phase relation between the individual molecules, and the occupation probability n_j, which indicates the excess number of vibrational quanta (or the excess energy) stored in the molecular system, were introduced. The two quantities $\langle q_j\rangle$ and n_j are governed by the individual time constants T_2 and T_1, respectively [see Eqs. (5) and (6)]. For the coherent amplitude $\langle q_j\rangle$, Eq. (5) predicts exponential decay of the vibrational system with the time constant T_2:

$$\langle q_j\rangle \propto \exp(-t/T_2) . \tag{18}$$

This time dependence results from the stochastic pro-

cesses assumed in the derivation of the damping term in Eq. (5). The validity range of Eq. (18) requires some discussion. Equation (18) does not hold for very short time intervals $\Delta t \cong \tau_C$, where τ_C is a correlation time connected with certain intermolecular interactions in the liquid, e.g., rapid translational motion (see, for example, Slichter, 1963). Since $\tau_C \sim 10^{-13}$ sec, no dynamical information on a time scale of several 10^{-13} sec may be deduced from Eq. (18) or, correspondingly, from Eq. (5). This condition, on the other hand, does not set a limitation to our experimental investigations with picosecond pulses. Information obtained with these pulses represents time averages over $\gtrsim 10^{-12}$ sec. A large number of individual physical events determine the relaxation time T_2 leading to an exponential decay. In liquids the exponential time dependence of Eq. (18) is expected for values of $T_2 > 1$ psec. Time constants of this magnitude are investigated in this paper.

Similar considerations hold for the excited-state population and the lifetime T_1 [see Eq. (6)]. The present arguments are strongly supported by the experimentally measured exponential time dependence of $\langle q_j \rangle$ and n_j (see Secs. V and VI).

We emphasize the need to clearly distinguish the two relaxation times. In a number of experiments where T_2 and T_1 were determined for the same normal mode and molecule, a considerable difference was observed for the two time constants. For instance, a ratio of $T_1/T_2 \cong 10^{11}$ was found for the fundamental vibrational mode of liquid N_2 (Laubereau, 1974; Calaway and Ewing, 1975a and b; Brueck and Osgood, 1976); for the symmetric CH_3 stretching mode of CH_3CCl_3 a ratio of $T_1/T_2 = 2.4$ was reported by Laubereau, von der Linde, and Kaiser (1972). These findings give experimental evidence of rapid vibrational relaxation processes which affect the phase of the molecular vibration but not the population of the excited vibrational state.

We call processes which are only concerned with loss of phase correlation "pure dephasing processes." Generally, the decay rate of $\langle q_j \rangle$ is affected by loss of phase correlation and by loss of vibrational energy (occupation density). For the experimental dephasing time T_2 we write (Fischer and Laubereau, 1975)

$$2/T_2 = 1/\tau_{ph} + 1/T_1 . \tag{19}$$

The time constant τ_{ph} in Eq. (19) represents "pure dephasing"; the second term denotes the contribution of energy dissipation. Experimental values of τ_{ph} are deduced from measurements of T_1 and T_2 of the same vibrational mode. For several vibrational modes a significant contribution of $1/\tau_{ph}$ was found, i.e., $T_1 > T_2/2$.

For a microscopic description of the vibrational time constants, the Hamiltonian for the interaction V between the vibrating molecule and the surrounding medium is expanded in the oscillator coordinate q:

$$H_{int} = \frac{\partial V}{\partial q} q + \frac{1}{2} \frac{\partial^2 V}{\partial q^2} q^2 + \cdots \tag{20}$$

V fluctuates with the time constant τ_C mentioned above. Model calculations retaining only the linear term in the expansion of Eq. (20) include only population decay and arrive at $T_1 = T_2/2$; i.e., these models are not sufficient to describe the dephasing and the population relaxation of the vibrating molecule. It has been shown by Fischer and Laubereau (1975) that the second term in Eq. (20) is important in order to account for the rapid dephasing processes observed experimentally. These authors have developed a semiclassical collision model for vibrational dephasing. The molecular interaction of Eq. (20) is described by quasielastic collisions during which the molecules experience an adiabatic change of vibrational frequency. In the quantum-mechanical picture the molecules undergo virtual excitation processes and end up in the initial energy state. The resulting time constant τ_{ph} depends on the frequency, masses, thermal energy, and time between elastic collisions. Values of 10^{-12}–10^{-10} sec were numerically estimated for τ_{ph} from the quasielastic collision model. Resonant transfer of vibrational quanta between molecules of the same kind may also contribute to pure dephasing. Similar ideas were discussed by Madden and Lynden-Bell (1976), Rothschild (1976), and Oxtoby and Rice (1976).

6. Comparison with spontaneous Raman spectroscopy

Until now, we have discussed the time constants connected with a macroscopic excitation of the molecular system. It is interesting to make a comparison with the vibrational dynamics at thermal equilibrium which is observed by conventional Raman spectroscopy. The analogy of a two-level vibrational system with a spin system suggests that T_2 is closely connected with the line broadening observed in spectroscopic investigations. This point will be discussed in the following.

It has been shown in a number of publications that an analysis of a spontaneous Raman line provides information on the vibrational relaxation and the rotational motion of the molecule (Gordon, 1964 and 1965a and b; Bratos and Marechal, 1971; Bartoli and Litovitz, 1972; Nafie and Peticolas, 1972). For these investigations the scattered light polarized parallel (VV) and perpendicular (VH) to the incident laser has to be measured. Under the condition that vibrational and rotational motion are statistically independent it is possible to separate the broadening contribution of reorientation from the intrinsic vibrational part. The results have been discussed in terms of the isotropic part $I_{is}(\omega)$ and the anisotropic component $I_{an}(\omega)$ of the spectral intensity distribution. For example, I_{is} is obtained from the experimental VV and VH spectra (under 90° scattering angle) using the relation $I_{is}(\omega) = I_{VV}(\omega) - \frac{4}{3} I_{VH}(\omega)$. It has been shown that $I_{is}(\omega)$ corresponds to the isotropic part of the scattering tensor and is independent of rotational motion; i.e., $I_{is}(\omega)$ contains the information on vibrational dynamics supplied by spontaneous Raman spectroscopy.

The spectral intensity distribution I_{is} is connected to a vibrational correlation function $\phi_V(t, t')$ by Fourier transformation (see, for example, Bailey, 1974):

$$\phi_V(t, t') = \frac{1}{2\pi} \int d\omega \exp[-i\omega(t - t')] I_{is}(\omega) , \tag{21}$$

ϕ_V contains the relaxation properties of the molecular vibration since the fluctuations of the molecular polarizability observed in the spontaneous scattering are pro-

portional to the vibrational coordinate q [see Eq. (3)]. ϕ_V is the autocorrelation function of the normal vibrational mode:

$$\phi_V(t,t') = \langle q_m(t) q_m(t') \rangle_{eq} . \tag{22}$$

q is here treated as a classical quantity and the brackets $\langle\rangle_{eq}$ denote an equilibrium ensemble average. The subscript m labels individual molecules. Equations (21) and (22) indicate that the Fourier transform of the Raman band provides directly (under certain conditions) the correlation function $\langle q_m(t) q_m(t') \rangle_{eq}$ of the system at thermal equilibrium.

With time-resolved techniques, on the other hand, a macroscopic excitation with amplitude $\langle q_m(t) \rangle$ is observed which is generated by the external driving light field [see Eq. (5)]. The time evolution of the two quantities $\langle q_m(t) q_m(t') \rangle_{eq}$ and $\langle q_m(t) \rangle$ is compared with the help of the fluctuation–dissipation theorem. We distinguish two situations: homogeneously and inhomogeneously broadened Raman lines.

First, a homogeneously broadened vibrational system ($\omega_j = \omega_0$) is considered. In this case, identical time behavior is expected for the correlation function $\langle q(t) q(t') \rangle_{eq}$ and the coherent amplitude $\langle q \rangle$. Proof of this statement is obtained by writing down explicitly the fluctuation-dissipation theorem (see, for example, Martin, 1968):

$$\langle q(t) q(t') \rangle_{eq} - \langle q(t) \rangle_{eq} \langle q(t') \rangle_{eq} = \frac{1}{2\pi} \int d\omega \exp[-i\omega(t-t')] 2\epsilon(\omega) \chi''(\omega)/\omega . \tag{23}$$

The second term on the left-hand side vanishes since $\langle q(t) \rangle_{eq} = 0$. $\epsilon(\omega)$ denotes the mean energy of an oscillator with frequency ω:

$$\epsilon(\omega) = \hbar\omega [\tfrac{1}{2} + (e^{\hbar\omega/kT} - 1)^{-1}] . \tag{24}$$

$\chi''(\omega)$ represents the imaginary part of the Fourier transform of the retarded response function $\chi(t-t')$ of the vibrational mode. This function is determined from the equation of motion. For an oscillator equation of the form of Eq. (5) one obtains

$$\chi''(\omega) = \frac{1}{mT_2} \frac{\omega}{(\omega^2 - \omega_0^2)^2 + (2\omega/T_2)^2} . \tag{25}$$

For the experiments to be discussed we are interested in a vibrational system with negligible population of the excited states, $\hbar\omega_0 \gg kT$, and small damping $1/T_2 \ll \omega_0$. Since $\chi''(\omega)$ has a sharp peak in the neighborhood of ω_0 [see Eq. (25)], we set $\epsilon(\omega) \simeq \hbar\omega_0/2$ and write:

$$\langle q(t) q(t') \rangle_{eq} = \frac{\hbar\omega_0}{2\pi} \int d\omega \exp[-i\omega(t-t')] \frac{\chi''(\omega)}{\omega} . \tag{26}$$

Comparison of Eqs. (21), (22), and (26) shows that the spectral intensity distribution $I_{is}(\omega)$ has the form χ''/ω. Using Eq. (25) we obtain for frequencies ω near the resonance frequency ω_0:

$$I_{is}(\omega) = \text{const} \frac{1/T_2}{(\omega - \omega_0)^2 + (1/T_2)^2} . \tag{27}$$

A line broadening of Lorentzian shape is predicted for the homogeneous vibrational system. Equation (27) yields the linewidth $\delta\tilde{\nu}_{hom}$ of the isotropic scattering component (FWHH, in units of cm^{-1}):

$$\delta\tilde{\nu}_{hom} = (\pi c T_2)^{-1} . \tag{28}$$

It is interesting to see that the linewidth is determined by the dephasing time. For highly polarized Raman lines one obtains $\delta\tilde{\nu}_{hom}$ directly from the linewidth of the polarized scattering component $I_{VV}(\omega)$ since I_{VH} is negligible. Equations (21), (22), and (27) yield Eq. (29):

$$\langle q(t) q(t') \rangle_{eq} = \cos[\omega_0(t-t')] \exp[-|t-t'|/T_2] . \tag{29}$$

Comparison of Eq. (29) and Eq. (18) indicates that both the vibrational correlation function and the coherent amplitude decay exponentially. Spontaneous measurements of a homogeneous line and time-resolved studies of the coherent excitation give the same time T_2.

For the inhomogeneously broadened Raman band, the autocorrelation function of Eq. (29) is no longer valid since the distribution of vibrational frequencies ω_j has to be included in the calculation of the ensemble average $\langle q_m(t) q_m(t') \rangle_{eq}$. The correlation function is not a simple exponential; it decays rapidly due to the spread of vibrational frequencies ω_j. Correspondingly, the spectral intensity distribution $I_{is}(\omega)$ of Eq. (27) has to be replaced by a convolution of the frequency distribution with the homogeneous lines. A broader bandwidth results with

$$\delta\tilde{\nu}_{inhom} > (\pi c T_2)^{-1} . \tag{30}$$

The inhomogeneous linewidth contains the integral information of three different processes: (i) distribution of molecules with different resonance frequencies according to their individual surroundings; (ii) dynamical contributions by pure dephasing; and (iii) dynamic contributions by population (energy) relaxation [see Eq. (19)].

B. Stimulated Raman scattering of a homogeneously broadened line with isotropic scattering tensor

In this section we discuss the essential features of transient stimulated Raman scattering. The physical situation considered here is straightforward from a theoretical point of view and is, fortunately, of considerable practical interest. Homogeneously broadened lines were found for a number of vibrational modes. Neglect of the anisotropy γ of the Raman tensor, $\gamma = 0$, is appropriate for many cases. In fact, most molecular vibrations where a stimulated Raman process has been observed possess a rather isotropic scattering tensor according to their small depolarization ratios of $\rho_s < 0.1$. The influence of rotational motion with $\gamma \neq 0$ will be investigated in Sec. II.C.

1. General solutions

Equations (12)–(17) are considerably simplified for isotropic scattering, $\gamma = 0$, and for a vibrational system where $\omega_j = \omega_0$ and $\Delta\omega_j = 0$. The Stokes component polarized perpendicular to the incident light field vanishes, $E_{Sy} = 0$, and the scattered light is independent of molecular orientation ($s_1 = 1$; $s_2 = 0$). The subscript j labeling the molecules may be dropped ($Q_j = Q$, $n_j = n$). Transformation to a moving coordinate frame, x', t' with $x' = x$ and $t' = t - x/v$, gives the following coupled differential

equations:

$$\frac{\partial}{\partial x'} E_S = \kappa_1 E_L Q^*, \tag{31}$$

$$\left(\frac{\partial}{\partial t'} + \frac{1}{T_2}\right) Q = \kappa_2 E_L E_S^*, \tag{32}$$

$$\left(\frac{\partial}{\partial t'} + \frac{1}{T_1}\right) n = \frac{a}{8\hbar}(E_L E_S^* Q^* + E_L^* E_S Q). \tag{33}$$

Solutions of Eqs. (31) and (32) have been published in terms of the Bessel functions I_0 and I_1 of complex arguments (Carman *et al.*, 1970).

$$E_S(x', t') = E_S(0, t') + (bx')^{1/2} E_L(t') \times \int_{-\infty}^{t'} dt'' \exp\left(\frac{t'' - t'}{T_2}\right) \times E_L(t'') E_S(0, t'')[W(t') - W(t'')]^{-1/2} \times I_1(2\{bx'[W(t') - W(t'')]\}^{1/2}) \tag{34}$$

where we use the abbreviations $b = \kappa_1 \kappa_2$ and

$$W(t) = \int_{-\infty}^{t} dt' |E_L(t')|^2,$$

the latter being a measure of the pump energy accumulated up to time t. Introducing solution (34) into Eq. (31), one finds

$$Q(x', t') = \kappa_1 \int_{-\infty}^{t'} dt'' \left(\exp \frac{t'' - t'}{T_2}\right) E_L(t'') E_S^*(0, t'') \times I_0(2\{bx'[W(t') - W(t'')]\}^{1/2}). \tag{35}$$

The Stokes field E_S and the coherent vibrational amplitude Q are determined as functions of position x' and retarded time t'. Equations (34) and (35) describe for large incident pump fields an exponential growth with distance x' of the Stokes light E_S and of the coherent vibrational amplitude Q. The amplification process starts from an initial Stokes field $E_S(0, t')$, while the initial vibrational amplitude $Q(0, t')$ is assumed to be zero. A discussion of the initial field $E_S(0, t')$ is given in Appendix C.

The excess population n of the first excited vibrational state, the incoherent vibrational excitation, is derived from Eq. (33):

$$n(x', t') = \frac{a}{8\hbar} \int_{-\infty}^{t'} dt''(E_L E_S^* Q^* + E_L^* E_S Q) \times \exp[(t'' - t')/T_1]. \tag{36}$$

Equation (36) allows us to calculate the excess occupation number $n(x', t')$ after evaluation of $E_S(x', t')$ and $Q(x', t')$.

2. Scattering efficiency and stimulated Stokes pulse

We have carried out a detailed study of the transient stimulated Raman process generated by ultrashort light pulses. The generated Stokes pulse is discussed relatively briefly since we are mainly interested in the vibrational excitation. A discussion of the delay and shortening of the Stokes pulse, the influence of color dispersion, and the frequency chirp, is given in the literature (Carman *et al.*, 1970; Akhmanov, 1972).

The experimental situation we have in mind is a traveling-wave Raman generator. The incident laser pulse traverses the liquid cell and builds up the Stokes field and the vibrational amplitude from quantum noise. Our calculations assume incident light pulses of Gaussian time dependence with duration t_p (FWHH). This choice of the pulse shape is a good approximation of the single picosecond pulses used in our experiments (von der Linde, Laubereau, and Kaiser, 1971).

On account of the highly nonlinear character of the stimulated Raman process, the intensity of the incident laser pulse has to be carefully adjusted to the experimental situation. In this connection, two important parameters are relevant: the gain G and the ratio of the pulse duration to the dephasing time t_p/T_2. The gain is defined by

$$G = gI_L x \tag{37}$$

where

$$g = (16\pi/c\mu_L)\kappa_1 \kappa_2 T_2.$$

I_L represents the maximum value of the incident pump intensity, x the amplification length, and g the gain factor. The latter contains the material parameters [see also Eq. (15)] and determines the degree of interaction between the light field and the specific molecular vibration. Throughout the literature values of g are compiled for numerous vibrations of gases, liquids, and solids (Kaiser and Maier, 1972; Wang, 1975). Several examples are given in Table I; the frequency of the vibrational mode ν_0 and the spontaneous Raman linewidth are listed together with values of the gain factor g. The depolarization factor ρ_s obtained from spontaneous Raman scattering is included in Table I to indicate the anisotropy of the Raman transition (see Appendix B). It should be emphasized that the gain factor g is of the order of several cm/GW; i.e., laser pulses of high intensity (10^9 W/cm^2) are required for stimulated Raman scattering in samples of several cm of length.

Under steady-state conditions, i.e., for $t_p/T_2 \gg 1$, the parameter G denotes the exponential amplification of the Stokes intensity: $I_S/I_{S0} = \exp G$. Values of $G \sim 25$ provide efficient Stokes conversion. In the transient case, the Stokes amplification is smaller than in the stationary situation. The transient amplification depends in a more complex form on the product $G = gI_L x$ and larger values of G are required to produce a certain degree of scattering efficiency.

Having introduced the relevant parameters we return to the question of efficient vibrational excitation under transient conditions. This situation is analyzed in Fig. 2 for two values of η_S, the energy conversion efficiency of laser into Stokes light. The energy conversion efficiency is of interest since it allows an estimate of the degree of excitation of the vibrational system. On account of the exponential growth of the excitation with distance, the major excitation occurs within a small interval at the end of the interaction length. The gain G required to produce stimulated Stokes scattering with efficiencies $\eta_S = 0.1\%$ and 1% is plotted as a function of the ratio t_p/T_2. Going from right to left in Fig. 2, i.e., for decreasing values of t_p/T_2, the transient character

TABLE I. Investigated molecules and vibrational frequencies $\tilde{\nu}_0$. Gain factor for stimulated Raman scattering g; depolarization ratio ρ_s and maximum amplification length x_{max}.

	$\tilde{\nu}_0$(cm^{-1})	$\delta\tilde{\nu}$(cm^{-1})	g(cm/GW)[a]	ρ_s	x_{max}(cm)	Remarks
N_2	2326	0.067	22±7	0.10	35	b,c
O_2	1552	0.117	22±7	0.11	56	b,c
CCl_4	459	1.4	1.5±0.5	0.004	48	d,e,f
C_6H_6	992	2.15	3.7	0.001	14	b,c,g
CH_3CCl_3	2939	4.3	5.6	0.004	7	h,g
CH_3OH	2942	26.6	1.8	0.06	11	g
C_2H_5OH	2928	17.4	5.1	0.056	8	g
Diamond	1332	2.04	9.2	•••	7	c
Calcite	1086	1.20	5.5	•••	6	g,i,k

[a]For excitation at 529 nm; cited values are corrected for this wavelength according to Eqs. (15) and (37).
[b]Clements and Stoicheff (1968).
[c]Grun *et al.* (1969).
[d]Linewidth of a single isotope component.
[e]Görner *et al.* (1974).
[f]Murphy *et al.* (1967).
[g]Colles (1969); Colles and Griffiths (1972).
[h]Wochner *et al.* (1977).
[i]Parks (1966 and 1967).
[k]Kiefer and Laubereau (1978).

of the stimulated Raman scattering becomes more dominant. Larger G values are necessary for shorter pulses in order to achieve the same scattering efficiency η_S. This interesting behavior reflects the less effective response of the vibrational system to shorter pulses. The two curves for $\eta_S = 1\%$ (solid curve) and $\eta_S = 0.1\%$ (broken line) are very close together, illustrating the high nonlinearity of the scattering process. Figure 2 may serve as a guide for selecting proper experimental parameters for the excitation process via stimulated Raman scattering. The dephasing time T_2 introduced in Eqs. (5) and (32) is the significant time constant for the excitation of the vibrational system. It should be noted that an energy conversion $\eta_S = 1\%$ corresponds to a ratio of peak intensities of approximately

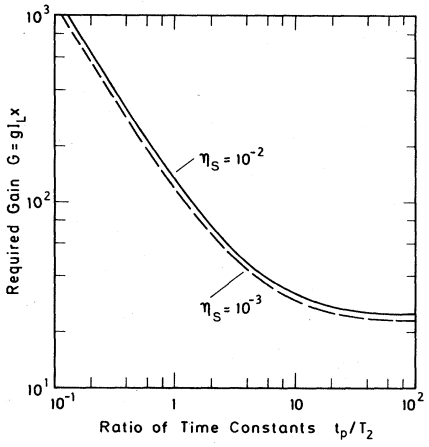

FIG. 2. Required stimulated Raman gain versus pulse duration t_p for two energy conversion efficiencies η_S of laser into Stokes light. Here T_2 is the dephasing time of the excited vibrational mode.

10% since the Stokes pulse has a shorter pulse duration and a smaller beam cross section than the incident laser pulse.

For larger conversion efficiencies the laser pulse is depleted by the Stokes radiation and the stimulated gain saturates. This situation will not be considered here.

The application of Fig. 2 is illustrated by the following numerical example: We wish to generate stimulated Raman scattering in CH_3CCl_3 (CH stretching vibration) with an efficiency of $\eta_S = 1\%$ using pulses of $t_p = 20$ psec. For $\delta\tilde{\nu} \simeq 5$ cm^{-1} (Table I) we estimate a ratio of $t_p/T_2 \simeq 10$ and deduce a necessary gain of $G \simeq 32$ from Fig. 2. For an amplification length of $x = 2$ cm and the value of the gain constant g listed in Table I the necessary incident laser peak intensity is estimated to be $I_L = 3 \times 10^9$ W/cm^2. If pulses of $t_p = 3$ psec were used experimentally we would need $G = 65$; i.e., a considerably higher pump intensity of $I_L = 9 \times 10^9$ W/cm^2 is required in order to achieve the same conversion efficiency of 1%.

Concerning the amplification length x [see Eq. (37)], the following two points have to be considered: (i) Small values of x require a high intensity level which may favor competing nonlinear processes, e.g., parametric four-photon scattering (Penzkofer, Laubereau, and Kaiser, 1973; Penzkofer and Kaiser, 1977) or dielectric breakdown (Bloembergen, 1976). (ii) Large values of x introduce the problem of group velocity dispersion. The group velocity is given by the equation $v = c(n - \lambda dn/d\lambda)^{-1}$, where c and λ are the light velocity and wavelength *in vacuo*, respectively. For normal dispersion the value of $dn/d\lambda$ is negative. As a result, the Stokes pulse travels faster than the incident pump pulse. This effect limits the amplification length to a maximum value x_{max} according to the relation: $x_{max} = t_p v_L v_S/2(v_S - v_L)$. Calculated values of x_{max} are listed in Table I for the case of a green pumping wavelength ($\lambda_L = 0.53$ μm) and a pulse duration of $t_p = 6$ psec. Note that the values of x_{max} are of the order of 10 cm.

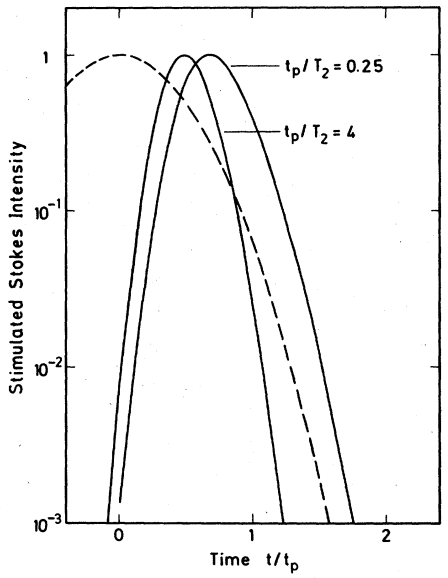

FIG. 3. Generated Stokes pulse vs time for a moderately transient, $t_p/T_2 = 4.0$, and a highly transient, $t_p/T_2 = 0.25$, situation. The Gaussian incident laser pulse of duration t_p is shown by the broken curve. Here $\eta_S = 10^{-2}$.

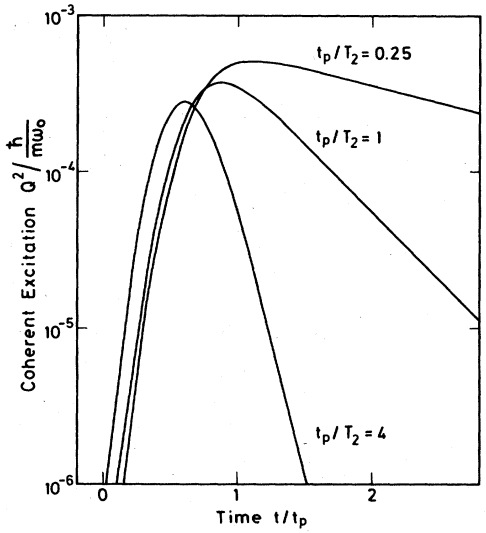

FIG. 4. Coherent vibrational excitation in units of $\hbar/m\omega_0$ vs time for three values of the parameter t_p/T_2 (duration of pump pulse t_p to dephasing time T_2). Note the exponential decay of the freely relaxing system with time constant $T_2/2$. Calculations are made for an energy conversion efficiency $\eta_S = 1\%$ and an interaction length $x = 1$ cm. Here m and ω_0 denote the reduced mass and the vibrational frequency, respectively.

Examples of the time dependence of two generated Stokes pulses are shown in Fig. 3. The intensity I_S of the Stokes light was evaluated from Eq. (34) and plotted as a function of time (in units of t_p, the half-power pulse width of the incident pulse). The parameter t_p/T_2 determines the time behavior of the coherent interaction between the laser pulse and the molecular system. Figure 3 represents a moderately transient situation of $t_p/T_2 = 4$ and a more transient case with $t_p/T_2 = 0.25$ (solid lines). The broken curve in the figure represents the incident Gaussian pulse assumed in the calculation. It is interesting to see the rapid rise and decay of the Stokes pulse, quite independent of the different values of t_p/T_2. The Stokes pulse is found to be notably shortened (Carman *et al.*, 1970). This effect is a consequence of the highly nonlinear character of the stimulated scattering process. Theory predicts a pulse shortening of approximately 2. The Stokes light rises over several orders of magnitude when the pump intensity changes only by a factor of approximately 2. The maximum of the Stokes pulses in Fig. 3 is shifted with respect to the maximum of the incident pulse (at $t = 0$); time is required to build up the material excitation and the stimulated light emission. The delay amounts to a fraction of the pulse duration depending upon the ratio t_p/T_2.

3. Material excitation

We turn now to the discussion of two important aspects of the vibrational excitation: the degree of coherent excitation and the excess population in the first vibrational state. The interaction of the incident light pulse and the generated Stokes pulse with the molecules may be visualized as follows: The coherent laser and Stokes pulse generate a force at the difference frequency $\omega_0 = \omega_L - \omega_S$ which drives resonantly the molecular vibration [see Eq. (32)]. A well-defined phase relationship is established between the vibrating molecules in the interaction volume. This collective excitation is represented by the ansatz [Eq. (11)] for the coherent vibrational amplitude where the phase relation is indicated by the wave vector $\mathbf{k}_0 = \mathbf{k}_L - \mathbf{k}_S$. We emphasize the abrupt onset and cutoff of the pumping process on account of the rapidly rising and decaying Stokes intensity (see Fig. 3). This point makes stimulated Raman scattering an attractive excitation mechanism for time-resolved studies of freely relaxing vibrational systems.

Examples of the coherent vibrational excitation $|Q|^2$ are presented in Fig. 4; they were calculated from Eqs. (34) and (35). $|Q|^2$ is plotted as a function of time t normalized to the pulse duration t_p for three values of the relevant parameter t_p/T_2. The ordinate is plotted in units of $\hbar/m\omega_0$, where m and ω_0 denote the reduced mass and the frequency of the molecular vibration, respectively. The calculations were made for a typical experimental situation of $x = 1$ cm and $\eta_S = 1\%$.

It is interesting to see in Fig. 4 that the excitation $|Q|^2$ grows very fast over more than two orders of 10 within a time interval of a fraction of t_p (almost independent of the dephasing time T_2). This behavior is expected from our discussion of the rapidly rising Stokes field which drives, together with the laser field, the coherent excitation. Similar to the Stokes pulse the position of the maximum value of $|Q|^2$ is shifted with respect to the maximum of the incident pump pulse at $t = 0$. This delay reflects the accumulative character of the pumping process. Figure 4 indicates that the delay of the position of the maximum $|Q|^2_{\max}$ increases with the dephasing time (i.e., with diminishing values of t_p/T_2).

When the pumping process has terminated, the vibra-

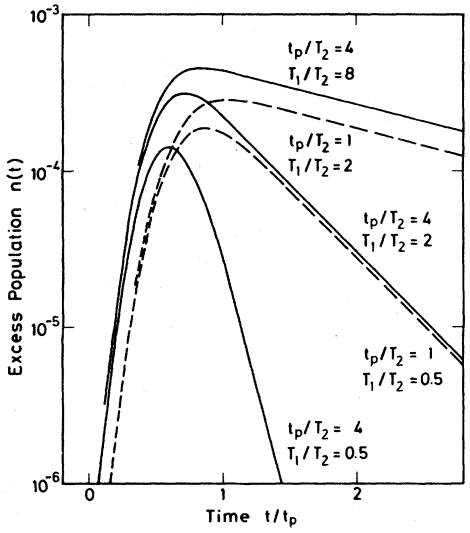

FIG. 5. Excess population n of the first excited vibrational state vs normalized time. Here n decays exponentially with the population relaxation time T_1. Parameters are the ratios t_p/T_2 and T_1/T_2, where t_p and T_2 are the duration of the pump pulse and the dephasing time, respectively. Calculations are performed for $\eta_S = 1\%$ and $x = 1$ cm.

tional excitation relaxes freely. The exponential decay of the curves in Fig. 4 provides directly the value of $T_2/2$. For short pump pulses, $t_p/T_2 = 0.25$ and 1.0, the exponential decay sets in shortly after the maximum. For longer pulses, $t_p/T_2 = 4$, on the other hand, the pumping process terminates more slowly and the exponential decay starts approximately a factor of 10 below the maximum of the $|Q|^2$ curve (see Fig. 4).

The second aspect of the vibrational excitation is illustrated in Fig. 5. We recall that for each Stokes photon emitted one molecule is promoted from the ground to the first vibrational state. The excess population of the upper vibrational state ($v = 1$) is plotted versus normalized time. The numerical examples are evaluated from Eq. (36); the calculation of the Stokes field and of the amplitude Q have been discussed earlier. Each curve in Fig. 5 has two dynamical parameters: the population lifetime (the energy relaxation time) T_1 and the dephasing time T_2. The time constants enter the computation as ratios t_p/T_2 and T_1/T_2. Calculated curves are presented in Fig. 5 for values of $t_p/T_2 = 1$ and 4 and of $T_1/T_2 = 0.5$, 2, and 8. The attained magnitude of the occupation probability n is typical and corresponds to the experimental situation of $x = 1$ cm and $\eta_S = 1\%$. The rapid rise of the excited-state population over orders of 10 is readily recognized from Fig. 5. A comparison of the three solid curves with parameter $t_p/T_2 = 4$ indicates that the magnitude and the time of the maximum increase with population lifetime T_1. This behavior is expected since the excess population n accumulates more effectively and over a longer time of the pumping process with increasing T_1.

Most important are the exponential parts of the curves in Fig. 5 for larger values of t. The individual energy relaxation time T_1 determines the decay of n. The exponential asymptote is quickly reached after the maximum for $T_1 \gtrsim t_p/2$ (see curve $T_1/T_2 = 2$ and $t_p/T_2 = 4$).

C. Stimulated Raman scattering of a homogeneously broadened line with anisotropic scattering tensor: Contribution of rotational motion

The more general case of a homogeneously broadened vibrational mode with anisotropic scattering tensor ($\Delta\omega_j = 0$, $\gamma \neq 0$) is treated now. Equations (12a) and (12b) of Sec. II.A contain orientational averages $\langle Qs_{1j}\rangle_{or}$ and $\langle Qs_{2j}\rangle_{or}$ which require the knowledge of a rotational relaxation time τ_{2R}. We drop the subscripts "or" and "j" in the following equations.

1. Solutions

It is shown in Appendix D that E_{Sz} and E_{Sy} may be evaluated separately. For the simple case of exponential rotational decay discussed there, Eqs. (12)–(14) are rewritten as follows:

$$\frac{\partial}{\partial x'} E_{Sz} = \kappa_1 E_L [\langle Q^* s_1\rangle_{is} + \langle Q^* s_1\rangle_{an}], \tag{38}$$

$$\left(\frac{\partial}{\partial t'} + \frac{1}{T_2}\right)\langle Qs_1\rangle_{is} = \kappa_2 E_L E^*_{Sz}, \tag{39a}$$

$$\left(\frac{\partial}{\partial t'} + \frac{1}{\tau_{an}}\right)\langle Qs_1\rangle_{an} = \frac{4}{45}\frac{\gamma^2}{a^2}\kappa_2 E_L E^*_{Sz}, \tag{39b}$$

$$\left(\frac{\partial}{\partial t'} + \frac{1}{T_1}\right) n = \frac{a}{8\hbar} E_L E^*_{Sz}(\langle Q^* s_1\rangle_{is} + \langle Q^* s_1\rangle_{an}) + \text{c.c.} \tag{40}$$

A similar set of expressions is obtained for the Stokes field E_{Sy}, polarized perpendicular to the incident laser, and for the material excitation $\langle Qs_2\rangle$. It is important to emphasize that the molecules with favorable orientation participate more strongly in the excitation process. As a consequence, the vibrational amplitude Q is connected in Eqs. (38)–(40) with averages over the angles θ. The collective vibrational amplitude $\langle Qs_1\rangle$ consists, according to Eqs. (39a) and (39b), of two components of different dynamical behavior: $\langle Qs_1\rangle = \langle Qs_1\rangle_{is} + \langle Qs_1\rangle_{an}$. The isotropic contribution $\langle Qs_1\rangle_{is}$ is governed by the vibrational dephasing time T_2 [Eq. (39a)]. The anisotropic contribution $\langle Qs_1\rangle_{an}$ is strongly affected by the rotational motion according to the relaxation time τ_{an}, where $1/\tau_{an} = 1/T_2 + 1/\tau_{2R}$ [see Eq. (39b)]. Two time constants, T_2 and τ_{2R}, now determine the evolution of the Stokes pulse and the material excitation produced in the stimulated scattering process. It will be shown below that $\langle Qs_1\rangle$ can be directly measured with picosecond probing techniques.

2. Stokes pulse

We first discuss the steady-state case where $t_p \gg T_2$. Under these conditions, Eqs. (38) and (39) readily yield exponential growth of the Stokes intensity $I_S \propto \exp(gI_L x)$. For the Stokes field polarized parallel to the laser field, the gain factor $g_\parallel$ is found to be

$$g_\parallel = \frac{16\pi}{c\mu_L}\kappa_1\kappa_2 T_2\left[1 + \frac{4}{45}\frac{\gamma^2}{a^2}\frac{\tau_{2R}/T_2}{1+\tau_{2R}/T_2}\right]. \tag{41}$$

Similarly, for the Stokes component polarized perpendicular to the laser field we find a gain factor $g_\perp$:

$$g_\perp = \frac{16\pi}{c\mu_L}\kappa_1\kappa_2 T_2 \frac{\gamma^2}{15a^2}\frac{\tau_{2R}/T_2}{1+\tau_{2R}/T_2}. \quad (42)$$

It is interesting to see in Eqs. (41) and (42) that the anisotropic tensor component γ contributes to the gain of the stimulated scattering depending upon the ratio τ_{2R}/T_2. Rapid rotational motion ($\tau_{2R}/T_2 \ll 1$) reduces the contribution of γ to the stimulated scattering process. When $\tau_R/T_2 \to 0$, we obtain the gain factor of the isotropic situation [Eq. (37)] for the parallel component E_{Sz} and a vanishing gain for the perpendicular field E_{Sy}. In the limiting case of very slow rotational motion $\tau_{2R}/T_2 \gg 1$, our equations reduce to formulas previously discussed in the literature (Bloembergen and Lallemand, 1966). We see from Eqs. (41) and (42) that both gain factors depend on τ_{2R}/T_2 in a different way. Quite generally, we can write for the ratio

$$g_\perp/g_\parallel \leq \rho_s \leq 0.75; \quad (43)$$

i.e., the gain factor $g_\perp$ of the depolarized Stokes field is always smaller than $g_\parallel$ of the polarized field. In a Raman generator the Stokes field starts from quantum noise and has to be amplified by a factor of 10^{11}; the smaller gain coefficient $g_\perp$ gives an amplification of less than 10^8, i.e., the depolarized Stokes field is negligible.

For the transient stimulated Raman process we do not present extensive numerical solutions of Eqs. (38) and (39). Several cases of practical interest have analytical solutions of the form discussed above in Sec. II.B. As an example we consider fast rotational motion with $\tau_{2R} \ll t_p$. In this case, elimination of $\langle Qs_1\rangle_{is}$ and $\langle Qs_1\rangle_{an}$ in Eq. (38) gives

$$\left\{\frac{\partial^2}{\partial t'\partial x'} + \frac{1}{T_2}\frac{\partial}{\partial x'} - \kappa_1\kappa_2|E_L|^2 \left[1+\frac{4}{45}\frac{\gamma^2}{a^2}\frac{\tau_{2R}/T_2}{1+\tau_{2R}/T_2}\right]\right\}\left(\frac{E_{Sz}}{E_L}\right) = 0. \quad (44)$$

This equation is equivalent to an expression which is readily derived from Eqs. (31) and (32) for the isotropic case $\gamma = 0$. As a result, the Stokes field given in Eq. (34) represents also a solution for Eq. (44) after replacing b by b' when $b' = \kappa_1\kappa_2\{1+4\gamma^2\tau_{2R}/[45a^2(\tau_{2R}+T_2)]\}$. The time dependence of the Stokes pulse described by Eq. (44) for $\gamma \neq 0$ and $\tau_R \ll t_p$ is identical to the situation for isotropic scattering (see Fig. 3).

3. Material excitation

Of special interest is the vibrational excitation produced in the anisotropic stimulated scattering. Once the stimulated Stokes field has been evaluated, Eqs. (39a) and (39b) yield the two components $\langle Qs_1\rangle_{is}$ and $\langle Qs_1\rangle_{an}$ of the coherent vibrational excitation. The ratio of the peak amplitudes is estimated to be

$$\left|\frac{\langle Qs_1\rangle_{an}^{max}}{\langle Qs_1\rangle_{is}^{max}}\right| \simeq \frac{4}{45}\frac{\gamma^2}{a^2}\frac{\tau_{an}}{T_2}. \quad (45)$$

Equation (45), which holds exactly for the steady state, gives an estimate of the relative contribution of the anisotropic part $\langle Qs_1\rangle_{an}$ resulting from molecular orientation. For most of the molecular vibrations investigated so far in stimulated Raman scattering, the right-hand side of Eq. (45) is smaller than 10^{-2}.

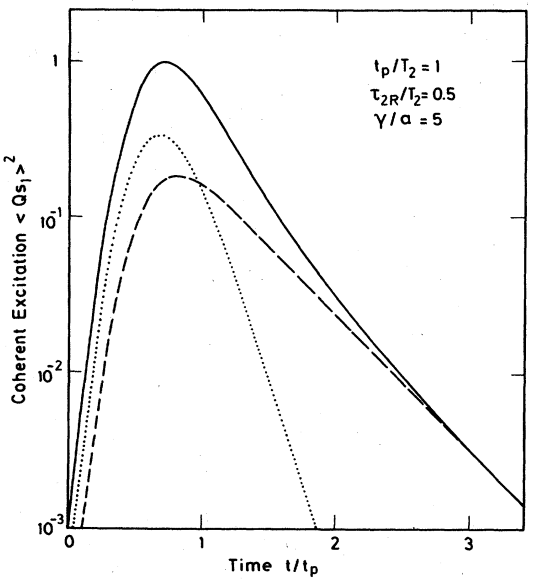

FIG. 6. Total coherent excitation vs time (solid curve) for a vibrational mode with anisotropic scattering tensor. Here a and γ are the symmetric and anisotropic contributions, respectively. The isotropic and anisotropic excitation is depicted by the broken and dotted curve. τ_{2R} denotes the rotational relaxation time.

Equation (45) gives a significant orientational contribution for large anisotropy and slow rotational motion.

The time dependence of the coherent excitation produced in the general case of $\gamma \neq 0$ is calculated as follows: The coherent vibrational excitation is numerically evaluated from Eqs. (38) and (39). The chosen parameters are $t_p/T_2 = 1$, $\tau_{2R}/T_2 = 0.5$, and $\gamma/a = 5$ ($\rho_s \simeq 52\%$). The isotropic and anisotropic components, $|\langle Qs_1\rangle_{is}|^2$ and $|\langle Qs_1\rangle_{an}|^2$, and the total vibrational excitation $|\langle Qs_1\rangle|^2 = |\langle Qs_1\rangle_{is} + \langle Qs_1\rangle_{an}|^2$ are plotted in Fig. 6 as functions of time. Time zero denotes the maximum of the incident laser pulse of Gaussian shape. The excitations $|\langle Qs_1\rangle_{is}|^2$ and $|\langle Qs_1\rangle_{an}|^2$ (broken and dotted curves in Fig. 6) rise to a maximum at slightly different times. A ratio of the peak values of 1.8 is seen in the figure. From Eq. (45) we estimate a ratio of 1.5 for the parameters given above. Of special interest is the time dependence for later times, where the stimulated excitation process has terminated and the molecular system relaxes freely. $\langle Qs_1\rangle_{is}$ decays according to the vibrational dephasing time T_2, while $\langle Qs_1\rangle_{an}$ decreases more rapidly at a rate of $1/\tau_{an} = 1/T_2 + 1/\tau_{2R}$. As a consequence, the time evolution of the total vibrational excitation is strongly affected by the orientational motion. During the excitation process, molecules with favorable orientation become preferentially excited. Immediately following the pumping process, the excitation decays considerably faster on account of orientational averaging. Two orders of magnitude below the maximum of $|\langle Qs_1\rangle|^2$, the coherent excitation turns to an exponential slope with time constant $T_2/2$. Our example of Fig. 6 demon-

strates that for our specific case, rotational motion contributes substantially to the relaxation of the coherent excitation. We note that molecular vibrations with depolarization factors of the magnitude chosen in this example have not yet been excited in stimulated Raman experiments.

In many practical cases, the values of γ and τ_{2R}/T_2 are small and the contribution of molecular rotation to the time evolution of the material excitation may be neglected. This fact is considered to be an important advantage of time-resolved investigations of molecular vibrations.

D. Stimulated Raman scattering of an inhomogeneously broadened line with isotropic scattering tensor

This section is devoted to the coherent excitation of more complex vibrational modes. First, we study normal modes with different isotope components (II.D.2). For molecular vibrations with a large isotope effect, the spontaneous Raman spectrum exhibits a distinct line splitting; for a small isotope effect, the spontaneous spectrum does not resolve the individual components. It will be shown below that coherent light scattering allows us to measure the dephasing time T_2 (i.e., the homogeneous linewidth) of individual isotope components even for unresolved Raman bands.

Next we investigate vibrational modes with a continuous distribution of frequencies. A distribution of resonance frequencies occurs on account of varying molecular surroundings. The best known examples are hydrogen bonded molecules where wide inhomogeneously broadened Raman and infrared bands have been observed. In general, spectroscopic investigations do not permit us to distinguish between homogeneous and inhomogeneous line broadening factors. In fact, there is very little quantitative information about an inhomogeneous contribution to the many vibrational modes. The *a priori* assumption of a homogeneously broadened vibrational line is not justified in many liquid systems. It will be demonstrated in Sec. II.D.3 that transient coherent excitation of condensed matter offers the possibility of measuring separately the homogeneous and inhomogeneous contribution to the Raman line of an individual vibrational mode.

1. Starting equations

We restrict our calculations to the case of an isotropic Raman scattering tensor. It has been pointed out in Sec. II.C that the anisotropy of the scattering tensor gives negligible contributions to the excitation process in most practical cases. The set of equations (12)–(17) simplifies considerably for $\gamma = 0$. The Stokes component polarized perpendicular to the incident light field vanishes, $E_{Sy} = 0$. The excitation proceeds independently of molecular orientation: $s_{1j} = 1, s_{2j} = 0$ [see Eq. (16)], and the brackets $\langle\ \rangle_{or}$ denoting an average over the orientational distribution may be omitted. Equations (12)–(14) are rewritten as follows:

$$\left(\frac{\partial}{\partial x}+\frac{1}{v}\frac{\partial}{\partial t}\right) E_{Sz} = \kappa_1 E_L \sum_j f_j Q_j^* \exp(-i\,\Delta\omega_j t)\,, \tag{46}$$

$$\left(\frac{\partial}{\partial t}+\frac{1}{T_2}\right) Q_j = \kappa_2 E_L E_{Sz}^* \exp(-i\Delta\omega_j t)\,, \tag{47}$$

$$\left(\frac{\partial}{\partial t}+\frac{1}{T_1}\right) n_j = \frac{a}{8\hbar} E_L E_{Sz}^* \exp(i\Delta\omega_j t) + \text{c.c.}\,, \tag{48}$$

where we used the abbreviations

$$\Delta\omega_j = \omega_L - \omega_S - \omega_j \tag{49}$$

and

$$\kappa_1 = \frac{a\pi\omega_S^2 N}{c^2 k_S}\ ;\quad \kappa_2 = \frac{a(1-2\bar{n})}{4m(\omega_L-\omega_S)}\,. \tag{50}$$

Equation (49) is identical to Eq. (17) and is repeated to give a complete set of equations. The subscript z of the Stokes field will be dropped in the following. We recall that the sum $\sum_j$ on the right-hand side of Eq. (46) has to be carried out over all components j of the vibrational system and that Eqs. (46)–(50) were derived for the ansatz of plane waves for the laser and Stokes field [see Eq. (2)]. The monochromaticity of the stimulated Stokes emission is considered in Appendix E. Phase-matching $k_j = k_L - k_S$ is established for all vibrational components during the stimulated excitation process.

One important aspect of the coherent excitation of a distribution of frequencies is readily seen from the limiting case of a very short excitation pulse where $|\Delta\omega_j t_p| \ll 1$. In this case the factors $\exp(-i\Delta\omega_j t)$ of Eqs. (46) and (47) are approximately equal to unity and may be neglected. As a result, the coherent amplitudes Q_j build up with equal gain; i.e., we obtain $|Q_j| = Q$. In addition, the short excitation pulse prepares the different molecular species with approximately equal initial phases. When the incident pump pulse has passed the medium the stimulated excitation process rapidly terminates and the molecular components relax freely. The collectively vibrating components decay with the dephasing time T_2. The total vibrational excitation, which is a superposition of the amplitudes $\langle q_j \rangle$, shows interference effects. For example, for the case of isotopic line splitting with constant frequency difference, a (damped) beating phenomenon is expected with repetitive maxima and minima.

Experimentally, we work with pulses of finite duration. To calculate the excitation process we introduce explicitly a phase factor ϕ_j for the vibrational component j:

$$Q_j = |Q_j| \exp(i\phi_j)\,. \tag{51}$$

Substituting this expression in Eqs. (46) and (47) readily gives the following set of coupled equations:

$$\left(\frac{\partial}{\partial x}+\frac{1}{v}\frac{\partial}{\partial t}\right) E_S = \kappa_1 E_L \sum_j f_j |Q_j| \cos(\Delta\omega_j t + \phi_j)\,, \tag{52}$$

$$\left(\frac{\partial}{\partial t}+\frac{1}{T_2}\right) |Q_j| = \kappa_2 E_L E_S \cos(\Delta\omega_j t + \phi_j)\,, \tag{53}$$

$$\frac{\partial}{\partial t}\phi_j + \frac{\kappa_2 E_L E_S}{|Q_j|} \sin(\Delta\omega_j t + \phi_j) = 0\,. \tag{54}$$

The field amplitudes E_L and E_S are taken to be real. It is pointed out in Appendix E that a constant phase of the Stokes field develops during the excitation (after an amplification of several orders of 10). The imaginary part of Eq. (46) yields a supplementary condition defin-

ing the frequency position of the Stokes pulse:

$$\sum_j f_j |Q_j| \sin(\Delta\omega_j t + \phi_j) = 0 . \tag{55}$$

ω_S enters Eq. (55) implicitly via Eq. (49). For a symmetric frequency distribution of the vibrational system the Stokes emission occurs according to Eq. (55) at the center frequency of the spontaneous Raman line (where $\Delta\omega_j = 0$).

Equations (52)–(55) describe the time evolution of the coherent vibrational excitation represented by the set of amplitudes Q_j and phases ϕ_j. Solutions are presented in the next two sections for two specific cases. The development of the excited-state population n_j determined by Eq. (48), is similar to the results of Sec. II.B for a homogeneous line and will not be discussed here.

2. Equidistant neighboring vibrational levels

Vibrational modes with discrete, equally spaced vibrational levels are investigated in this section. Such a situation occurs, for example, when the molecules consist of different isotope species. Due to the slightly different masses of the vibrating atoms, the resonance frequencies are shifted. The present discussion is restricted to constant frequency spacing $\Delta\omega$ of the vibrational levels. We assume a small line splitting and correspondingly small phase factors during the excitation process. The condition $|\Delta\omega_j t + \phi_j| \ll 2\pi$ is equivalent to moderately short pulses, $|\Delta\omega_j t_p| \lesssim 1$, and applies to the experimental situation discussed in Sec. V.B.

Expanding the phase factors in Eqs. (52)–(55) to first order we obtain:

$$\left(\frac{\partial}{\partial x} + \frac{1}{v}\frac{\partial}{\partial t}\right) E_S = \kappa_1 E_L Q , \tag{56}$$

$$\left(\frac{\partial}{\partial t} + \frac{1}{T_2}\right) Q = \kappa_2 E_L E_S , \tag{57}$$

$$\frac{\partial \phi_j}{\partial t} + \frac{\kappa_2 E_L E_S}{Q}(\Delta\omega_j t + \phi_j) = 0 , \tag{58}$$

$$\omega_S = \omega_L - \sum_j f_j \omega_j . \tag{59}$$

f_j denotes the relative number density of molecules ($\sum_j f_j = 1$). Equations (56) and (57) show that phase-dependent terms have canceled in first order. As a result, the individual components are excited with equal absolute value $Q = |Q_j|$ of the vibrational amplitude. Equations (56) and (57) are identical to the case of a single vibrational component [see Sec. I.B, Eqs. (31) and (32)]; they may be solved independently of Eq. (58). A Stokes pulse is produced in the same way as calculated for a homogeneously broadened molecular vibration. Solutions of E_S and Q have been discussed in Eqs. (34) and (35) in terms of Bessel functions of complex arguments. The transient stimulated Stokes emission grows as if the small frequency shifts $\Delta\omega_j$ were absent. Accordingly, the total number density N contained in the parameter κ_1 enters the stimulated gain factor G in the present calculation: $G = 2T_2\kappa_1\kappa_2 E^2_{L\,\max} l$, where l denotes the length of the sample [see Sec. II.B, Eq. (37)]. This result differs from the steady-state stimulated Raman process ($t_p \gg T_2$), where the maximum gain is proportional to $N\sum f_j/[1+(\Delta\omega_j T_2)^2]$.

With E_S and Q known, the phase factors ϕ_j of the individual species j can be evaluated with the help of Eq. (58). We find

$$\phi_j = -\Delta\omega_j t + \psi_j , \tag{60a}$$

where

$$\psi_j = \Delta\omega_j \int_{-\infty}^{t} dt' \exp\left(\frac{t'-t}{T_2}\right)\frac{Q(t')}{Q(t)} . \tag{60b}$$

ψ_j denotes the phase shift between the individual vibrations and the driving force; numerical calculations indicate that ψ_j is weakly time dependent during the stimulated excitation process. The phase factor ϕ_j contains the term $-\Delta\omega_j t$. Consequently, Eq. (11) together with Eqs. (49), (51), and (60a) gives a coherent amplitude $\langle q_j \rangle$ oscillating with frequency $\omega_0 = \omega_L - \omega_S$. In fact, the molecular species are coherently driven with the frequency difference $\omega_L - \omega_S$ of the total exciting field. The situation is similar to the well-known behavior of harmonic oscillators, which are excited under off-resonance conditions.

The magnitude of ψ_j depends on the ratio t_p/T_2, pulse duration to dephasing time. Short excitation gives small values of ψ_j as is illustrated by the following numerical examples. In the steady-state situation, $t_p/T_2 \gg 1$, Eq. (60b) yields $\psi_j = \Delta\omega_j T_2$. In the transient case we find values of $\psi_j \simeq 0.4\Delta\omega_j T_2$, $0.1\Delta\omega_j T_2$, and $0.02\Delta\omega_j T_2$, respectively, for Gaussian pulses of duration $t_p/T_2 = 25$, 0.5, and 0.1. For very short pulses, one finds $\psi_j \simeq 0$, as was pointed out at the beginning of this section.

When the excitation process has terminated, each vibrational component oscillates with its resonance frequency ω_j. At times $t \gtrsim t_p$ the phase factor ϕ_j has reached a constant value:

$$\phi_{j,\infty} = -\Delta\omega_j \frac{\int_{-\infty}^{\infty} dt\, t\, E_L E_S \exp(t/T_2)}{\int_{-\infty}^{\infty} dt\, E_L E_S \exp(t/T_2)} . \tag{61}$$

Equation (61) determines the phase relation of the different vibrational components at the end of the excitation process. The results derived here hold for an ensemble of vibrational systems disregarding intermolecular forces. The spatial variation of $\phi_{i,\infty}$ will be discussed in Sec. III.A.4.

A numerical example for the coherent excitation of a vibrational system with isotopic substructure is shown in Fig. 7. Calculations were made for three molecular species of relative abundance 1 : 0.5 : 0.5 and the parameter values $\Delta\omega T_2 = \pi/4$, $t_p/T_2 = 0.5$, using Eqs. (57)–(59). The parameters chosen refer to the tetrahedron vibration of carbon tetrahalides. The total vibrational excitation Q_{tot} of the system is represented by the coherent superposition of vibrational states:

$$Q_{\text{tot}} = \left|\sum_j f_j \langle q_j \rangle\right| = \left|\sum f_j Q \exp(-i\omega_j t + \phi_j)\right| . \tag{62}$$

$|Q_{\text{tot}}|^2$ is plotted in Fig. 7 as a function of time (solid curve). $t = 0$ marks the maximum of the excitation pulse. The vibrational excitation rapidly rises to a delayed

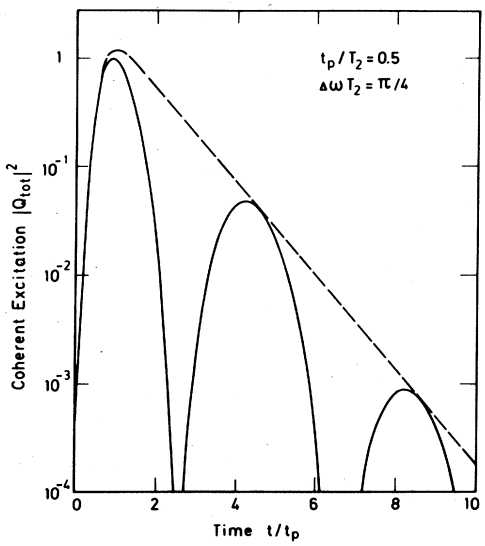

FIG. 7. Calculated coherent vibrational excitation of three molecular components vs time t/t_p (equal frequency spacing $\Delta\omega$; relative abundance 1 : 0.5 : 0.5). The solid curve represents the beating due to the superposition of the vibrational excitations. The broken line indicates the vibrational excitation of one molecular component.

maximum at $t/t_p \simeq 0.9$. For later times t the stimulated process rapidly terminates and the three isotopic components relax freely. It is interesting to see the beating phenomenon which decays exponentially with dephasing time T_2 (note broken envelope line). The oscillatory behavior shown in Fig. 7 is a direct consequence of the phase relationship established in the excitation process and the frequency spacing $\Delta\omega$ of the isotopic species. The $|Q_{tot}|^2$ curve in the figure displays the resulting maxima and minima with beat period of $2\pi/\Delta\omega$. Experimental data on the collective beating are presented in Sec. V.B.

3. Distribution of vibrational components

After the discussion of a vibrational system with discrete levels of a small frequency difference, we investigate the more general case where a normal mode is frequency broadened by a continuous distribution of vibrational states. The set of differential equations which governs the vibrational system has been derived above [Eqs. (52)–(55)]. The phase terms in these equations will be retained to account for frequency shifts $\Delta\omega_j$ and associated phases ϕ_j. We have obtained numerical solutions of the coupled differential equations and will briefly discuss our results in the following. A distribution function $f(\Delta\omega_j)$ of Gaussian shape is assumed for the vibrational mode. This special choice is supported by theoretical arguments for stochastic processes.

At this point, we should comment on the use of the subscript j to characterize individual components of the vibrational distribution. It is advantageous for the theoretical treatment and for the present discussion to consider a quasicontinuous distribution where molecules within a small frequency spread $\delta\omega$ belong to a vibrational component j with number density Nf_j. In our calculations we make $\delta\omega \ll 1/T_2$ for each molecular component j with resonance frequencies $\omega_j \pm \delta\omega/2$. The molecules of each subgroup display equal phase shifts during the stimulated excitation process. The notation used here is certainly not unique. Equations (52) and (55) may easily be converted to a continuous distribution replacing the sum $\sum_j$ by an integral $\int d(\Delta\omega)$ and using $f(\Delta\omega)$, $Q(\Delta\omega)$, and $\phi(\Delta\omega)$ instead of f_j, Q_j, and ϕ_j, respectively. Introduction of integrals in the coupled partial differential equations (52)–(56) does not change the physical situation. In numerical calculations one returns to the quasicontinuous distribution discussed here.

We present now our numerical results for the coupled differential equations (52)–(55). The time dependence of the stimulated Stokes pulse is found to be similar to the case of a single vibrational constituent (see Fig. 3 in Sec. II.B). Our main interest is focused on the vibrational excitation which has a time evolution as depicted in Fig. 8. A fairly broad distribution of width $\delta\omega_{inh}T_2 = 45$ and a duration of the pumping light pulse $t_p/T_2 = 0.5$ are assumed in the calculation. The excitation $|Q_j|^2$ is plotted versus time in units of the pulse duration t_p for the band center $\Delta\omega_j = 0$ (broken line). The exponential decay with time constant $T_2/2$ should be noted. Of interest are the data on the total vibrational excitation $|Q_{tot}|^2$ (solid curve in Fig. 8), where Q_{tot} represents the coherent superposition of the vibrational distribution defined by Eq. (62). We emphasize the different time behavior of the $|Q_{tot}|^2$ curve. The ac-

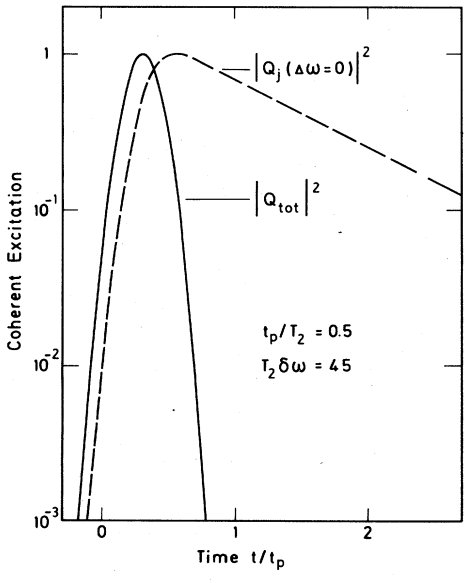

FIG. 8. Calculated coherent excitation of a vibrational system with a (Gaussian) distribution of transition frequencies. The solid curve represents the total vibrational excitation with rapid nonexponential decay due to destructive interference of the various components. The broken line shows the time behavior of a molecular subensemble with negligible spread of transition frequencies; the exponential decay with time constant $T_2/2$ should be noted.

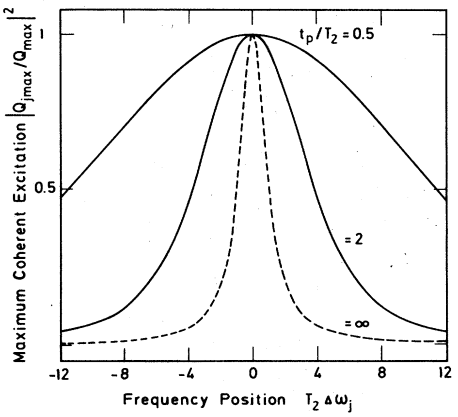

FIG. 9. Maximum coherent excitation of an inhomogeneously broadened vibrational system vs frequency position for different values of t_p/T_2. $\Delta\omega_j = 0$ denotes the band center.

celerated, nonexponential decay of the solid curve results from destructive interference between the vibrational components which are excited with well-defined phases ϕ_j. It is obvious from Fig. 8 that we have to select one vibrational component out of the total excitation in order to learn the value of T_2. It will be shown below that indeed one vibrational component can be studied by probe scattering under carefully selected experimental conditions.

The vibrational amplitudes of the various components depend on their frequency position $\Delta\omega_j$. This point is elucidated in Fig. 9. The maximum excitation $|Q_{j\max}|^2$ is plotted as a function of the distance $\Delta\omega_j$ from the center of the frequency distribution (where $\Delta\omega_j = 0$). Figure 9 presents theoretical data for different values of the ratio pulse duration to dephasing time, t_p/T_2. The solid curves are calculated for values of $t_p/T_2 = 0.5$ and 2, respectively. The broken line represents the steady-state situation, $t_p/T_2 \to \infty$, and corresponds to the well-known resonance curve of a driven harmonic oscillator under stationary conditions. It is interesting to see in Fig. 9 that the bandwidth of the components which participate in the stimulated Raman process is significantly larger in the transient case than in the steady-state situation. For example, the excitation of the molecules occurs over a frequency bandwith $\delta\omega_{\rm exc} T_2 = 22$ for $t_p/T_2 = 0.5$. This value exceeds the steady-state value by a factor of 11. Figure 9 shows that a larger fraction of the total molecular ensemble interacts with the incident laser pulse when the excitation process becomes more transient.

As discussed in the previous section, the vibrational components do not oscillate with their resonance frequencies during the excitation process; they display driven vibrations close to the frequency difference $\omega_L - \omega_S$ of the light fields. This behavior is illustrated in Fig. 10 for a transient situation with $t_p/T_2 = 1$. The normalized instantaneous frequency $T_2\Delta\omega = T_2\partial\phi_j/\partial t$ is plotted versus time t for several vibrational components j. $t = 0$ marks the maximum of the exciting laser pulse. It is readily seen from the figure that the instantaneous frequency is pulled towards $\Delta\omega \simeq 0$ during the excitation process. When the vibrational excitation has terminated, i.e., for $t/t_p > 1$, the vibrational components j shift to their respective resonance frequencies ω_j where $\Delta\omega = \Delta\omega_j$. The frequency changes of the individual components j during the free relaxation are important for the investigation of the vibrational distribution with coherent probe pulses. This point will be treated in Sec. III.A.

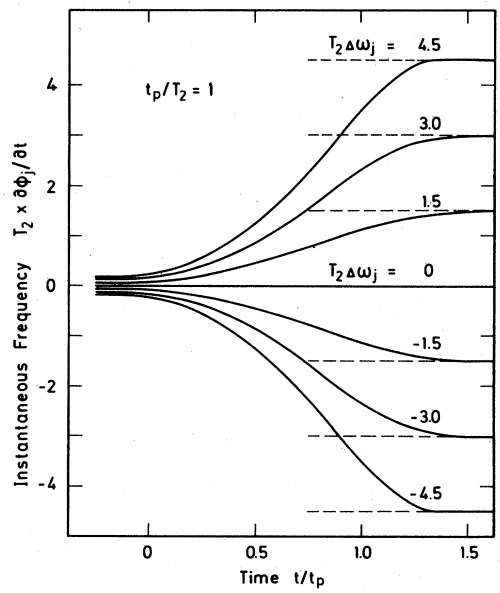

FIG. 10. Instantaneous frequency $\partial\phi_j/\partial t$ of various subensembles of the vibrational system (labeled by their transition frequency position $\Delta\omega_j$) during and after the excitation process. Here $t = 0$ denotes the maximum of the pump pulse. During the excitation process ($t/t_p \sim 0$) the molecules are driven with the same frequency $\omega_L - \omega_S$; after the excitation they return to their individual resonance frequencies ω_j.

E. Excitation by resonant infrared absorption

In the previous sections the excitation of one normal vibrational mode via stimulated Raman scattering has been discussed. The frequency of the incident light pulse is not in resonance with the vibrational (or electronic) transition frequencies of the molecular system. In this case the interaction Hamiltonian of Eq. (4) provides the relevant coupling mechanism. This section is devoted to a different physical situation. The frequency of the incident light pulse coincides with the resonance frequency of the vibrational mode of interest. For optically allowed transitions the electric dipole coupling determines the propagation of the resonant incident pulse.

The frequency of the required light pulses ranges—corresponding to the normal mode frequencies—from a hundred to a few thousand wavenumbers; i.e., dynamical investigations using electric dipole interaction necessitate ultrashort pulses in the infrared. The absorption properties of specific liquid samples in this spectral range are available from standard infrared absorption spectroscopy. In this section we investigate the

vibrational excitation generated by infrared absorption of an intense resonant pulse of picosecond duration. Both the coherence and the time scale of the incident pulse introduce new and interesting features to the absorption process.

1. Macroscopic variables

In the past decade the electric dipole interaction between light pulses and two-level systems has received considerable attention (for reviews see Kryukov and Letokhov, 1969, Courtens, 1972, and Sargent, Scully and Lamb, 1974). Several striking phenomena have been predicted and experimentally observed fo r the propagation of short pulses in resonant media (Kurnit, Abella, and Hartmann, 1964; Tang and Silverman, 1966; McCall and Hahn, 1967; Patel and Slusher, 1967 a and b; Gibbs and Slusher, 1970; Brewer and Shoemaker, 1971; Grieneisen *et al.*, 1972; Grischkowsky, 1973; Aartsma and Wiersma, 1976). Photon echo, optical nutation, and self-induced transparency are optical counterparts to the coherent phenomena observed for magnetic dipole transitions of spin systems. We point to the extensive literature on the latter subject (Abragam, 1961; Slichter, 1963).

Previous optical investigations were performed on metal vapors or molecular gases at low pressure and with doped solids at low temperature. In these systems the dephasing times T_2 are long (>10^{-8} sec) and it is possible to work with standard electronically switched light pulses of $t_p < T_2$. Relatively high population densities are readily generated with these long laser pulses of medium-intensity levels. The present treatment considers the situation in liquids where a high molecular density is combined with very short dephasing times of the order of 10^{-12} sec. Our calculations differ from previous publications in various respects:

(i) Rapid rotational motion of the molecules which proceeds in many liquids at rates comparable to the vibrational dephasing is included.

(ii) Analytic solutions of the equations of motion for arbitrary values of the incident pulse duration t_p and time constants T_1 and T_2 of the vibrational transition are presented. These results are obtained for small changes of the excited-state population $n \ll 1$. As shown below, such a situation prevails in many liquid systems.

Our discussion starts with the ansatz for the electromagnetic field

$$\vec{E} = \tfrac{1}{2} E(x,t) \exp(ikx - i\omega t) + \text{c.c.}\,, \tag{63}$$

where E is the complex amplitude of a light pulse of frequency ω. For simplicity we assume linear polarization of the field in the z direction. The propagation of the light pulse in the x direction is governed by the wave equation [Eq. (1)],

$$\frac{\partial^2 \tilde{E}}{\partial x^2} - \frac{\bar{\mu}^2}{c^2}\frac{\partial^2(\tilde{E})}{\partial t^2} - \frac{\bar{\gamma}}{c}\frac{\partial \tilde{E}}{\partial t} = \frac{4\pi}{c^2}\frac{\bar{\mu}^2+2}{3}\frac{\partial^2 \tilde{P}}{\partial t^2}\,. \tag{64}$$

$\bar{\mu}$ and $\bar{\gamma}$ denote the index of refraction and absorption coefficient, respectively, resulting from the nonresonant part of the interaction of the field with the medium. The resonant part of the interaction is described by the macroscopic polarization on the rhs of Eq. (64). A local field correction is included.

The ansatz for the induced polarization is

$$\tilde{P} = \tfrac{1}{2} P(x,t) \exp(ikx - i\omega t) + \text{c.c.} \tag{65}$$

Since the incident field is assumed to be polarized in the z direction, only the z component of the induced polarization is considered in Eq. (65). As in Sec. II.A (for the Raman transition) we use the slowly varying envelope approximation; i.e., the envelope functions $E(x,t)$ and $P(x,t)$ are assumed to vary little within an optical period or wavelength. Neglecting second-order derivatives of E and P as well as $\partial P/\partial t$ and $\bar{\gamma}\partial E/\partial t$ we obtain from Eqs. (63)–(65)

$$\left(\frac{\partial}{\partial x} + \frac{1}{v}\frac{\partial}{\partial t} + \frac{\bar{\gamma}}{2}\right) E = i\frac{2\pi\omega}{c\bar{\mu}}\frac{\bar{\mu}^2+2}{3} P\,. \tag{66}$$

The group velocity v is calculated from the nonresonant parameters of the medium. Equation (66) relates the coherent electromagnetic pulse described by the field amplitude E to the polarization P of the resonant medium; the latter contains the dynamic response of the molecular system. The specific properties of P have to be calculated from a microscopic theory before the pulse propagation in the medium is evaluated.

2. Equations of motion

The resonant coupling of the incident electromagnetic field to the vibrational transition is expressed by the Hamiltonian

$$H = H^0 - \tilde{p} E_{\text{loc}} \cos\theta\,. \tag{67}$$

H^0 refers to the unperturbed system; the second term in Eq. (67) represents the interaction Hamiltonian with dipole operator $\tilde{p}$. The factor $E_{\text{loc}} \cos\theta$ is the local field component parallel to the induced dipole moment of the individual molecule. The angle θ denotes the molecular orientation with respect to the z axis. It should be noted that vibrational and rotational coordinates are separated in the interaction potential of Eq. (67). In contrast to the vibrational motion, the molecular rotation will be treated purely classically. This approach is justified since the rotational quanta are much smaller than kT and the rotational motion is strongly hindered.

On account of the sharp resonance of the interaction potential in Eq. (67), only two levels, the ground and first excited state of the specific vibrational mode, interact with the incident field. Higher vibrational transitions may be neglected because of anharmonic frequency shifts. The equations of motion of the two-level system are discussed in Appendix A. The strong analogy with the Raman interaction is pointed out in this appendix. For simplicity we restrict our discussion to a homogeneously broadened vibrational system excited exactly at resonance. Writing for the expectation value of the induced dipole moment

$$\langle \tilde{p} \rangle = \tfrac{1}{2} \langle p \rangle \exp(ikx - i\omega t) + \text{c.c.}\,, \tag{68}$$

one arrives at the differential equations

$$\left(\frac{\partial}{\partial t} + \frac{1}{T_2}\right)\langle p \rangle = i\frac{p_{ab}^2}{\hbar}\frac{\bar{\mu}^2+2}{3} E \cos\theta\,[1 - 2(n+\bar{n})]\,, \tag{69}$$

$$\left(\frac{\partial}{\partial t}+\frac{1}{T_1}\right)n = i\,\frac{1}{4\hbar}\,\frac{\bar{\mu}^2+2}{3}\,E\,\langle p\rangle\cos\theta + \text{c.c.} \tag{70}$$

Two quantities describe the instantaneous state of the molecular ensemble: the amplitude $\langle p\rangle$ of the transition dipole moment and the occupation probability n of the first excited vibrational state in excess of the equilibrium value $\bar{n}$. The two dynamic variables behave differently in time according to the individual time constants T_2 and T_1 which have been discussed in Sec. II.A. p_{ab} denotes the off-diagonal matrix element of the transition dipole moment. A local field correction $(\bar{\mu}^2+2)/3$ is introduced in Eqs. (69) and (70) (Pantell and Puthoff, 1968). Comparing the dipole coupling in Eq. (67) with the Raman interaction of Eq. (4) we see a close relationship between the dipole transition moment $\langle\tilde{p}\rangle$ [Eqs. (67), (68)] and the expectation value of the normal mode operator $\langle q\rangle$, [Eqs. (11) and (13)]. In fact, the two quantities $\langle\tilde{p}\rangle$ and $\langle q\rangle$ are proportional with the proportionality factor depending upon the specific molecule and the symmetry of the specific vibrational mode. $\langle\tilde{p}\rangle$ is connected to a local separation of charges and is represented by a vector, while $\langle q\rangle$ is a scalar measuring the vibrational amplitude. As a result, molecular rotation affects the time evolution of $\langle\tilde{p}\rangle$ and $\langle q\rangle$ quite differently. In order to evaluate the component P of the total polarization which points in the direction of the external field we have to calculate the average of $\langle\tilde{p}\rangle\cos\theta$ over the rotational subensemble. After integration of Eq. (69), the orientational average has the form

$$\langle\langle p\rangle\cos\theta\rangle_{\text{or}} = i\,\frac{p_{ab}^2}{\hbar}\,\frac{\bar{\mu}^2+2}{3} \times\int_{-\infty}^{t} dt'\exp\left(\frac{t'-t}{T_2}\right)E(t') \times[1-2(n+\bar{n})]\langle\cos\theta(t)\cos\theta(t')\rangle_{\text{or}}\,. \tag{71}$$

We recognize the rotational correlation function $\langle\cos\theta(t)\cos\theta(t')\rangle_{\text{or}}$, which has been discussed in connection with the analysis of infrared absorption bands; it is different from the rotational correlation function entering the Raman effect (Lascombe, 1974) (see Sec. II.C).

The effect of orientational motion on the dynamical response of the liquid molecules is illustrated for an exponential decay of the rotational correlation. This time dependence is expected for the case of rotational diffusion and for times $t \geq 1$ psec.

$$\phi_{1R} \equiv \langle\cos\theta(t)\cos\theta(t')\rangle_{\text{or}} \simeq \tfrac{1}{3}\exp(-|t-t'|/\tau_{1R})\,. \tag{72}$$

Equation (72) defines an orientational relaxation time τ_{1R} which differs from the time constant τ_{2R} by a factor of 1–3, depending upon the physical processes which determine the rotational relaxation (Bartoli and Litovitz, 1972).

Substitution of Eq. (72) in Eq. (71) and differentiation give the desired expression for $\langle\langle p\rangle\cos\theta\rangle_{\text{or}}$ replacing Eq. (69):

$$\left(\frac{\partial}{\partial t}+\frac{1}{T_2}+\frac{1}{\tau_{1R}}\right)\langle\langle p\rangle\cos\theta\rangle_{\text{or}} = i\,\frac{p_{ab}^2}{\hbar}\,\frac{\bar{\mu}^2+2}{9}\,E[1-2(n+\bar{n})]\,. \tag{73}$$

We note that the rate of vibrational dephasing and orientational motion add in the relaxation term of Eq. (73).

3. Fundamental equations

We are now in a position to present the differential equations describing the resonant interaction of an infrared pulse with a molecular vibration of the liquid. The component of the polarization P parallel to the incident field is the linear superposition of the corresponding dipole moments of the molecular ensemble with number density N; i.e., $P = N\langle\langle p\rangle\cos\theta\rangle_{\text{or}}$. From Eqs. (66), (70), and (73) we obtain the following set of differential equations:

$$\left(\frac{\partial}{\partial x}+\frac{1}{v}\,\frac{\partial}{\partial t}+\frac{\bar{\gamma}}{2}\right)E = i\lambda_1 P\,, \tag{74}$$

$$\left(\frac{\partial}{\partial t}+\frac{1}{T}\right)P = i\lambda_2 E[1-2(n+\bar{n})]\,, \tag{75}$$

$$\left(\frac{\partial}{\partial t}+\frac{1}{T_1}\right)n = i\lambda_3(EP^*-E^*P)\,, \tag{76}$$

where we use the abbreviations

$$\lambda_1 = \frac{2\pi\omega(\bar{\mu}^2+2)}{3\bar{\mu}c}\,,\qquad \lambda_2 = \frac{\bar{\mu}^2+2}{9}\,\frac{p_{ab}^2}{\hbar}\,N\,,\qquad \lambda_3 = \frac{\bar{\mu}^2+2}{12\hbar N}\,. \tag{77}$$

We define an effective dephasing time T of the polarization by

$$\frac{1}{T} = \frac{1}{T_2}+\frac{1}{\tau_{1R}}\,; \tag{78}$$

i.e., both vibrational dephasing and orientational motion lead to a decay of the macroscopic polarization P in the liquid. Equations (75) and (78) indicate that dynamic studies of the induced polarization do not, in general, provide the dephasing time T_2 associated with the vibrational transition. Correspondingly, measurements of the line shape in ir spectroscopy represent a convolution of the vibrational dephasing and rotational motion.

Equations (74)–(76) predict transient phenomena connected with the resonant absorption of a homogeneously broadened vibrational transition. For small light intensities enhanced transmission of short pulses was calculated by Crisp (1970) and experimentally observed in gases by Hamadani *et al.* (1974). Nonlinear coherent phenomena (e.g., self-induced transparency) are described by the same equations [(74)–(76)] for intense pulses with considerable population changes n (see literature on gaseous systems cited above).

In liquids, the excess population which can be generated by ultrashort pulses is quite small. Experimentally we have values of $n \lesssim 10^{-2}$ even for high peak intensities of 10^9 W/cm^2. We note that the electric dipole transition moments in the infrared have moderate values and that the ultrafast relaxation processes in liquids require excitation pulses of a few picoseconds. The following numbers should illustrate the situation: a CH stretching mode of $\bar{\nu} = 3000$ cm^{-1} with maximum absorp-

tion coefficient of $\gamma = 500\ \mathrm{cm}^{-1}$ is excited with a pulse of peak intensity $I = 10^9\ \mathrm{W/cm^2}$ and duration $t_p = 4$ psec. In a liquid with number density of $N = 10^{22}\ \mathrm{cm}^{-3}$ we estimate $n = 5 \times 10^{-3}$ from the formula $n = 2\gamma I t_p / N\hbar\omega$ (population relaxation is neglected).

For $n \ll 1$, Eqs. (74) and (75) may be solved independently of Eq. (76). Transforming to a moving frame, $x' = x$, $t' = t - x/v$, and eliminating P in Eq. (74), we obtain a partial differential equation of second order:

$$\left[\frac{\partial^2}{\partial x' \partial t'} + \frac{1}{T}\frac{\partial}{\partial x'} + \frac{\bar{\gamma}}{2}\frac{\partial}{\partial t'} + \lambda_1\lambda_2 + \frac{\bar{\gamma}}{2T}\right] E = 0 . \tag{79}$$

Substitution of the field amplitude E in Eqs. (74) and (75) gives the same expression for the macroscopic polarization P. Equation (79) has to be integrated for the initial conditions: A known input pulse enters the sample at position $x' = 0$; no field E and no polarization P are present for $t' \to -\infty$:

$$\begin{aligned} &E(x', -\infty) = 0 ; \\ &E(0, t') = E_0(t') ; \\ &P(x', -\infty) = 0 . \end{aligned} \tag{80}$$

The initial field E_0 is assumed to be real. Using Riemann's method we find the following solution of Eq. (79) satisfying our initial conditions [Eqs. (80)]:

$$E(x', t') = E_0(t') \exp(-\bar{\gamma}x'/2) - \lambda_1\lambda_2 x' \exp(-\bar{\gamma}x'/2) \times \int_{-\infty}^{t'} dt'' \exp[-(t' - t'')/T] E_0(t'') J_1(2[\lambda_1\lambda_2 x'(t' - t'')]^{1/2}) [\lambda_1\lambda_2 x'(t' - t'')]^{-1/2} . \tag{81}$$

Using Eq. (81) in Eq. (74) yields the corresponding solution for the polarization:

$$P(x', t') = i\lambda_2 \exp\left(\frac{-\bar{\gamma}x}{2}\right) \int_{-\infty}^{t'} dt'' \exp\left(-\frac{t' - t''}{T}\right) E_0(t'') J_0(2[\lambda_1\lambda_2 x'(t' - t'')]^{1/2}) . \tag{82}$$

J_0 and J_1 denote the Bessel functions of zero and first order. The factor i on the rhs of Eq. (82) indicates a phase shift of $\pi/2$ of the polarization with respect to the light field E. Using the expressions for E and P, the excess population generated by the interaction process is readily evaluated from Eq. (76):

$$n(x', t') = 2\lambda_3 \int_{-\infty}^{t'} dt'' \exp\left(-\frac{t' - t''}{T_1}\right) |E(x', t'') P^*(x', t'')| . \tag{83}$$

We recall that Eqs. (81)–(83) are valid for homogeneous vibrational systems at resonance and for small changes of the occupation number, $n \ll 1$. The equations hold for arbitrary values of the time constants T, T_1, and t_p; in addition, they are applicable to any shape of the incident pulse.

4. Discussion

First we investigate the solutions (81)–(83) for two limiting cases. Input pulses are considered which are very long or very short as compared to the time constants T and T_1. Analytical expressions can be derived which provide direct insight into the nature of the incoherent and coherent absorption process. The intermediate situation, where the three parameters T, T_1, and t_p are of comparable magnitude, is discussed subsequently.

The limiting case of long pulses, $t_p \gg T, T_1$, represents the steady-state situation of conventional infrared transmission spectroscopy. Under these conditions the amplitude E_0 is treated as a constant factor in Eqs. (81) and (82). Integration over the Bessel functions yields

$$E(x', t') = E_0(t') \exp[-(\bar{\gamma}/2 + \lambda_1\lambda_2 T)x'] , \tag{84}$$

$$P(x', t') = (i\lambda_2 T) E(x', t') . \tag{85}$$

From Eq. (83) we find

$$n(x', t') = 2\lambda_2\lambda_3 T T_1 |E(x', t')|^2 . \tag{86}$$

We note that Eqs. (84)–(86) may directly be obtained from Eqs. (74–(76), neglecting time derivatives of P and n. In Eq. (84) we see the well-known exponential decrease of the light field with distance in a resonant medium (Beer's law). The absorption coefficient may be used to determine the dipole transition moment p_{ab} contained in the coupling coefficient λ_2 [see Eq. (77)]. We introduce the maximum absorption coefficient γ of the infrared absorption band. Neglecting the nonresonant absorption, $\bar{\gamma} \ll \gamma$, we have

$$\gamma \simeq 2\lambda_1\lambda_2 T , \tag{87a}$$

which gives

$$p_{ab}^2 = \frac{27\bar{\mu}c}{4\pi(\bar{\mu}^2 + 2)^2} \frac{\hbar}{NT} \frac{\gamma}{\omega} . \tag{87b}$$

This expression refers to a homogeneously broadened absorption line at resonance. The linewidth $\delta\tilde{\nu}_{ir}$ observed in ir spectroscopy, on the other hand, allows an estimate of the time constant T which is the relevant lifetime for the induced polarization P in the absorption process. The exponential relaxation of Eq. (75) leads to a Lorentzian band shape of width (FWHH) in units of cm^{-1}:

$$\delta\tilde{\nu}_{ir} = (\pi c T)^{-1} . \tag{88}$$

Equations (88) and (78) show that vibrational dephasing and rotational motion contribute to the width of the absorption band (Gordon, 1965).

Next, we briefly discuss the limiting case of the transient response of the absorbing medium to a very short excitation pulse. t_p should be small in comparison to the relaxation time T for a given interaction length $\gamma x'$, i.e.,

$$t_p \ll T \text{ and } T/\gamma x' . \tag{89}$$

In this case, the factors $J_1(x)/x$ and $J_0(x)$ under the integrals of Eqs. (81) and (82) are approximately constant during a small time interval around the maximum of the short incident pulse at $t' = t_{max}$. Equation (81) gives

$$E(x', t') = E_0(t') \exp(-\bar{\gamma} x'/2) - \frac{\gamma x'}{T} \exp[-\bar{\gamma} x'/2 - (t' - t_{max})/T] \times \frac{J_1([2\gamma x'(t' - t_{max})/T]^{1/2}}{[2\gamma x'(t' - t_{max}/T]^{1/2}} \int_{-\infty}^{t'} dt'' E_0(t'') . \tag{90}$$

A corresponding expression is obtained from Eq. (82) for the polarization P. It is interesting to notice a significant change of pulse shape due to the second term on the rhs in Eq. (90). The pulse propagation in the medium displays an extended decaying part with oscillatory time behavior which results from the Bessel function J_1. Most important, the electromagnetic pulse travels—apart from the nonresonant absorption term—essentially without losses through the resonant medium. This transparency effect occurs without notably populating the upper vibrational state ($n \ll 1$); it is independent of the intensity level of the input pulse and differs from self-induced transparency. The transient transparency predicted by Eq. (90) is a consequence of the short duration of the interaction; dephasing processes do not disturb the coherent response of the medium (small area pulse propagation).

We turn now to the intermediate situation where the parameters T, T_1, and t_p are of comparable magnitude. This case is of particular interest for our experimental investigations. We have evaluated numerical examples with the help of Eqs. (81) and (82). Input pulses of Gaussian shape and half-width (FWHH) t_p were assumed in the following calculations.

We consider a physical system with a constant linear absorption coefficient γ; i.e., according to Eq. (87b) we have $p_{ab}^2 T = \text{const}$. The penetration depth x_e into the resonant medium was calculated for a decrease of peak intensity of the input pulse by a factor of e and plotted in Fig. 11 versus the ratio of pulse duration t_p to effective dephasing time T. For large values of t_p (rhs of Fig. 11) the interaction process approaches the steady-state situation where $\gamma x_e = 1$; i.e., we have Beer's law. For shorter pulses (lhs of Fig. 11) the increasing values of the penetration depth x_e and the corresponding smaller propagation losses are due to the transient character of the absorption process. The phenomenon is demonstrated by the following numbers (solid line): For $t_p = T$ the pulse propagates twice the distance γ^{-1} before the peak intensity of the pulse decays to the $1/e$ value. For $t_p = T/10$ the penetration depth is found to be approximately 15 times larger than for long pulses under stationary conditions.

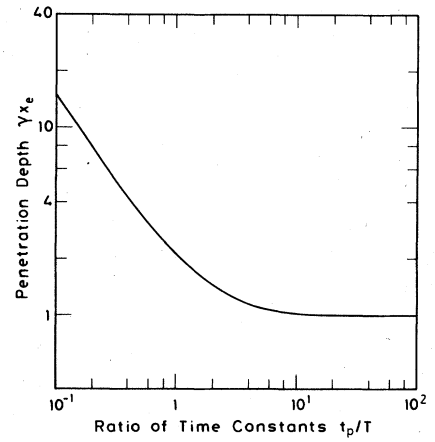

FIG. 11. Penetration depth x_e for constant intensity transmission vs ratio of pulse duration t_p to effective dephasing time T. Here γ denotes the absorption coefficient derived from Beer's law.

The incident and two transmitted pulses are presented in Fig. 12. The normalized intensity $|E/E_0|^2$ of the pulse after propagation of a distance $x = 4\gamma^{-1}$ through the absorbing medium is plotted as a function of time t/t_p for two parameter values $t_p/T = 1$ and 2 (solid and broken lines, respectively). The dotted curve represents the incident pulse of Gaussian shape. The striking

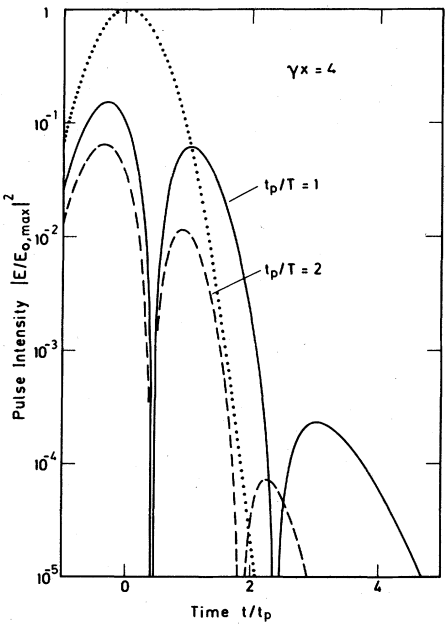

FIG. 12. Intensity vs time of a light pulse after propagation of a distance $x = 4\gamma^{-1}$ through an absorbing medium of absorption coefficient γ. Solid and broken curves correspond to the material parameters $t_p/T = 1$ and $t_p/T = 2$, respectively (T is the effective dephasing time of the medium). The dotted curve represents the Gaussian input pulse.

breakup of the propagating pulse is of special interest. Three maxima and additional zero points have developed as a result of the interaction of the incident field and the resonant medium. The intensity peaks in the figure are found to have opposite phases of the electric field. The reshaping of the pulse originates from the transient character of the resonant absorption and may be visualized as follows:

The incident field builds up a (delayed) macroscopic polarization P with 90° phase shift which radiates an electric field component again phase-shifted by 90° [see Eqs. (74) and (75)]. The primary incident field component and the secondary induced field have opposite phase and different time behavior. The pulse components are separated by zero values in the electric field. In the examples of Fig. 12 ($t_p/T=1$ and 2), the first zero points occur at $t \simeq 0.2t_p$. The second part of the electric field again generates a third field contribution. The positions of the maxima and minima depend on the propagation length γx and the ratio of pulse duration t_p to dephasing time T. Comparison of the broken curve ($t_p/T=2$) and solid line ($t_p/T=1$) in Fig. 12 shows larger intensities for shorter pulses. The relative amplitudes of the secondary maxima are found to increase with propagation length x. In fact, the area under the electric field approaches the asymptotic value $\int E(t)dt=0$ where the individual peaks of the electric field give equal contributions of opposite sign.

We emphasize that the pulse breakup and the transient transparency of weak short pulses in Fig. 12 do not involve significant population changes of the vibrational states. The phenomenon results from the coherent interaction of the pulse with the macroscopic excitation of the vibrational system. The signal velocity is only slightly affected. The situation is different for self-induced transparency where large population changes introduce substantial reduction of the propagation velocity of the transmitted pulses.

We have calculated the material excitations, the coherent polarization P, and the vibrational excess population n, for a variety of parameters. As examples, we present in Fig. 13 numerical results of $|P|^2$ and n as a function of time evaluated for a distance $x=4\gamma^{-1}$ within the medium and for the parameter $t_p/T=1$. The $|P|^2$ curve should be compared with the corresponding data of the light intensity in Fig. 12. We note a time delay of the maxima and minima of $|P|^2$ resulting from the cumulative effect of the vibrational system. Of special value for our investigations is the excess population n of the upper vibrational state. Using Eq. (83), calculations were made for two parameters $T_1=t_p$ and $T_1=2t_p$. According to Fig. 13, the excess population n rises rapidly with time to a delayed maximum and is followed by some slight oscillations resulting from the time dependence of the electric field and the polarization. For longer times t, the excess population n decays exponentially with the population lifetime T_1; i.e., from the asymptotic time behavior of n it is possible to determine the important material parameter T_1 independent of other parameters such as the effective dephasing time T. In Sec. VI.B we shall present experimental data where T_1 of a well-defined vibrational normal mode was measured after short infrared excitation.

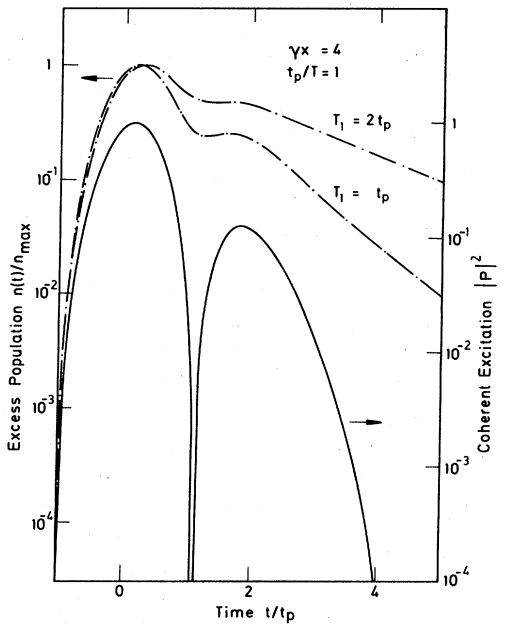

FIG. 13. Coherent polarization $|P|^2$ (solid curve) and vibrational excess population n (dash-dotted curve) vs time at a penetration depth of $x=4\gamma^{-1}$ (γ = the absorption coefficient of the medium). Calculations are made for a pulse duration t_p equal to the effective dephasing time T of the medium. The excess population decays with the population lifetime T_1; two examples with $T_1=t_p$ and $T_1=2t_p$ are depicted.

Concluding the theoretical discussion on excitation processes, some remarks should be made concerning Figs. 2 and 11, where data on Raman interaction and resonant absorption, respectively, are depicted. The figures demonstrate the effect of transient excitation. Both the Raman gain required for a fixed Stokes conversion (i.e., for a certain vibrational excitation) and the penetration depth for a given intensity loss (i.e., for a certain material excitation) increase for shorter laser pulses. Figures 2 and 11 show quantitatively that the interaction of light and matter becomes weaker for shorter coherent light pulses. Deviations from the steady-state values occur when the interaction time t_p is of the order of the effective dephasing time of the system.

III. THEORY OF PROBING PROCESSES

Having introduced two excitation processes in Sec. II we are now in a position to discuss methods for the study of the instantaneous state of the physical system during the excitation and during the return to thermal equilibrium. It has been shown above that the coherent vibrational amplitude and the excited-state population are important factors of the vibrational excitation. Different techniques are required to measure the relevant physical parameters of the vibrational dynamics. In Sec. III.A we discuss coherent Raman scattering as an experimental tool for investigating the coherent excitation of the molecular system. Methods of observing

the excited-state population and energy transfer processes are treated in Secs. III.B and III.C.

A. Coherent Raman probe scattering

We repeat the experimental situation considered here. A powerful light pulse first excites the vibrational mode of interest via stimulated Raman scattering. A second weak light pulse with variable time delay with respect to the pumping pulse traverses the sample subsequently and probes the instantaneous degree of excitation as a function of delay time t_D. The probe wave interacts with the coherent vibrational amplitude $\langle q\rangle$ giving rise to scattered radiation. The interaction process is called coherent Raman scattering. The significance of the coherent material excitation was first emphasized in a paper on lattice vibrations of calcite by Giordmaine and Kaiser (1966). The first application of coherent Raman scattering for the determination of the dephasing time of molecular vibrations in liquids was performed by von der Linde, Laubereau, and Kaiser (1971). At the same time, Alfano and Shapiro (1971) investigated a molecular vibration in calcite. The lifetime of a lattice mode (TO phonon lifetime) of diamond was measured by Laubereau, von der Linde, and Kaiser (1971).

There exists some analogy of the coherent Raman scattering to the interaction of light with coherent sound waves. The molecules in the excited volume vibrate with a definite phase relation and produce a macroscopic modulation of the optical refractive index via the coupling parameter $\partial\alpha/\partial q$. The system behaves like an oscillating three-dimensional phase grating. Scattering off this phase grating produces sidebands shifted by the vibrational frequency to higher (anti-Stokes) and smaller (Stokes) frequencies.

Comparing coherent Raman scattering with conventional spontaneous Raman scattering, we note drastic differences: The latter process is known to scatter an exceedingly small fraction of the incident light ($\sim 10^{-6}$) into the whole solid angle of 4π, quite independent of the specific experimental geometry. Coherent scattering, on the other hand, is more intense by many orders of magnitude and generates a scattering signal which is highly collimated close to the forward direction. Most important, the scattering efficiency depends critically on the scattering geometry according to the k-matching condition (see below).

1. Fundamental equations

The following treatment reveals the close relationship of the coherent probing process to the stimulated excitation discussed above. Both processes are produced by the same macroscopic polarization proportional to the coherent amplitude $\langle q\rangle$. The experimental conditions, however, are significantly different for coherent or stimulated scattering. The latter mechanism generates the vibrational excitation required for the subsequent coherent probe scattering. The scattered radiation in both cases is coherent and is described by the amplitude of an electromagnetic field which obeys a classical wave equation.

The electromagnetic field of the probing process is written in the form

$$\mathbf{E}_{\rm pr} = \tfrac{1}{2}\mathbf{e}_y\{E_{L2}\exp(ik_{L2}x - i\omega_{L2}t) + \sum_j E_{Sj}\exp(ik_{Sj}x - i\omega_{Sj}t) - \sum_j E_{Aj}\exp(-ik_{Aj}x + i\omega_{Aj}t) + \text{c.c.}\}. \quad (91)$$

The subscripts $L2$, Sj, and Aj refer to the incident probe pulse, the Stokes scattered light, and the anti-Stokes radiation, respectively. In several of the following equations we shall use the subscript $\overline{S}$ for the scattered Stokes component in order to differentiate between the Stokes field of the excitation and the probe scattering process.

Propagation in the x direction is assumed; i.e., we consider scattering in the forward direction parallel to the exciting beam. Extension to an off-axis scattering geometry will be discussed below. Equation (91) assumes parallel polarization of the incident probe pulse and scattered probe light. Scattering components of perpendicular polarization are not relevant here and have been omitted. The probing field is polarized in the y direction which is perpendicular to the laser and Stokes field of the excitation process [see Eq. (2)]. This choice has the advantage that components of the excitation and probing field with equal frequency can be discriminated by their different planes of polarization. A negative sign has been chosen for the anti-Stokes field components to take into account the proper phase of the scattering component.

The propagation of the probe field is governed by the wave equation [Eq. (1)], which is repeated here:

$$\Delta\mathbf{E}_{\rm pr} - \frac{1}{c^2}\frac{\partial^2}{\partial t^2}(\mu^2\mathbf{E}_{\rm pr}) = \frac{4\pi}{c^2}\frac{\partial^2}{\partial t^2}\mathbf{P}_{\rm pr}. \quad (92)$$

μ denotes the refractive index. The coupling of the field to the collectively vibrating molecules is described by the macroscopic polarization $\mathbf{P}_{\rm pr}$. The component of $\mathbf{P}_{\rm pr}$ parallel to the incident probe field is expressed by the first term of Eq. (9) (Sec. II.A):

$$\mathbf{P}_{\rm pr} = \mathbf{E}_{\rm pr}N\sum_j f_j\langle\langle q_j\rangle[a + \gamma(\cos^2\theta_{3j} - \tfrac{1}{3})]\rangle_{\rm or}. \quad (93)$$

Equation (93) describes the general case of an inhomogeneously broadened vibrational system with the anisotropic Raman scattering tensor discussed in Sec. II.A. The subscript j labels the component of the vibrational system with number density Nf_j according to its resonance frequency ω_j. The orientation of the molecular symmetry axis with respect to the laboratory frame is denoted by the angle θ_{3j}. The bracket $\langle\rangle_{\rm or}$ indicates that the orientational average has to be taken over the subensemble j. The constants a and γ represent, respectively, the isotropic and anisotropic part of the Raman polarizability tensor ($\partial\alpha/\partial q$), defined by Eqs. (3) and (8) in Sec. II.A. The coherent vibrational amplitude is written in the form of Eq. (11):

$$\langle q_j\rangle = \tfrac{1}{2}iQ_j\exp(ik_jx - i\omega_jt) + \text{c.c.} \quad (94)$$

Inserting Eqs. (93) and (94) in the wave equation we find

under similar approximations as used in Sec. II.A

$$\frac{\partial}{\partial x'} E_{Sj} = \kappa_S E_{L2}(t' - t_D) f_j \langle Q_j^* s_{1j} \rangle_{or} \exp(i \Delta k_{Sj} x') , \quad (95a)$$

$$\frac{\partial}{\partial x'} E_{Aj} = \kappa_A E_{L2}^*(t' - t_D) f_j \langle Q_j^* s_{1j} \rangle_{or} \exp(i \Delta k_{Aj} x') . \quad (95b)$$

t_D denotes the time delay between the maxima of the pumping and the probing pulse. The amplitudes $\langle Q_j s_{1j} \rangle_{or}$ in Eqs. (95) represent given functions of time and space generated by the preceding excitation process. The following abbreviations are used [see Eqs. (15)–(17)]:

$$\kappa_S = \frac{\pi \omega_{\bar{S}}^2}{c^2 k_{\bar{S}}} aN , \kappa_A = \frac{\pi \omega_A^2}{c^2 k_A} aN;$$

$$s_{1j} = 1 + (\gamma/a)(\cos^2\theta_{3j} - \tfrac{1}{3}) . \quad (96)$$

The frequencies of the scattered Stokes and anti-Stokes components are found to be

$$\omega_{Sj} = \omega_{\bar{S}} + \Delta\omega_j , \quad \omega_{Aj} = \omega_A - \Delta\omega_j ,$$

where

$$\omega_{\bar{S}} = \omega_{L2} - \omega_L + \omega_S , \quad \omega_A = \omega_{L2} + \omega_L - \omega_S . \quad (97)$$

$\omega_{\bar{S}}$ denotes the central Stokes frequency of the scattered probe pulse; $\Delta\omega_j$ indicates the frequency difference between the component j and the primary material excitation: $\Delta\omega_j = \omega_L - \omega_S - \omega_j$ [Eq. (17)]. The Δk values in Eqs. (95) represent the wave-vector mismatch of the Stokes and anti-Stokes scattered fields; they are important parameters for the subsequent discussion. We recall that the excitation of all frequency components is described by the wave vector $k_j = k_L - k_S$ [see Eq. (17)]. For the mismatch of the probe beams we find

$$\Delta k_{Sj} = k_{L2} - k_{Sj} - k_j \quad (98)$$

and

$$\Delta k_{Aj} = k_{Aj} - k_{L2} - k_j . \quad (99)$$

It should be noted that Eqs. (95a) and (95b) refer to a retarded time $t' = t - x/v$ and to $x' = x$; in this way $E_{L2} = E_{L2}(t')$ depends on t' only. v is the group velocity of the probe radiation. Group velocity dispersion will be neglected. This approximation is valid for interaction lengths between probing pulse and vibrational excitation of a few centimeters, a condition which is readily fulfilled in our experiments. On the other hand, color dispersion has to be considered in Eqs. (95a) and (95b) for the Δk_j values. The wave-vector mismatch has different magnitudes for the Stokes and anti-Stokes process and for the different components j. We shall return to this point in the following discussion.

Equations (95a) and (95b) represent the growth of the coherent field components at the Stokes and anti-Stokes frequency in the probing process. This probe scattering affects the vibrational excitation via the interaction Hamiltonian of Eq. (4) analogously to the stimulated scattering process (Sec. II.A). Expressions similar to Eq. (13) may be derived for the buildup or loss of the vibrational amplitudes Q_j resulting from Stokes and anti-Stokes probe scattering.

The disturbance of the vibrational excitation is negligible if we work with incident probe pulses of sufficiently low intensity. We find the following condition for the peak intensity I_{L2} of the incident probe pulse:

$$\frac{16\pi}{c\mu_{L2}} \kappa_S \kappa_2 T_2 \Delta l \; I_{L2} \ll 1 . \quad (100)$$

Δl denotes the effective interaction length of the probe scattering and will be discussed below. The coupling parameter κ_2 has been defined by Eq. (15). Equation (100) should be compared with the stimulated gain G of Eq. (37). Condition (100) is readily fulfilled in our experimental investigations with probe pulses of much smaller intensity than the excitation pulses:

$$I_{L2} \ll I_L . \quad (101)$$

Our ultrashort light pulses are too short for direct time-resolved observation with standard electronic detectors. With photomultipliers we observe time-integrated scattering signals. We introduce the coherent probe scattering signal S^{coh} measured at the end of the sample, $x = l$:

$$S^{coh}(t_D) = \frac{c\mu_{AS}}{8\pi} \int_{-\infty}^{\infty} \Big| \sum_j E_{AS,j}(l, t') \Big|^2 dt' . \quad (102)$$

The subscript AS indicates probe scattering at the anti-Stokes (A) or Stokes (S) side. The evaluation of the field components is carried out with the help of Eqs. (95a) and (95b). Integration is facilitated using the properties of the stimulated excitation process. It was shown in connection with Eqs. (34) and (37) that the stimulated Stokes pulse grows approximately exponentially with distance:

$$|E_S|^2 \propto \exp(x'/\Delta l) . \quad (103)$$

The effective excitation length Δl is readily estimated for a Raman generator. In this case a large amplification of ~exp(25) builds the intense stimulated Stokes radiation up from quantum noise in a sample of length l. The excitation length Δl,

$$\Delta l \simeq l/25 , \quad (104)$$

denotes the interval at the end of the interaction path l where the maximum excitation occurs.

There are no general analytic solutions of Eqs. (95a) and (95b) and for S^{coh}, since the $Q_j(x,t)$ values are found from numerical calculations. For several special cases approximate expressions may be derived which reveal the relevant properties of the coherent probe signal $S^{coh}(t_D)$.

2. Coherent probing of a homogeneously broadened line: Isotropic and anisotropic scattering tensor

For a transition with a homogeneous line we have $\omega_j = \omega_0, \Delta\omega_j = 0$, and the subscript j may be dropped. The laser field E_{L2} and the amplitude Q are chosen to be real and Eqs. (95a) and (95b) reduce to

$$\frac{\partial}{\partial x'} E_{AS} = \kappa_{AS} E_{L2}(t' - t_D) \langle Q s_1 \rangle_{or} \exp(i \Delta k_{AS} x') . \quad (105)$$

The phase mismatch Δk_{AS} has the form:

$$\Delta k_S = k_{L2} - k_{\bar{S}} - k_L + k_S\,,$$
$$\Delta k_A = k_A - k_{L2} - k_L + k_S\,. \tag{106}$$

Equation (105) is integrated with the help of Eqs. (39) and (103); substitution in Eq. (102) yields

$$S^{\mathrm{coh}}(t_D) = \frac{c\,\mu_{AS}}{2\pi}\,\frac{\kappa_{AS}^2 \Delta l^2}{1+(2\Delta k_{AS}\Delta l)^2} \times \int_{-\infty}^{\infty} dt' E_{L2}(t'-t_D)^2 \langle Q s_1(t', x'=l)\rangle_{\mathrm{or}}^2\,. \tag{107}$$

Equation (107) represents a convolution of the coherent vibrational excitation $\langle Qs_1\rangle^2$ and the probing light pulse. It is interesting to see that the magnitude of the scattering signal strongly depends upon the wave-vector mismatch Δk_{AS}. Perfect phase matching $\Delta k_{AS}=0$ represents the optimum situation. A mismatch of $\Delta k_{AS} = (2\Delta l)^{-1}$ reduces the value of S^{coh} by a factor of 2. We note that Δk_A differs from Δk_S due to color dispersion $k_{AS} = \mu_{AS}\omega_{AS}/c$ and $\mu_A \neq \mu_S$. Simultaneous perfect k matching of Stokes and anti-Stokes probe beams is not possible for the collinear geometry. Equation (107) indicates that the delay dependence of $S^{\mathrm{coh}}(t_D)$ is identical for the two scattered sidebands.

A numerical example for the scattering signal S^{coh} is presented in Fig. 14. The simple case of an isotropic Raman scattering tensor is considered where $\gamma=0$ and $\langle |Q|s_1\rangle = |Q|$. The coherent (Stokes or anti-Stokes) probe signals are evaluated from Eq. (107) and plotted as a function of delay time t_D between the exciting and probing light pulses. A Gaussian shape and an equal pulse duration t_p are assumed for the excitation and the probe pulse. The calculations are made for the parameters $t_p/T_2 = 0.25$, 1, and 4 which are identical to those of Fig. 4. The signal curves rise to a peak value which is delayed with respect to the maximum of the pump pulse at $t_D=0$. The delay of the maximum of the vibrational excitation (see Fig. 4) and the convolution of $|Q|^2$ with the probe pulse lead to the observed delay of $S^{\mathrm{coh}}_{\mathrm{max}}$. It is interesting to see the effect of T_2 on the trailing part of the signal curve. For $t_p/T_2 = 0.25$ the signal curve shows an exponential decay shortly after the maximum. For values of $t_p/T_2 \geq 1$, i.e., for longer pulses, time is required to establish the asymptotic behavior of the signal curve. Exponential decay starts approximately a factor of 3 and 20 below the maximum for $t_p/T_2 = 1$ and 4, respectively. The time constant $T_2/2$ is directly obtained from the exponential slopes of the signal curves.

We have investigated the effect of the shape of the probing pulse on the scattering signal S^{coh}. Our calculations show that a rapid rise and decay of the probe intensity is important for relatively long pulses, i.e., for $t_p > T_2$. Figure 14 illustrates that pulses of Gaussian shape allow the determination of relaxation times T_2 which are notably shorter than the pulse duration t_p. For pulses with extended wings the situation is less favorable; e.g., for a pulse represented by a hyperbolic secant function and for $t_p/T_2 = 1$, the signal curve approaches asymptotic behavior more slowly, and the exponential decay starts a factor of 20 below the maximum. This number has to be compared with the factor of 3 mentioned above for Gaussian pulses with the same parameter $t_p/T_2 = 1$.

We turn now to the more general case of an anisotropic scattering tensor, $\gamma \neq 0$. To illustrate the effect of γ, we first consider a large anisotropy of $\gamma/a = 5$ and values of $\tau_{2R}/T_2 = 0.5$ and $t_p/T_2 = 1$. The orientational relaxation time τ_{2R} was introduced in Sec. II.C. According to Eq. (107), the S^{coh} curves in Fig. 15 repre-

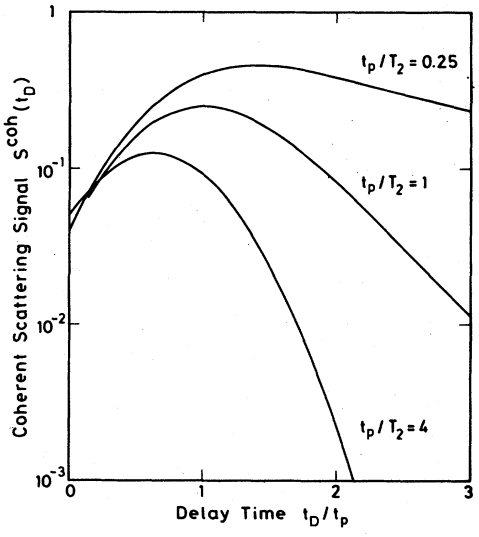

FIG. 14. Coherent (Stokes or anti-Stokes) scattering signal $S^{\mathrm{coh}}(t_D)$ as a function of delay time t_D. Calculations are made for an isotropic Raman scattering tensor and for a homogeneously broadened line with three different dephasing times T_2. The corresponding coherent vibrational excitation is depicted in Fig. 4.

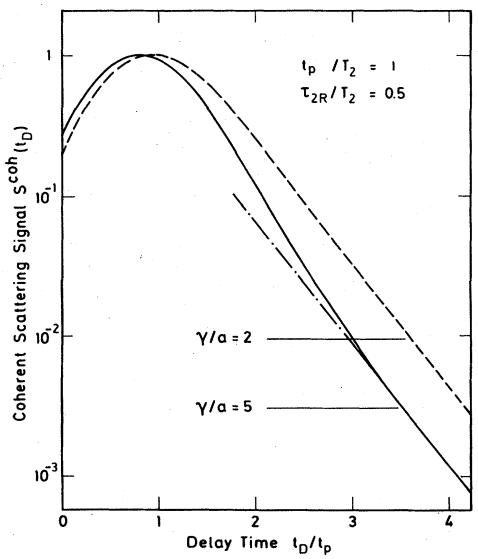

FIG. 15. Coherent (Stokes or anti-Stokes) scattering signal $S^{\mathrm{coh}}(t_D)$ vs delay time t_D. The solid and broken curves are calculated for an anisotropic Raman tensor with anisotropy $\gamma/a = 5$ and 2, respectively. The corresponding coherent excitation (for $\gamma/a = 5$) is presented in Fig. 6.

sent the folding of the probe pulse with the material excitation $|\langle Qs_1\rangle|^2$ (see Fig. 6). After the maximum, the signal curve first decays quickly. For larger values of t_D the decrease of S^{coh} is less pronounced and reaches an exponential tail which starts approximately a factor of 400 below the maximum. The similarity between the S^{coh} curve in Fig. 15 and the material excitation in Fig. 6 should be noted. The rapid decay shortly after the maximum is closely connected with the rotational motion of the vibrating molecules which affects the probe scattering via the anisotropy γ. The exponential asymptote of the signal curve, on the other hand, represents pure vibrational relaxation. From the slope of this later part of $S^{coh}(t_D)$, the time constant $T_2/2$ is directly obtained.

It is interesting to note that the time constant T_2 can be measured with our coherent probe scattering technique even for the unfavorably large anisotropy of the scattering tensor. In most practical cases the influence of rotational motion is much smaller. The broken curve in Fig. 15 illustrates an example where a smaller depolarization factor of $\rho_s \simeq 0.2$ is considered. The corresponding ratio of $\gamma/a = 2$ and the same time constants as used above ($\tau_{2R}/T_2 = 0.5, t_p/T_2 = 1$) were assumed in the calculation. In this case the S^{coh} curve quickly turns to an exponential slope providing the time constant $T_2/2$. The vibrational dephasing time T_2 can be directly determined from the signal curve, without influence of the rotational motion of the molecules in the liquid.

3. Coherent probing of an inhomogeneously broadened line: Isotropic scattering tensor

We wish to discuss now the general case of vibrational systems with inhomogeneous broadening. This situation is of considerable practical interest. To avoid unnecessary complications in the theoretical discussion we consider a vibrational system with an isotropic scattering tensor. It has been pointed out above that the anisotropic part of the tensor, which is small in many practical cases, contributes little to the time evolution of the coherent scattering signal, even for moderately large values of the depolarization factor.

We use the same notation as introduced in Sec. II.D for the excitation process and write, for the complex coherent vibrational amplitude Q_j,

$$Q_j = |Q_j| \exp(i\phi_j), \tag{108}$$

where ϕ_j denotes the phase of the component j of the vibrational distribution. Substitution of Eq. (108) in Eq. (95) yields for the case of an isotropic scattering tensor ($\gamma = 0, s_{1j} = 1$)

$$\frac{\partial}{\partial x'} E_{AS_j} = \kappa_{AS} E_{L2}(t' - t_D) \times f_j |Q_j| \exp(i\Delta k_{AS_j} x' - i\phi_j). \tag{109}$$

The field E_{L_2} of the probe pulse is taken to be real. The amplitudes $|Q_j|$ and phases ϕ_j of the vibrational system in Eq. (109) are prepared by the independent excitation process. The values of the phase mismatch Δk_{AS_j} have been defined by Eqs. (98) and (99). Two ways of coherent probing should be distinguished: nonselective k matching and selective k matching.

a. Nonselective k matching. Coherent superposition of states

A solution of Eq. (109) obviously depends on the x dependence of the exponent $\Delta k_j x' - \phi_j(x', t')$. First, we are interested in the limiting case where the exponent is approximately constant over the effective interaction length Δl defined by Eqs. (103) and (104). Since $|\Delta k_j - \partial\phi_j/\partial x'| \leq |\Delta k_j|$, this situation is established for

$$|\Delta k_j \Delta l| \ll 1. \tag{110}$$

Condition (110) will be called nonselective k matching. Using Eqs. (53) and (103) in Eq. (102) yields an approximate analytic expression for the coherent probe signal at the end of the sample $x' = l$:

$$S^{coh}(t_D) = \frac{c\mu_{AS}}{2\pi} \frac{(\kappa_{AS}\Delta l)^2}{1 + (2\Delta k_{AS}\Delta l)^2} \int_{-\infty}^{\infty} dt' E_{L2}(t' - t_D)^2 \times \Big| \sum_j f_j |Q_j(l, t')| \exp[i\Delta\omega_j t' + i\phi_j(l, t')] \Big|^2. \tag{111}$$

The mismatch Δk_{AS} of the Stokes or anti-Stokes process is indicated by Eqs. (106). Equation (111) represents a convolution of the total excitation $|Q_{tot}|^2$ [see Eq. (62)] with the probe pulse E_{L2}^2. All components j contribute to the scattered signal according to their relative number densities f_j, amplitudes $|Q_j|$, and their individual phases; i.e., Eq. (111) represents a coherent superposition of vibrational states. Due to the frequency differences $\Delta\omega_j$, the superposition of the individual components gives rise to an interference phenomenon. For a discrete substructure of the vibrational system with constant frequency difference $\Delta\omega$ of the vibrational components, the sum on the rhs of Eq. (111) contains oscillating terms $\propto \cos\Delta\omega t_D$; i.e., the probe signal is expected to display a beating phenomenon. For a continuous frequency distribution the superposition of states in Eq. (111) leads to destructive interference; $S^{coh}(t_D)$ decreases rapidly with a nonexponential time dependence.

Numerical calculations for a vibrational mode with discrete substructure and constant frequency distance $\Delta\omega$ of the individual components are presented in Fig. 16. Three molecular species of relative abundance 1:0.5:0.5 and the parameter values $\Delta\omega T_2 = \pi/4$ and $t_p/T_2 = 0.5$ are assumed. The physical situation is the same as for the material excitation depicted in Fig. 7 (Sec. II.D). The scattering signal $S^{coh}(t_D)$ is plotted in Fig. 16 versus delay time. The broken line in the figure represents the calculated signal that would be observed from a single component of the vibrational system. A measurement of the decaying part with slope $2/T_2$ of this signal curve provides directly the dephasing time T_2 of the molecular vibration. It will be discussed below that this information may be supplied by a selective k-matching geometry. Probe scattering with nonselective k matching [Eq. (111)] is shown by the solid curve in Fig. 16. It is interesting to see the minima and maxima of $S^{coh}(t_D)$, which reflect the beating phenomenon of the coherent vibrational excitation; the beats occur at time intervals of $2\pi/\Delta\omega$. Comparison of the vibrational excitation (Fig. 7) and the probe scattering (Fig. 16)

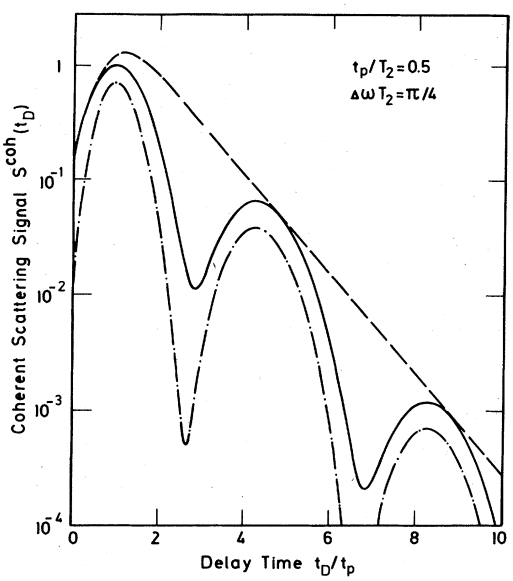

FIG. 16. Coherent (Stokes or anti-Stokes) probe scattering signal $S^{\rm coh}(t_D)$ of a normal mode consisting of three isotope species with relative abundances 1 : 0.5 : 0.5 and with equal frequency spacing $\Delta\omega$. Selective k matching allows us to measure the exponential decay of one isolated molecular component (i.e., provides $2/T_2$) (broken curve). Nonselective k matching gives a beating effect due to coherent superposition of the vibrational components. The solid and dash-dotted curves correspond to probe pulses of duration t_p and $t_p/2$, respectively (t_p is duration of excitation pulse). The corresponding coherent vibrational excitation is depicted in Fig. 7.

shows less pronounced minima of $S^{\rm coh}(t_D)$. This result is explained by the finite duration t_p of the probe pulse in the probing process. To illustrate this point, the scattered signal is calculated for two durations of the probe pulse, t_p and $t_p/2$ (t_p is the pulse duration of the pumping pulse). Stronger oscillations of the signal curve result from shorter probe pulses.

b. Selective k matching. Observation of a molecular subgroup

In the preceding section, the coherent probe scattering of a substructured vibrational system was discussed for a short interaction length Δl [see Eq. (110)]. In this case, the spatial phase relation of the collective material excitation entering the starting differential equation (109) may be neglected. Now we discuss the integration of Eq. (109) under more general conditions. For geometries with sufficiently large Δl, the collective phase relation $\phi_j(x,t)$, the collective phase relation $\phi_j(x,t)$ is important for the t_D dependence of the coherent probe signal. It will be shown that the dephasing of a molecular subensemble may be observed under selective k-matching conditions for systems displaying wave-vector conservation.

For simplicity, our discussion is restricted to long times, $t \gg t_p$, after the excitation process, where the vibrational system relaxes freely. In this time domain, analytic solutions of Eq. (109) are possible, since the phase factors $\phi_j(x,t)$ have reached asymptotic values $\phi_{j,\infty}(x)$. The variation of $\phi_{j,\infty}$ with local coordinate x should be noted; it depends upon the specific nature of the physical system. We expand the asymptotic phases $\phi_{j,\infty}$ around $x=l$, the end of the sample where the maximum excitation occurs:

$$\phi_{j,\infty}(x)=\phi_{j,\infty}(l)+\frac{\partial\phi_j}{\partial x}(x-l)+\cdots . \tag{112}$$

The second term vanishes for systems where the k vectors, prepared during the excitation process, are conserved. Higher-order terms are neglected. Equation (109) for the scattered probe field is integrated with the help of Eqs. (53), (103), and (112). The following expression gives the time-integrated scattering signal $S^{\rm coh}$ [Eq. (102)] at the end of the sample, $x=l$:

$$S^{\rm coh}(t_D)=\frac{c\mu_{AS}}{2\pi}(\kappa_{AS}\Delta l)^2\int_{-\infty}^{\infty}dt' E_{L2}(t'-t_D)^2 \times\left|\sum_j f_j[1+(2\Delta\tilde{k}_{AS,j}\Delta l)^2]^{-1/2} \times|Q_j(l,t')|\exp(i\Delta\omega_j t'+i\delta_{AS,j})\right|^2 . \tag{113}$$

Equation (113) is approximately valid for large time delay $t_D \gtrsim 2t_p$. $\Delta\tilde{k}_{AS,j}$ denotes the k mismatch of the probing process which is modified by the spatial phase dependence $\partial\phi_j/\partial x$ of the molecular subensemble j. One finds

$$\Delta\tilde{k}_{AS,j}=\Delta k_{AS,j}-\frac{\partial\phi_j}{\partial x}=\Delta k_{AS}+\frac{\Delta\omega_j}{v_{AS}}-\frac{\partial\phi_j}{\partial x}, \tag{114a}$$

where

$$\Delta k_S=k_{L2}-k_{\bar{S}}-k_L+k_S;\quad \Delta k_A=k_A-k_{L2}-k_L-k_S . \tag{114b}$$

The phase factors $\delta_{AS,j}$ in the exponent of Eq. (113) have the form

$$\delta_{AS,j}=\phi_{j,\infty}(l)+\arctan(2\Delta\tilde{k}_{AS,j}\Delta l) . \tag{114c}$$

Δl denotes the effective interaction length of the probing process introduced by Eq. (104).

Equation (113) indicates that the magnitude of the probe signal $S^{\rm coh}$ and the relative contribution of the various components j to the scattering signal strongly depend upon the k-matching situation through the products $\Delta\tilde{k}_{AS,j}\Delta l$. This product may differ strongly for different vibrational components j. Components m with $\Delta\tilde{k}_m\Delta l \leq 0.5$ contribute predominantly to $S^{\rm coh}$. For these vibrational components m with good phase matching, we define a frequency spread of $\delta\omega_{\rm ph}$ of the resonance frequencies ω_m. The magnitude of $\delta\omega_{\rm ph}$ determines Δl. The dephasing time T_2 of a vibrational subgroup may be measured if $\delta\omega_{\rm ph} \ll 1/T_2$. According to Eq. (114a), this condition leads to the following expression for the interaction length Δl:

$$\Delta l \gg v_{AS}T_2\left(1-\frac{v_{AS}}{\Delta\omega_j}\frac{\partial\phi_j}{\partial x}\right)^{-1} . \tag{115}$$

Equation (115) represents the necessary condition of selective k matching: A small number of vibrational components m which have approximately equal phase factors and display identical time behavior contribute to the scattering signal. Equations (113) and (115) yield (for $t_D \gtrsim 2t_p$)

$$S^{\mathrm{coh}}_{(t_D)} = \mathrm{const}\int_{-\infty}^{\infty} dt' E_{L\,2}(t'-t_D)^2 \left|Q_m(l,t')\right|^2$$

$$\propto \exp(-2t_D/T_2)\,. \tag{116}$$

It is interesting to see that the probe signal has the form of Eq. (107) derived for a homogeneously broadened line. Equation (116) shows that S^{coh} decays exponentially with time constant $T_2/2$; i.e., selective k matching allows the direct measurement of the dephasing time T_2 of a small group of molecules within a distribution of vibrational frequencies. Molecules with frequencies outside of $\delta\omega_{\mathrm{ph}}$ do not contribute to the scattering signal of Eq. (116) because of their large values of $\Delta\tilde{k}_j$.

Nonselective k matching discussed above in Eq. (110) is repeated here for completeness. For a short interaction length Δl, the k-matching situation may be made similar for many components m of the vibrational system. An upper limit of the vibrational distribution is the spontaneous Raman linewidth $\delta\omega_{\mathrm{spon}}$.

For $\delta\omega_{\mathrm{ph}} \gtrsim \delta\omega_{\mathrm{spon}}$ we observe scattering of all excited vibrational components. With the help of Eq. (114a) we estimate the following sufficient condition for nonselective k matching:

$$\Delta l \lesssim v/\delta\omega_{\mathrm{spon}}\,. \tag{117a}$$

Equation (117a) complements Eq. (110). As pointed out above in the context of Eq. (111), a coherent superposition of vibrational states may be observed under nonselective k-matching conditions.

Besides the limiting cases (a) and (b) intermediate situations are possible. When the temporal decay of S^{coh} varies according to the specific k-vector geometry (e.g., when it varies with sample length l), one has a direct indication of a distribution of vibrational frequencies with $\Delta\tilde{k}_j \neq 0$. For a homogeneous line, on the other hand, the time evolution of $S^{\mathrm{coh}}(t_D)$ does not depend on the k-matching condition of the probe scattering.

The analytic expressions derived above for $S^{\mathrm{coh}}(t_D)$ are valid during the free relaxation regime, i.e, for delay times $t_D \gtrsim 2t_p$. To show the time dependence of the signal curve for shorter times (when the excitation process has not yet terminated) we present some computer results. The numerical calculation starts from a solution of Eq. (109); using Eq. (103) one evaluates the probe scattering signal from Eq. (102). A broad quasicontinuous distribution of resonance frequencies ($\delta\omega_{\mathrm{inh}}T_2 = 45$) and perfect wave-vector conservation $\partial\phi_j/\partial x = 0$ are assumed in Fig. 17 with $t_p/T_2 = 0.5$. The parameters are the same as in the example of Fig. 8 in Sec. II.D for the coherent vibrational excitation. The broken curve in Fig. 17 represents the time dependence of the scattering signal S^{coh} evaluated for selective k matching [Eq. (115)] of the vibrational component situated at the center of the frequency distribution with $\Delta\omega_j = 0$. The rise and decay of the signal curve strongly resembles the results of Fig. 14 for a homogeneously broadened line. The exponential slope for larger values of t_D should be noted, which allows the determination of T_2 of the selected vibrational component. The probe scattering signal under nonselective k-matching conditions [Eqs. (111), (117a)] is depicted by the solid curve in Fig. 17. In this case, S^{coh} is connected with the total vibrational excitation $|Q_{\mathrm{tot}}|^2$ and should be compared with the solid curve in Fig. 8. We point to the nonexponential decay of the solid curve. This time dependence reflects the destructive interference between the various vibrational components having received well-defined phases during the stimulated process.

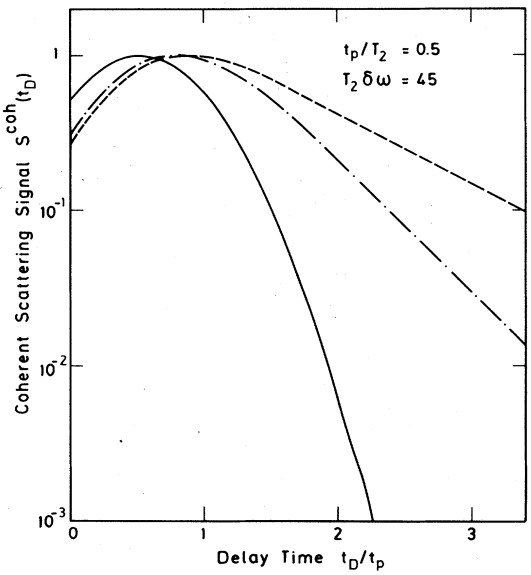

FIG. 17. Calculated coherent Stokes signal $S^{\mathrm{coh}}(t_D)$ of an inhomogeneously broadened vibrational mode as a function of delay time t_D/t_p. Selective k matching gives the time dependence of a small vibrational subgroup at the center of the frequency distribution (broken curve). Nonselective k matching shows destructive interference of various vibrational components (solid curve). For conditions of medium k selectivity see text (dash-dotted curve). The corresponding coherent vibrational excitation is presented in Fig. 8.

Finally, we discuss a moderate k selectivity where the frequency spread $\delta\omega_{\mathrm{ph}}$ of good k matching ($\Delta k_{AS,j}\Delta l \lesssim 0.5$) is equal to the homogeneous linewidth $1/T_2$. This condition is equivalent to the relation $\Delta\tilde{k}_{AS,j}\Delta l = \Delta\omega_j T_2/2$ [$\Delta k_{AS} = 0$, see Eq. (114)]. Numerical results of S^{coh} are depicted by the dash–dot curve in Fig. 17. It is readily seen that the signal curve for this k-matching condition decays more rapidly than the broken line representing the selective k-matching situation. The k resolution is not sufficient to observe the true dephasing time of a small selected subgroup of molecules. Our calculations indicate that larger values of Δl by a factor of approximately 5 (and a corresponding reduction of the observed frequency spread) would be required to give a value of $T_2/2$ approximately 20% smaller than the true number.

We briefly summarize at this point: Time-resolved measurements of the coherent probe signal depend upon the wave-vector geometry and the spatial phase correlation ($\partial\phi_j/\partial x$) prepared by the excitation process. Under favorable conditions information may be obtained (i) on the question of whether a vibrational transition is inhomogeneously broadened, and (ii) on the dephasing time T_2 of a small vibrational subensemble of the inhomogeneously broadened transition.

4. Spatial phase correlation of liquid systems

In the preceding section, we have derived the condition (115) for coherent probing with selective k-matching geometry. Information on the relaxation time of a vibrational subgroup is obtained when Eq. (115) holds. This means that $|\partial\phi_j/\partial x| \ll |\Delta\omega_j/v_{AS}|$ is necessary. Obviously, the spatial phase relation $\partial\phi_j/\partial x$ prepared in the excitation process requires special consideration.

An ensemble of spatially independent molecules is discussed first. The excitation of such a system by transient stimulated Raman scattering was treated in Sec. II. The phase relation of the vibrational excitation was described by the functions $\phi_j(x,t)$ governed by the differential equation (54). For small frequency differences $\Delta\omega_j$ a solution was presented [Eqs. (60) and (61)]. We are interested here in the spatial phase relation after excitation, $\phi_{j,\infty}(x)$ or correspondingly $\partial\phi_j/\partial x$. Equations (61) and (112) give

$$\frac{\partial\phi_j}{\partial x}=\frac{\Delta\omega_j}{v}. \tag{117b}$$

This result is due to the propagation of the external fields which drive the molecular vibration by the product $E_L E_S = E_L(t-x/v)E_S(t-x/v)$. Switching off of the external force occurs at different sites at different times. The frequency shift $\partial\phi_j/\partial t$ discussed in context with Fig. 10 is accompanied by the spatial phase change of Eq. (117b). Consequently, the values of $\Delta\tilde{k}_{AS,j}$ [Eq. (114)] entering the coherent signal [Eq. (113)] are identical for all subgroups j, and selective k matching is not possible for an ensemble of spatially uncoupled molecules.

It is felt that an ensemble of spatially independent molecules does not properly describe a real liquid system as far as spatial phase correlation is concerned. The large number density of molecules of 10^{21} cm^{-3} suggests the introduction of some intermolecular coupling. In fact, the interaction between molecules has been shown in numerous papers to affect the vibrational motion of high-pressure gases and condensed media (Buckingham, 1958 and 1960a and b; Monson *et al.*, 1968; see also reviews by Knaap and Lallemand, 1975 and by Bauer *et al.*, 1976). The frequency position, linewidth, and band shape of a vibrational mode is found to depend on the molecular environment. We investigate here briefly the influence of intermolecular forces on the spatial phase correlation of a coherently excited vibrational mode. The Hamiltonian of Eq. (4) for an individual molecule j of the liquid ensemble is extended by an interaction potential which is assumed to be quadratic in the vibrational coordinates:

$$H_j = H_j^0 - \frac{1}{2}q_j\sum_{h,i}\left(\frac{\partial\alpha}{\partial q}\right)_{h,i}E_hE_i + m\sum_{(\Delta V)}\Gamma_{kj}(q_k+q_j)^2. \tag{118}$$

k denotes the index of summation over the neighborhood of the considered molecule j, which extends over an interaction volume ΔV. The coupling parameters Γ_{kj} are due to dipole–dipole interaction or repulsive intermolecular forces and depend on the fluctuating distances between the molecules k and j (see, for example, Buckingham, 1958). The magnitude of the Γ_{kj} may be estimated from the normal mode frequency shift of the liquid molecule as compared to the gas.

The interaction potential term in the Hamiltonian [Eq. (118)] leads to somewhat modified equations of motion for the molecular ensemble, Eqs. (53) and (54) for $|Q_j|$ and ϕ_j, respectively. While the time evolution of $|Q_j|$ is not affected significantly, the phases ϕ_j are influenced by the intermolecular interaction, particularly during the decay of the external force $\sim E_L E_S$. The spatial phase shift noted above for the uncoupled ensemble does not occur. The nonpropagating intermolecular interaction determines the return of the driven vibrations to the resonance frequencies. The wave vector $k_j = k_L - k_S$ generated during the excitation process is conserved. One arrives at

$$\partial\phi_j/\partial x \simeq 0. \tag{119}$$

The effect of the intermolecular coupling obviously leads to a collective, nonlocalized character of the vibrational modes related to optical phonons in solids. In Sec. V of this paper we present experimental results of selective k matching in several liquids. These findings give strong support to the conservation of the k vectors [Eq. (119)].

In conclusion, we note that our knowledge of the spatial phase correlation is in a preliminary state. More work is necessary to understand the microscopic nature and the physical consequence of intermolecular coupling.

5. Wave-vector geometries

It is apparent from the previous sections that the k vectors of the excitation and of the probe process are of major importance for the generated scattering signal. A collinear geometry was considered where all k vectors are parallel. We now discuss in more detail the angular dependence of the coherent Raman probe scattering. The various angles of the excitation and probe fields are assumed to be small, approximately a few degrees. This condition is fulfilled in the following experimental investigations. The expressions derived above for the probe signal $S^{\mathrm{coh}}(t_D)$ are still valid for these small angles. Probe scattering on the anti-Stokes and Stokes side will be treated separately.

Several aspects of the anti-Stokes probing process are illustrated in Fig. 18. The collinear geometry is depicted in Fig. 18(a). Parallel laser and Stokes waves produce via stimulated Raman scattering the wave vector $\mathbf{k}_j = \mathbf{k}_L - \mathbf{k}_S$ of the material excitation which also points in the forward direction. The probe pulse with parallel wave vector $\mathbf{k}_{L2}$ coherently interacts with the vibrational excitation, generating scattered light in the forward direction with wave vectors $\mathbf{k}_{Aj}$. The wave vector k_{Aj} refers to a specific frequency (within the distribution f_j) which we want to study after the excitation has terminated. On account of the discussion given in connection with Eq. (119) we write $\Delta\tilde{k}_{AS,j} = \Delta k_{AS,j}$ [see Eq. (114a)]. The magnitude of Δk_{Aj} determines whether we are able to observe this vibrational component j efficiently. The wave-vector mismatch Δk_{Aj} [Eq. (99)] depends upon the angles and frequencies of the excitation and probing pulses. Phase matching of

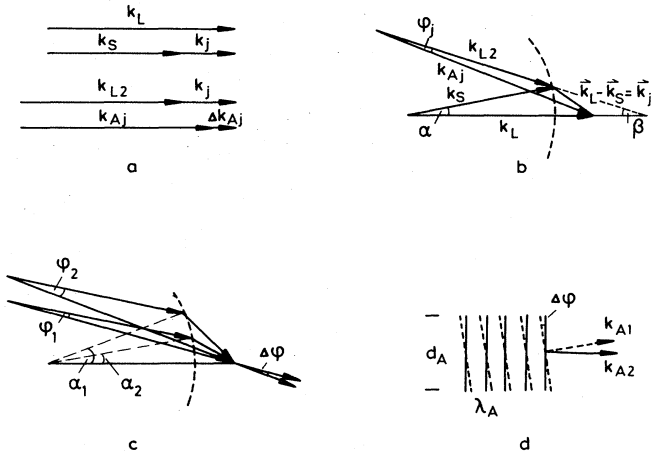

FIG. 18. Wave-vector geometries for the anti-Stokes probing process. (a) Collinear scattering geometry with $k_j = k_L - k_S$, the wave vector of the material excitation. (b) Noncollinear k matching for Stokes emission angle α; the angle between excitation (k_L) and interrogating pulse (k_{L2}) is denoted by β. (c) Noncollinear k matching for two vibrational components. The anti-Stokes emission occurs under different angles φ_1 and φ_2 with respect to the incident probe beam. (d) Wave fronts of two interfering anti-Stokes beams.

the noncollinear wave-vector geometry is illustrated by Fig. 18(b). It is known that stimulated Stokes light is generated within a cone of small angles $\alpha \lesssim \alpha_{max}$ with respect to the forward direction, where α_{max} represents the Stokes divergence. One estimates $\alpha_{max} \simeq d/2l$, with d being the beam diameter of the laser pulse. Corresponding to the cone of wave vectors $k_S(\alpha)$, the material excitation displays a distribution of wave vectors $\mathbf{k}_j(\alpha) = \mathbf{k}_L - \mathbf{k}_S(\alpha)$ of different directions. The absolute value $|\mathbf{k}_j(\alpha)|$ is found from a simple geometrical consideration:

$$k_j(\alpha) = (k_L^2 + k_S^2 - 2k_L k_S \cos\alpha)^{1/2}. \tag{120}$$

Note that the magnitude of $|\mathbf{k}_j(\alpha)|$ depends on the off-axis angle, while the values of $|\mathbf{k}_L|$ and $|\mathbf{k}_S(\alpha)|$ are independent of α and are determined by their frequencies and indices of refraction, $k_{L,S} = \omega_{L,S}\mu_{L,S}/c$. The interaction of the incident probe pulse ($\mathbf{k}_{L2}$) with the cone of material wave vectors $\mathbf{k}_j(\alpha)$ depends on the mismatch $\Delta\mathbf{k}_{Aj}(\alpha)$. Using geometrical arguments the mismatch $k_{Aj}(\alpha) = k_{Aj} - |\mathbf{k}_{L2} + \mathbf{k}_L - \mathbf{k}_S|$ is calculated to be

$$\Delta k_{Aj}(\alpha) = k_{Aj} - [k_{L2}^2 + k_L^2 + k_S^2 + 2k_{L2}k_L\cos\beta - 2k_{L2}k_S\cos(\alpha+\beta) - 2k_L k_S\cos\alpha]^{1/2}. \tag{121}$$

The angle between the exciting and interrogating beam is denoted by β in Fig. 18. For a proper choice of the angle β perfect matching $\Delta k_{Aj}(\alpha_j) \simeq 0$ may be achieved for a certain part of the k-vector distribution. These wave vectors $k_j(\alpha_j)$ contribute dominantly to the probe scattering.

The highly collimated anti-Stokes emission occurs under an angle φ_j with respect to the probe pulse (see Fig. 18). One finds

$$\tan\varphi_j = \frac{k_S\sin(\alpha+\beta) - k_L\sin\beta}{k_{2L} + k_L\cos\alpha - k_S\cos(\alpha+\beta)}. \tag{122}$$

It is recalled that the angles α, β and φ_j are small and amount to a few degrees.

As an example we consider now the phase-matching geometry for two different vibrational components labeled 1 and 2. Figure 18(c) shows schematically that the probe pulse ($\mathbf{k}_{L2}$) has to interact with k vectors of different directions of the two vibrational excitations in order to make $\Delta k_{Aj} \simeq 0$. As a result, the anti-Stokes wave vectors k_{A1} and k_{A2} of the two vibrational components have slightly different angles φ_1 and φ_2, respectively. The anti-Stokes scattering signal contains different information as a function of emission angle φ with respect to the incident probe pulse. Using highly collimated beams of the excitation and probing pulses and selecting the angle of acceptance by the help of an aperture, the angular dispersion of the probe scattering allows us to isolate a single vibrational component.

For a sufficiently large angle of acceptance the light beams scattered off different vibrational components are simultaneously detected. Beating of the vibrational states corresponds to the interference of the scattered light waves. Figure 18(d) illustrates schematically the wave fronts of the two light beams. It is readily seen that the resulting interference signal depends on the beam diameter d and the angle $\Delta\varphi = \varphi_1 - \varphi_2$ between the scattered components. For a beam diameter

$$d_{AS} < \lambda_{AS}/\Delta\varphi \tag{123}$$

coherent superposition of the vibrational components can be observed. Using green probe light ($\lambda = 0.5\ \mu$m) and $\Delta\varphi = 10^{-3}$ we estimate $d_{AS} < 500\ \mu$m. Experimentally we are able to work with beam diameters as small as 30 μm.

Quantitative values of the k mismatch are presented in Figs. 19 and 20. Calculations are made for specific experimental situations discussed in Sec. V. Figures 19(a) and 19(b) illustrate the k matching of an anti-Stokes scattering process. Pump and probe beams of equal frequency $\tilde{\nu}_L = \tilde{\nu}_{2L} = 18\,910$ cm^{-1} are considered. They interact with the symmetric tetrahedron vibration of $SnBr_4$ at 30°C, where the two isotopes ^{79}Br and ^{81}Br produce five lines around 221 cm^{-1} in the vibrational spectrum.

Figure 19(a) refers to parallel pump and probe beams, $\beta = 0$. Using Eq. (121), the wave-vector mismatch Δk_{Aj} is calculated with the help of known refractive indices (Gmelin, 1972) and plotted in Fig. 19(a) as a function of the Stokes emission angle α for the five isotope components $j = 1$–5. The frequency difference between neighboring isotope species was taken to be $\Delta\omega/2\pi c = 0.67$ cm^{-1}. The Δk_{Aj} curves display minima in the forward direction $\alpha = 0$ and rise quickly with increasing Stokes angle. Four species display perfect phase matching $\Delta k_{Aj} = 0$ for Stokes emission angles $\alpha_j \simeq 1.8$, 7.3, 10.0, and 12.6 mrad. It is interesting to note that color dispersion incidentally leads for the component $j = 4$ to almost perfect phase matching, $\Delta k_4 \simeq 0.3$ cm^{-1}, in the forward direction. Substantial mismatch, $\Delta k_3 \simeq -7.8$ cm^{-1}, is found at $\alpha = 0$ for the most abundant isotope component $j = 3$. These facts allow the design of a

highly selective system. In a collinear geometry where the Stokes divergence is made very small (e.g., $\lesssim 3$ mrad) one observes efficient scattered signals of the component $j=4$ while the other components $j \neq 4$ do not contribute.

Figure 19(b) shows the k-matching situation for an angle $\beta = 2.6°$ between pump and probe beam. The wave-vector mismatch Δk_{Aj} of the five $SnBr_4$ isotope species is plotted versus Stokes emission angle α. It is readily seen that the Δk_{Aj} curves rise rapidly as a function of Stokes divergence. Phase matching, $\Delta k_{Aj}=0$, occurs at different values of the Stokes angle α_j for the individual molecular species j. For example, values of $\alpha_j = 2.8$, 1.9, and 1.0 mrad are found, respectively, for $j=1$, 2, and 3 in Fig. 19(b). The anti-Stokes probe emission of components 1–3 occurs within a narrow cone with only slightly different angles φ_j. From Eq. (122) we calculate values of $\varphi_j = 2.1$, 1.3, and 0.5 mrad for $j=1-3$, respectively. These numbers indicate that coherent superposition for the vibrational components of $SnBr_4$ may be experimentally observed for the considered off-axis geometry.

We now discuss coherent Stokes scattering. k matching of the Stokes emission is easier to achieve as may be seen from Eq. (114b), where k_S and $k_{\bar{S}}$ have opposite signs. Figure 20(a) illustrates the special case of $\mathbf{k}_{L2} = \mathbf{k}_L$ (i.e., equal frequencies of the excitation and probing pulse) and a collinear geometry $\alpha = \beta = 0$. It is interesting to see that perfect phase matching, $\Delta k_{Sj}=0$, is achieved at the band center $\Delta\omega_j = 0$ [see Eqs. (114)]. This point is of advantage in experimental applications. There is a serious problem with this geometry. We have to observe the weak probe signal at the Stokes frequency in the presence of the intense Stokes emission of the stimulated excitation process. As discussed in Sec. IV, this difficulty may be overcome experimentally by the proper choice of the polarization directions.

The Stokes process with noncollinear geometry is depicted in Fig. 20(b). The situation is analogous to the anti-Stokes process of Fig. 18(b). The incident probe pulse ($\mathbf{k}_{L2}$) interacts with the cone of material wave

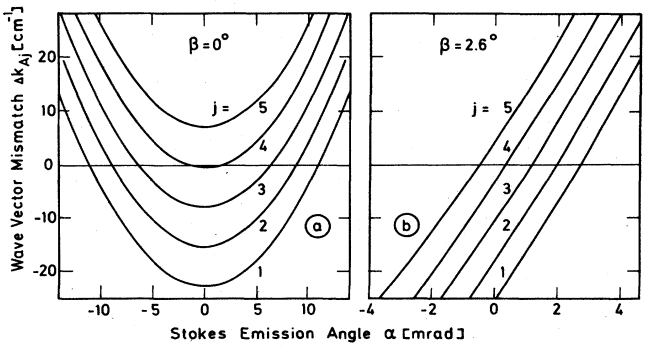

FIG. 19. Wave-vector mismatch of anti-Stokes scattering Δk_{Aj} vs Stokes emission angle α. The five isotope components of the tetrahedron mode of $SnBr_4$ around 221 cm^{-1} are considered with pump and probe pulses of frequency 18 910 cm^{-1}. (a) Collinear excitation and probing beam, $\beta = 0$. (b) Probe angle $\beta = 2.6°$.

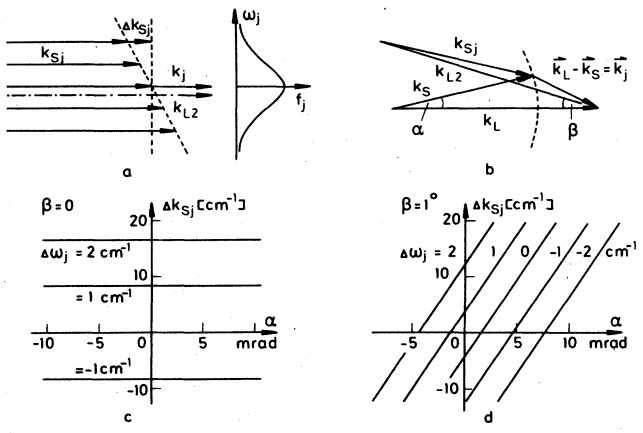

FIG. 20. Wave-vector geometries for the Stokes probing process. (a) Collinear excitation and probing. Vector k_j denotes the wave vector of the material excitation. Perfect phase matching, $\Delta k_j = 0$, exists for Stokes waves close to the center of the vibrational distribution f_j. (b) Noncollinear Stokes scattering, k_{Sj}. (c) and (d) Wave-vector mismatch of Stokes scattering Δk_{Sj} vs angle α. Calculations are made for the C–H stretching mode of methanol at 2835 cm^{-1}, and for pump and probe frequencies of 18 910 cm^{-1}. (c) Collinear excitation and probing beam, $\beta = 0$. (d) Probe angle $\beta = 1°$.

vectors $k_j(\alpha)$ defined by Eq. (120). Replacing the vectors k_{Aj} and k_{L2} of the anti-Stokes scattering by the vectors k_{L2} and k_{Sj}, respectively, for the Stokes probing, we immediately obtain from Eq. (121) the following expression for the mismatch $\Delta k_{Sj}(\alpha) = k_{L2} - |\mathbf{k}_{Sj} + \mathbf{k}_L - \mathbf{k}_S|$:

$$\Delta k_{Sj}(\alpha) = [k_{L2}^2 + k_L^2 + k_S^2 - 2k_{L2}k_L\cos\beta + 2k_{L2}k_S\cos(\alpha+\beta) - 2k_Lk_S\cos\alpha]^{1/2} - k_{Sj}. \quad (124)$$

The Stokes emission occurs under a small angle φ_j with respect to the incident probe pulse. φ_j may be calculated from Eq. (122), changing the sign of k_{L2}.

Figures 20(c) and 20(d) give numerical results [Eq. (124)] for the k mismatch, Δk_{Sj} for a specific example. The CH_3 stretching mode of methanol at 2835 cm^{-1} is considered. The situation $\beta = 0$ is illustrated in Fig. 20(c). It is interesting to see that the k mismatch for various components j is independent of α. This result differs substantially from the anti-Stokes process depicted in Fig. 19(a), where the k mismatch varies strongly with α. In Fig. 20(a) the mismatch Δk_{Sj} increases with frequency difference $\Delta\omega_j$ according to Eq. (114): $\Delta k_{Sj} \simeq \Delta\omega_j\mu/c = 2\pi\Delta\tilde{\nu}_j\mu$. Frequency components which are only $\Delta\tilde{\nu}_j = 1$ cm^{-1} away from the center of the vibrational distribution have a mismatch of $\Delta k_{Sj} \simeq 9$ cm^{-1}. As a result, the corresponding scattered Stokes signal S^{coh} is very small [see Eq. (113)] when an effective interaction length of $\Delta l \gtrsim 0.4$ cm is used. On the other hand, the vibrational frequencies very close to the center of the distribution are strongly favored because $\Delta k_{Sj} \simeq 0$ makes the scattered signal S^{coh} large. In Fig. 20(d) we present the k mismatch for $\beta = 1°$ where the values of Δk_{Sj} significantly depend on α. To select a group of molecules with small frequency spread $\delta\omega_{ph}$ one has to use a small acceptance angle φ of

the scattered beam. Comparing Figs. 20(c) and 20(d) we recognize a better k selectivity for the case of $\beta = 0$.

Our discussion of the coherent Raman probe scattering has shown that the k-matching geometry of the interacting beams as well as the observation geometry are essential for the measured scattering signal S^{coh}. For special arrangements it is possible to select a certain frequency component out of a distribution of closely spaced frequencies and study the dynamic properties of this single constituent. Even more interestingly, selective k matching allows us to investigate a small group of molecules within a distribution of vibrational frequencies. In this way we are in a position to obtain dynamic information on this molecular subgroup independent of the broad frequency distribution. For example, the dephasing time T_2 was measured in methanol for an inhomogeneously broadened vibrational mode (see Sec. V).

The following points are important for experimental investigations. (i) For sufficiently large values of t_D the signal curve approaches an exponential slope $2/T_2$. This part of the $S^{\text{coh}}(t_D)$ curve is most important for experimental investigations. Measurements should be carried out over several orders of 10 in order to determine the correct value of the dephasing time T_2. (ii) It has to be ascertained that additional nonlinear processes do not generate significant radiation in the frequency range of interest. In particular, the probe scattering mechanism has to be distinguished from stimulated four-photon parametric interaction of the excitation and probing light pulses via $\chi^{(3)}_{\text{NR}}$, the nonresonant part of the third-order susceptibility (see Levenson, 1974). The latter process can produce radiation at the anti-Stokes and Stokes frequency position of the probe scattering for times when the excitation and probing light pulses overlap, i.e., for small values of t_D. The contribution of $\chi^{(3)}_{\text{NR}}$ is not connected to the coherent excitation of the vibrational mode of interest. For concentrated samples (e.g., pure liquids) and for vibrational modes with large Raman cross section this mechanism is negligible close to the resonance frequencies. On the other hand, in highly diluted specimens, the effect of $\chi^{(3)}_{\text{NR}}$ was recently observed by Zinth *et al.* (1978).

B. Incoherent Raman probe scattering

In the preceding section we were concerned with coherent probe scattering. Our main aim was the determination of the vibrational dephasing time T_2 of a specific molecular mode and a definite group of molecules. In simple cases, i.e., for a homogeneous line, this time constant is closely connected to the linewidth observed in spontaneous Raman spectroscopy.

We discuss now methods which allow time-resolved studies of the population of vibrational quantum states. It is possible to measure directly the population lifetime T_1, to observe the transfer of vibrational energy, and to follow the decay routes of excited states. Information on these energy relaxation processes cannot be obtained by conventional spectroscopic techniques. The first measurement of the population lifetime T_1 of a vibrational mode in a liquid (electronic ground state) was reported by Laubereau, von der Linde, and Kaiser in 1972. A related method was used earlier by DeMartini and Ducuing (1966) for T_1 measurements in gases on the time scale of 10^{-4} sec.

The measuring technique consists of two steps. First, a powerful short light pulse traverses the sample and excites the vibrational mode of interest. As discussed in Sec. II, stimulated Raman scattering or resonant infrared absorption can produce an excess population of the first excited vibrational state. Subsequently, a second weak pulse of different frequency probes the instantaneous vibrational excitation via spontaneous anti-Stokes Raman scattering. The scattered intensity observed under a large scattering angle (e.g., 90°) is proportional to the instantaneous population of the upper vibrational state (and to the incident laser intensity).[2] Experimentally, a time-integrated signal is observed with a photomultiplier. The time-integrated incoherent scattering signal produced by the excess population n of a vibrational state is denoted by S^{inc}. We find

$$S_i^{\text{inc}}(t_D) = \frac{c\mu_A}{8\pi} N \left(\frac{d\sigma}{d\Omega}\right)_i \Delta\Omega \int_{x_0-\Delta x/2}^{x_0+\Delta x/2} dx' \times \int_{-\infty}^{\infty} dt' n_i(x', t') \, |E_{L2}(t' - t_D)|^2 . \tag{125}$$

x' denotes the propagation direction of the excitation pulse which generates the excess population n_i. Δx represents the observed local interval in the sample ($0 < x_0 < l$). N is the number density of the molecules in the liquid. $(d\sigma/d\Omega)_i$ corresponds to the spontaneous Raman cross section of the observed (excited) vibrational mode i and $\Delta\Omega$ to the solid angle of acceptance of the detection system. E_{L2} is the field amplitude of the probing pulse. Equation (125) represents a convolution of the probe pulse of delay time t_D with the vibrational population n_i. Experimentally, a primary excess population is produced in one vibrational mode by the exciting pulse. A secondary excess population resulting from energy transfer processes to some other vibrational state may be studied by the same incoherent probing techniques. The frequency of the probe signal S_i^{inc} is centered at $\omega_{L2} + \omega_i$, where ω_i denotes the frequency of the vibrational mode of interest. In general, S_i^{inc} is measured in a frequency interval somewhat larger than the spontaneous linewidth connected with the mode i.

Time- and frequency-resolved investigations are possible with probing pulses of several picoseconds duration. Two factors contribute to the spectral intensity distribution of the probe signal: the spontaneous Raman line shape of the vibrational mode with frequency ω_i and the line shape of the incident probe pulse at frequency ω_{L2}. Measurements of $S_i^{\text{inc}}(t_D = \text{const})$ as a function of frequency provide direct information on the instantaneous distribution of population among different vibrational modes (see Sec. VI).

Time-resolved data on the instantaneous population

[2] At this large scattering angle the phase mismatch for coherent scattering is very large. One estimates that the coherent scattering signal is down by ten orders of magnitude in this direction and can be neglected.

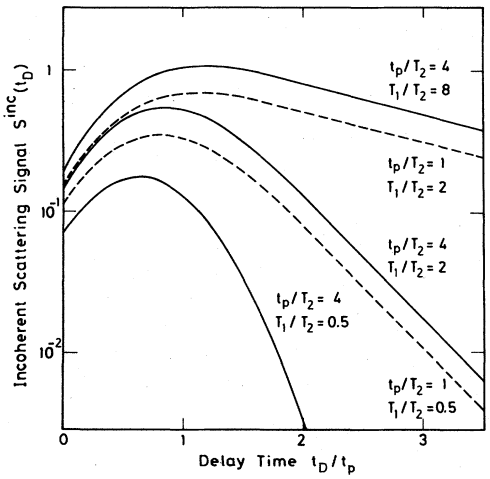

FIG. 21. Incoherent (anti-Stokes) probe signal $S^{inc}(t_D)$ monitoring the excess population n of the first excited vibrational state as a function of delay time t_D between probe and pump pulse. The signal curves decay exponentially with the population lifetime T_1. Comparison should be made with Fig. 5, where the excess population n is calculated for the same parameters.

n_i are presented in Fig. 21. Examples of the scattering signal $S^{inc}(t_D)$ are plotted versus delay time t_D. The interaction of a Gaussian probe pulse with the excess population n was calculated using Eq. (125). The time duration t_p of the probe and exciting pulse is assumed to be equal. The parameters correspond to the vibrational excitation illustrated in Fig. 5. The ratios of the relevant time constants, t_p/T_2 and T_1/T_2, determine the time evolution of $S^{inc}(t_D)$. The signal curves in the figure show the expected exponential tails. At these later times the probe pulse interacts with the freely relaxing molecules. The slope of the exponentially decaying part of $S^{inc}(t_D)$ is a direct measure of the population lifetime (energy relaxation time) T_1.

The low intensity of the spontaneous probe signal should be emphasized. It results from the limited number of photons in the ultrashort probe pulse, from the exceedingly small value of the Raman cross section $(d\sigma/d\Omega)_i$, and from the small excess population $n_i \ll 1$ which is produced experimentally. For a typical experimental situation we have a maximum occupation number $n \simeq 10^{-3}$ within an excitation length of $\Delta x \simeq 10^{-1}$ cm (number density of the liquid $N \simeq 5 \times 10^{21}$ molecules/cm^3). For a Raman scattering cross section of 2×10^{-30} cm^2/sr and a solid angle of acceptance of 10^{-1} sr, we estimate from Eq. (125) the scattering efficiency of the probing process to be $S^{inc}/I_L t_p \simeq 10^{-13}$. This number gives the fraction of photons of the incident probe pulse which are scattered in the solid angle of the detection system for the optimum setting of the delay time t_D. The frequency of the probe pulse ω_{L2} has to be carefully chosen ($\omega_{L2} > \omega_L$) in order to avoid background signals generated by the powerful pump pulse at the detected frequency position $\omega_{L2} + \omega_i$ of the incoherent probe signal.

C. Fluorescence probing

Here we discuss a probing technique for an excited vibrational state which is more sensitive by several orders of magnitude than the incoherent Raman probing of the previous section. The method is particularly well suited for highly diluted systems.

The molecular transitions involved in the excitation and probing process are illustrated schematically in Fig. 22. Vibrational levels (2) of energy $\hbar\omega_1$ above the ground state (1) are first populated by an exciting pulse (see Sec. II. E). The excess population of the excited states is subsequently interrogated by a second pulse of frequency ω_2. A fraction of the excited molecules is promoted to a level (3) close to the ground state (4) of the first excited singlet state S_1. The fluorescence originating from the S_1 state is a measure of the instantaneous degree of the vibrational excitation in the ground state. The time-integrated fluorescence signal is observed as a function of delay time t_D between the excitation pulse and the probing pulse. It should be noted that the frequency ω_2 of the probe pulse is adjusted in such a way that vibrational modes of energy $E < \hbar\omega_1$ do not participate in the probing process; dynamic information on vibrational levels in a small frequency band around $\hbar\omega_1$ is obtained. These levels contribute to the probe signal according to their occupation number and their Franck–Condon factors (i.e., absorption cross sections). Thermal occupation of the levels $E > \hbar\omega_1$ provides a background fluorescence signal. When the pulse interrogates the medium without preceding excitation, the background fluorescence is readily determined. The method outlined here was first used by Laubereau, Seilmeier, and Kaiser (1975) for dynamic vibrational investigations of dye molecules in liquid solution and more recently in the vapor phase (Maier *et al.*, 1977). Our technique is related to the probing method of Allamandola and Nibler (1974), who studied C_2^- in solid low-temperature matrices on a microsecond time scale.

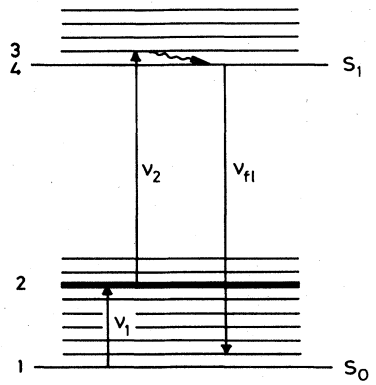

FIG. 22. Two pulse fluorescence technique. Schematic of the relevant molecular energy states. Vibrational level (2) is excited by an infrared pulse of frequency ν_1. The time dependence of the population of level (2) is monitored with a second delayed pulse of frequency ν_2. The (integrated) fluorescence at ν_{fl} is a measure of the population lifetime T_1 of level (2).

The dynamic processes involved in the probing technique are analyzed theoretically using the four-level model indicated in Fig. 22. Several time constants affect the probing process besides the relaxation times T_1 and T_2 of the excited vibrational level (2). The lifetime of the excited state T_1 is the time constant of interest. The transition (2) → (3) of the probing process has a dephasing time $T_{2,\mathrm{pr}}$ and a population decay time τ_{vib} of the upper level (3). The excess population of the lowest S_1 level decays with the fluorescence lifetime τ_{fl}. In general, molecular rotation affects the probing processes. We restrict our discussion to a simplified model:

(i) We consider (large) molecules where the rotational relaxation time is considerably larger than the time constant T_1: i.e., molecular rotation is neglected.

(ii) We assume the dephasing time $T_{2,\mathrm{pr}}$ of the excited-state absorption to be much smaller than the pulse duration of the probe pulse: $T_{2,\mathrm{pr}} \ll t_p$. The time constant $T_{2,\mathrm{pr}}$ is connected to the macroscopic polarization of the probe absorption in analogy to the dephasing time T_2 of the infrared absorption discussed in Sec. II.E. Dephasing processes of both levels (2) and (3) contribute to the decay rate $1/T_{2,\mathrm{pr}}$ of the induced polarization. On account of the rapid relaxation processes in the excited electronic state S_1, one estimates $T_{2,\mathrm{pr}} < 10^{-12}$ sec for many molecules. Assumption (ii) allows one to describe the probe process of the population of level (2) by rate equations.

(iii) The light intensity of the probe pulse is kept small in order not to affect the population of level (2) notably; i.e., the probing process represents a small perturbation of the vibrational system.

For the assumptions (i)–(iii) the occupation probabilities n_i of level i are described by the following differential equations:

$$\frac{\partial n_2}{\partial t} = f(x,t) - (n_2 - \bar{n}_2)/T_1 - \sigma_2 I_2 (n_2 + \bar{n}_2 - n_3)\,, \tag{126a}$$

$$\frac{\partial n_3}{\partial t} = \sigma_2 I_2 (n_2 + \bar{n}_2 - n_3) - n_3/\tau_{\mathrm{vib}}\,, \tag{126b}$$

$$\frac{\partial n_4}{\partial t} = n_3/\tau_{\mathrm{vib}} - n_4/\tau_{\mathrm{fl}}\,. \tag{126c}$$

Equations (126) are supplemented by the equation for the photon flux density I_2 of the probing pulse:

$$\left(\frac{\partial}{\partial t} + \frac{1}{v}\,\frac{\partial}{\partial x}\right) I_2 = -\sigma_2 N I_2 (n_2 + \bar{n}_2 - n_3)\,. \tag{127}$$

The excess population n_2 of the excited vibrational state of interest is generated by the pumping term $f(x,t)$ in Eq. (126a). $\bar{n}_2$ denotes the thermal equilibrium value. The population of level (2) depends on the excitation rate, the population lifetime T_1, and the probing light pulse of intensity I_2. The probing pulse excites level (3) where rapid redistribution occurs with a time constant τ_{vib} to the fluorescent states represented by level (4). Experimentally, we observe the time-integrated fluorescence signal:

$$F(t_D) = (\mathrm{const})\, N \frac{\eta}{\tau_{\mathrm{fl}}} \int_{-\infty}^{\infty} dt\, n_4(t - t_D) - F_b\,. \tag{128}$$

The constant factor in Eq. (128) combines various experimental parameters, e.g., excitation volume, solid angle of detection, observed wavelength, bandwidth of the fluorescence signal, and spectrometer transmission. The quantum efficiency of the fluorescence is denoted by η. $F(t_D)$ represents the fluorescence signal produced by the excess population of the vibrational level (2). The background signal F_b in Eq. (128) denotes the fluorescence emission observed without an excitation process, $f(x,t) \equiv 0$ [Eq. (126a)]. Clearly, F_b is independent of t_D. For the assumptions (i)–(iii) discussed above, Eq. (126) may be solved independently of Eq. (127) (propagation of the probe pulse). We have made detailed calculations of the four-level system depicted in Fig. 22 and of more extended systems involving energy redistribution between vibrational levels (2). Some of our theoretical results are briefly summarized as follows: For weak probing pulses, i.e., for

$$I_2 \ll (\sigma_2 \tau_{\mathrm{vib}})^{-1}\,, \tag{129}$$

the population of state (3) remains small ($n_3 \ll n_2$) during the probing process, and the time behavior of the fluorescence signal $F(t_D)$ does not depend on the relaxation times τ_{vib} and τ_{fl} of the levels (3) and (4), respectively. Accurate values of these time constants are not available for many molecular systems. Condition (129) ensures that the observed fluorescence signal decays exponentially with time constant T_1 after the excitation process has terminated:

$$F(t_D) \propto \exp(-t_D/T_1)\,. \tag{130}$$

Equation (130) indicates that the decaying part of the signal curve gives direct information on the vibrational dynamics of level (2). The measured time constant T_1 results from energy decay processes to lower-lying levels (which cannot interact with the probing pulse) and/or from energy transfer to adjacent vibrational levels of approximately equal frequency position. In the model described by Eqs. (126) it is assumed that levels populated by secondary redistribution processes do not notably contribute to the probe signal. In the general case, the decay of the fluorescent signal gives information on the time evolution of an ensemble of vibrational states with a nonexponential time dependence. A detailed knowledge of the Franck-Condon factors for the electronic transitions of the probing process is necessary for a full understanding of the vibrational information supplied by the fluorescence probing technique. Comparing this experimental method with the incoherent Raman probing of Sec. III.B we note that the selection rules of the latter process are more favorable for the investigation of the population of a single vibrational level, independent of other energy states of approximately the same frequency. In other words, the high sensitivity of the fluorescence technique is gained at the expense of a more difficult interpretation of the experimental data. Additional investigations are required to link the observed time constant to specific vibrational levels and to distinguish between energy decay and redistribution processes.

Fortunately, the fluorescence technique is very flexible. Tunable infrared pulses allow one to excite various vibrational levels of the same molecule and properly adjusted probe frequencies reduce the number of interacting states.

At the end of this section on probe techniques we emphasize the importance of knowing the temporal shape of the probe pulse. This fact is essential for relatively long pulses, i.e., for $t_p \gtrsim T_2, T_1$. Gaussian pulses which rise and decay rapidly are well suited for our investigations. Improvement of the experimental time resolution is possible by cutting the wings of the probe pulse with the help of a nonlinear absorber, e.g., a bleachable dye. This technique requires the transmission of the absorber to be adjusted to the peak intensity of the light pulse (Penzkofer *et al.*, 1972). For any pulse shape it is desirable to measure the probe scattering signals over an intensity range as large as possible to clearly interrogate the free relaxation of the system.

IV. EXPERIMENTAL

In the previous part of this paper we presented the theoretical background for the excitation and the probing of normal modes in the condensed phases.

We now wish to make several remarks as to the required quality of the picosecond pulses. Next, the generation of tunable infrared pulses is discussed. Subsequently, three experimental systems are presented which were used successfully to obtain new information on ultrafast dynamical processes in liquids and solids.

A. Generation of ultrashort laser pulses

To obtain reliable experimental data in picosecond investigations it is important to work with well-defined single picosecond pulses for the excitation and for the probing of the material excitation. One has to measure the pulse duration and one should work with bandwidth-limited pulses in many applications. It is desirable to know the peak intensity and the pulse shape of the pulses used. All parameters should be kept constant during the experimental run. The application of the whole mode-locked pulse train of a high-gain solid-state system should be avoided since the important pulse parameters, pulse duration, bandwidth, peak intensity, and pulse shape, vary from the beginning to the end of the pulse train (Duguay *et al.*, 1970; Eckardt *et al.*, 1971; von der Linde, 1972). The selection of chirp-free pulses from the pulse train is discussed by Zinth *et al.* (1977).

In our experimental systems we work with mode-locked Nd-glass lasers operating at a frequency $\tilde{\nu}_L = 9455\ \text{cm}^{-1}$. Satellite pulses on a picosecond time scale are eliminated by contacting the dye cell to one mirror of the oscillator (Bradley *et al.*, 1969). A single picosecond pulse is cut from the leading part of the pulse train using an electro-optic switch. This switch consists of a high-pressure spark gap in conjunction with an optical Kerr cell (von der Linde, Bernecker, and Laubereau, 1970). When one pulse of the mode-locked train reaches a certain power level, the spark gap operates and the Kerr shutter transmits the subsequent pulse. The pulse duration was measured by a quantitative application of the two-photon fluorescence (TPF) technique (Giordmaine *et al.*, 1967; von der Linde, Bernecker, and Kaiser, 1970; Zinth *et al.*, 1977; 1978), by the use of a fast streak camera of ~3 psec time resolution (Malyutin and Shchelev, 1969; Bradley *et al.*, 1971), and by a nonlinear optical technique using a rapidly rising and decaying material excitation for probing the laser pulse (von der Linde and Laubereau, 1971). The latter system has the advantage that the wings of the laser pulse can be measured several orders of ten below the peak of the pulse.

The various parameters of our ultrashort light pulses are as follows: pulse duration $t_p \simeq 6$ psec; frequency bandwidth $\Delta\tilde{\nu}_L = 3\ \text{cm}^{-1}$ $t_p \times \Delta\nu_L = 0.5$, i.e., our pulses are essentially bandwidth limited; peak power $P_L = 10^9$ W; pulse shape approximately Gaussian; peak to background ratio 10^4; and mode pattern TEM_{00}.

B. Infrared pulses for direct vibrational excitation

In Sec. II, we discussed two excitation processes for well-defined vibrational modes: stimulated Raman scattering and resonant infrared absorption. The latter process requires intense, tunable, ultrashort light pulses in the infrared part of the spectrum. We wish to comment briefly on the generation of such pulses (Laubereau, Greiter, and Kaiser, 1974).

When a coherent laser pulse passes through a properly oriented nonlinear crystal, two new pulses are generated at the signal and idler frequency. The physical process, parametric three-photon amplification, has been studied extensively in oscillators at moderate power levels (Giordmaine and Miller, 1965; for reviews see Smith, 1972, and Byer, 1975). The high peak intensities available in ultrashort pulses allow efficient generation of infrared pulses by one transit through the nonlinear crystal. It was found that with single picosecond laser pulses, conversion efficiencies of several percent are possible without crystal damage. The generated frequencies depend upon the nonlinear material and the crystal orientation with respect to the beam axis. For $LiNbO_3$ we found a practical tuning range from approximately 6800 cm^{-1} to 2700 cm^{-1} with a laser pulse at 9455 cm^{-1}. The frequency bandwidth of the generated pulses is a critical function of a number of parameters such as tuning curve of the material, crystal length, pump beam divergence, and signal divergence. In early experiments we obtained with one $LiNbO_3$ crystal a bandwidth of approximately 100 cm^{-1} at an infrared frequency of 3000 cm^{-1}. The bandwidth and divergence of the parametric pulse is substantially reduced when working with two nonlinear crystals in a distance of roughly 50 cm. The first crystal acts as a broadband, large-divergence generator, while a small frequency component is amplified in the second crystal determined by the (small) divergence of the pump beam and the distance between the crystals. More recently, careful measurements with two $LiNbO_3$ crystals gave infrared pulses of 8 cm^{-1} close to the Fourier transform limit (Seilmeier *et al.*, 1978). The infrared pulses have rapidly rising and falling wings on account of the highly nonlinear generation process. This fact is responsible for the favorable time resolution of

$\lesssim 0.5$ psec which we found when working with these infrared pulses.

C. Coherent excitation and probe techniques

Stimulated Raman scattering has the advantage of being able to coherently excite known vibrations of different molecules with a single laser frequency. In many cases, only one vibrational mode is excited for every polyatomic molecule.

Two experimental systems for coherent probe scattering with off-axis and collinear wave-vector geometry are depicted schematically in Figs. 23 and 24, respectively. The mode-locked laser oscillator is followed by an electro-optic switch, which cuts one pulse from the leading part of the pulse train. The selected pulse passes through an optical amplifier with gain of approximately 100 and is subsequently converted (in most experiments) to the second harmonic at 18 910 cm^{-1} or 0.53 μm in a potassium dihydrogen phosphate crystal. The powerful light pulse traverses the sample, a cell containing the liquids or a single crystalline specimen. Stimulated Raman scattering is effectively generated in samples of several millimeters to several centimeters in length. In our measurements the energy conversion of laser to Stokes emission is kept at a few percent in order to stay within the validity of our calculations and to avoid depletion of the input pulse. The stimulated Stokes pulse is simply measured by a fast photodiode and suitable filters (Fig. 23). More detailed information was obtained using a high-resolution spectrometer in conjunction with an optical multichannel analyzer system. We were able to study the spectra of the transmitted laser pulse, the generated Stokes pulse, and—in Fig. 24—the spectra of the scattered probe pulses at various delay times (see, for example, Fig. 32).

A beam splitter in the path of the input pulse provides

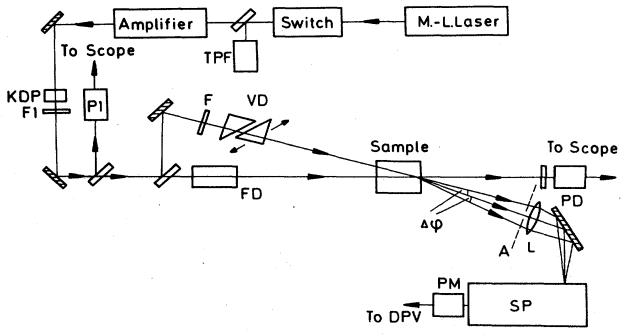

FIG. 23. Schematic of the experimental system to measure coherent probe scattering in an off-axis geometry. The mode-locked laser is followed by an electro-optic switch which cuts one pulse out of the pulse train. The picosecond pulse is controlled by a two-photon fluorescence technique (TPF). The energy of the input and of the generated Stokes pulse is monitored with fast photodiodes *P*1 and *PD*, respectively. A beam splitter provides a weak probe pulse which travels through a variable delay system (VD) before interrogating the momentary material excitation in the sample. The aperture *A* determines the divergence of the observed scattered probe beam.

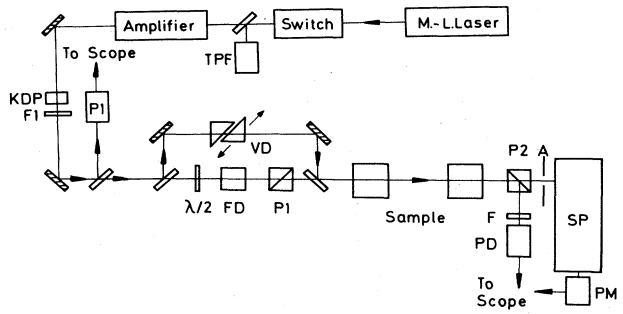

FIG. 24. Experimental setup to measure coherent probe scattering in a collinear geometry. A beam splitter generates the probe pulse, which is properly delayed before traveling collinearly to the exciting pulse. The scattered signals of the pump and probe pulses are separated by the polarizer P_2.

a second pulse of smaller intensity, approximately 10^{-2} of the exciting pulse. This weak pulse serves as an interrogating pulse of a variable delay time t_D. Our optical delay system of high precision consists of two movable prisms. The delay times were carefully determined taking into account the group velocities of various optical components. The accuracy of the t_D scale is better than 2%. The properly delayed probe pulse interacts with the instantaneous coherent vibrational excitation of the sample.

In the off-axis geometry of Fig. 23 the coherent anti-Stokes Raman scattering of the probe pulse is observed close to the forward direction. The spectrometer serves as a transmission filter for the anti-Stokes signal with a bandwidth of 20 cm^{-1}. The aperture *A* determines the solid angle of acceptance of the detection system. As pointed out above, the size and the position of the aperture *A* determine which material excitation we observe with our photodetector (PM). The phase-matching angle of the probe scattering geometry is determined by the color dispersion of the medium and by the Raman shift (i.e., the vibrational frequency) of the specific sample. The following experimental parameters are relevant for the off-axis k-matching situation: sample length (determining the interaction length Δl); beam diameter (affecting the Stokes divergence α_{max}); probing angle β; and angle of detection $\Delta\varphi$. Experimentally, we typically have $\alpha_{max} \simeq 2°$ and $\beta \simeq 3°$.

In Fig. 24, the weak probing pulse is generated by a first beam splitter and is subsequently properly delayed by a variable optical delay system. A second beam splitter is adjusted carefully to make the probe pulse travel collinearly to the exciting pulse through the medium. In this way we work with a probing angle $\beta = 0$. Two polarizers P1 and P2 are inserted into the light path. When both polarizers are parallel, we observe the strong ($\eta_S \sim 1\%$), highly polarized Stokes pulse and a much weaker (non-phase-matched) anti-Stokes signal, both generated by the powerful pumping pulse. With crossed polarizers these two signals and the laser pulse are attenuated by a factor of 10^5–10^6. It is then possible to observe the scattered Stokes or anti-Stokes signals of the interrogating pulse and to study their magnitude as a function of delay time. Since the probe pulse has

the same conversion efficiency into Stokes and anti-Stokes light as the pump pulse (~1%), we are able to measure the scattered probe signal over approximately three orders of magnitude. We note that the Stokes component of the probing pulse is always k-matched in the collinear geometry, while the anti-Stokes signal is k-matched for a slightly different frequency. These facts were used in experiments discussed below.

D. Incoherent probing

1. Spontaneous anti-Stokes Raman scattering

The experimental system to measure the energy relaxation time T_1 is presented schematically in Fig. 25. A powerful single picosecond pulse at $\nu_L = 9455$ cm^{-1} traverses the sample, generating vibrational excitation at the normal mode with the largest Raman gain. The KDP crystal in the second beam produces a light pulse at the second harmonic frequency ($\nu_{2L} = 18\,910$ cm^{-1}), which serves as a probe pulse with variable delay t_D. The probe pulse interacts with the excited molecules of the sample and the incoherent (spontaneous) anti-Stokes Raman signal $S^{\text{inc}}(t_D)$ is observed at a scattered angle of 90°. A monochromator or a set of dielectric filters is used for the detection of the weak spontaneous Raman signal. With approximately 10^{16} photons in the probe pulse, one estimates for an occupation number of $n \sim 10^{-3}$ an anti-Stokes signal of 10^3 photons in a solid angle of $\Delta\Omega \simeq 0.2$ sr.

2. Two-pulse fluorescence technique

The vibrational excitation by resonant infrared absorption and the physics of the fluorescence probe signal were discussed in Secs. II.E and III.C, respectively. The experimental system of the two-pulse technique is very similar to the setup presented in the previous section (see Fig. 25). The powerful laser pulse at $\tilde{\nu}_L = 9455$ cm^{-1} passes through two $LiNbO_3$ crystals (broken line), generating the desired infrared pulse. After filtering out the laser frequency, the infrared radiation is focused into the sample. At a frequency of $\nu_1 = 3000$ cm^{-1}, the pulse duration is ~3 psec and the pulse energy corresponds to 10^{14} quanta. The frequency and the bandwidth of the infrared pulse are monitored by an infrared spectrometer. A beam splitter in the input beam produces the second pulse which is—in the experiments discussed below—converted to the second harmonic frequency $\tilde{\nu}_{2L} = 18\,910$ cm^{-1} in a KDP crystal. The dye cell after the beam splitter provides a special pulse shaping of the laser pulse (Penzkofer *et al.*, 1972). The leading part of the transmitted pulse is efficiently steepened by the nonlinear dye absorber. The pulse at frequency ν_{2L} travels through an optical delay line and finally crosses the infrared beam, i.e., passes through the vibrationally excited volume. The fluorescence of the sample is measured with a spectrometer and photomultiplier.

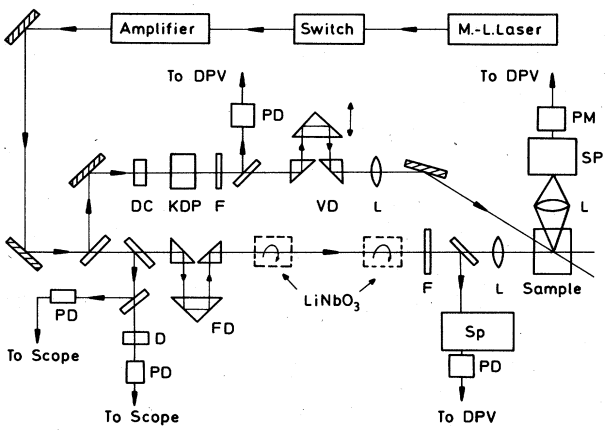

FIG. 25. Experimental system to measure energy relaxation times. A single-picosecond laser pulse either generates stimulated Raman scattering in the sample or produces ultrashort infrared pulses when the two nonlinear crystals (broken line) are inserted. The infrared frequency is tuned by crystal rotation. The probe pulse travels through the upper delay system and interrogates the excited volume. With spectrometer (SP) and photomultiplier (PM) a spontaneous anti-Stokes signal or a fluorescence signal can be measured. The input intensity is determined by two fast photodiodes (PD) in conjunction with a nonlinear absorber (D).

V. RESULTS AND DISCUSSIONS OF DEPHASING PROCESSES IN LIQUIDS

The following three sections are concerned with the determination of the dephasing time for a variety of vibrational modes. In Sec. V. A, we begin with the simplest case of a single molecular vibration with a homogeneously broadened Raman line. In the next step (Sec. V.B) we investigate vibrational modes with discrete but closely spaced vibrational components. In particular, we present a collective beating phenomenon originating from neighboring isotope species. The more complex situation of inhomogeneously broadened Raman lines, where a broad spectrum of vibrational modes is excited in the pumping process, is discussed in Sec. V.C. Several comments on the resolution of the wave-vector spectroscopy are given at the end of Sec. V.

A. Normal modes with homogeneously broadened Raman lines

First we investigate vibrational modes where all molecules have the same resonance frequency. The coherent scattering signal was measured for a variety of molecules using experimental systems presented in Figs. 23 and 24. One normal vibrational mode was excited for each molecular system. The mode with the largest gain factor [Eq. (37) and Fig. 2] dominates in the stimulated excitation process. We discuss the dephasing time of two different molecular vibrations of the molecules CH_3CCl_3 and liquid N_2. Experimental data for CH_3CCl_3 and liquid N_2 are presented in Figs. 26 and 27, respectively.

The coherent Stokes or anti-Stokes scattering signal $S^{\text{coh}}(t_D)$ is plotted as a function of delay time between the pump and the probing pulse. Time zero marks the maximum of the pump pulse. Both curves exhibit the main features predicted by the calculated curves in Fig. 14.

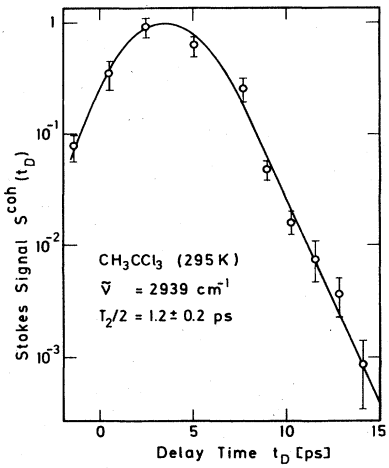

FIG. 26. Coherent Stokes scattering signals vs delay time t_D. The CH_3 stretching mode at 2939 cm^{-1} of CH_3CCl_3 is found to have a dephasing time $T_2/2 = 1.2$ psec.

The scattered probe signal rises to a delayed maximum and decays exponentially with a time constant characteristic of the molecule and the specific vibrational mode. It is possible to collect numerous data points along the exponential slope and determine the dephasing time with considerable accuracy of approximately 10%. We note that in Fig. 27 the exciting pulse has left the sample for over 200 psec while the freely relaxing molecules still show an observable phase relation within the excited volume.

In Fig. 26 the dephasing time $T_2/2$ of the CH_3 stretching mode at 2939 cm^{-1} is found to be 1.2 psec for CH_3CCl_3. Measurements were made under highly selective k-matching conditions where vibrational modes of other

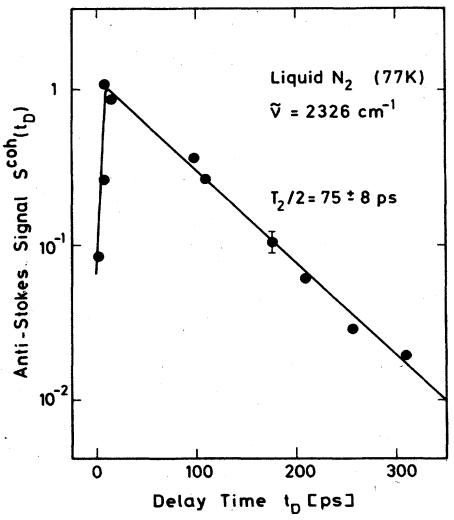

FIG. 27. Coherent anti-Stokes scattering signals vs delay time t_D. The fundamental mode of liquid N_2 at 2326 cm^{-1} gives a value of $T_2/2 = 75$ psec.

TABLE II. Measured dephasing times of several modes and molecules. Comparison with spontaneous Raman linewidth.

	$\tilde{\nu}_0$(cm^{-1})	$T_2/2$ (10^{-12} sec) Measured	From linewidth
N_2(77K)	2326	75 ±8	79 ±8
CCl_4	459	3.5±0.4	3.8±0.5
$SiCl_4$	425	3.0±0.5	2.8±0.5
$SnCl_4$	368	2.8±0.3	2.5±0.5
CH_3CCl_3	2939	1.2±0.2	1.2±0.1
$SnBr_4$	221	3.0±0.3	>1.6
CH_3OH	2835	2.3±0.5	>0.25
$(CH_2OH)_2$	2935	3.0±0.5	>0.1

molecules (see Table II) showed considerably longer dephasing times. On the other hand, independent tests of our experimental system gave a lower time resolution of 0.3 psec. It is important to note that the same dephasing time of $T_2/2 = 1.2$ psec was measured under different k-matching conditions including off-axis geometries. We conclude from these measurements that the observed value of 1.2 psec is the dephasing time $T_2/2$ of the observed vibration without indication of an inhomogeneous broadening. We have measured the energy relaxation time of the same vibrational mode (see Sec. VI.A.1) and found a value of $T_1 = 5.3$ psec; i.e., we have $T_1/T_2 = 2.2$. It is interesting to compare our time constants with the spontaneous Raman linewidth of the same vibration (and molecule). From the linewidth of $\delta\tilde{\nu} = 4.3$ cm^{-1} a time $T_2/2 = 1.2$ psec is calculated [see Eq. (28)]. The agreement between the two time constants supports our conclusion that the observed vibrational mode is predominantly homogeneously broadened.

Our experimental data on the coherent scattering signal of the fundamental vibration of N_2 at 2326 cm^{-1} are presented in Fig. 27. From the exponential slope of the experimental curve, a relaxation time of $T_2/2 = 75$ psec is deduced at 77 K (Laubereau, 1974). This number represents the longest dephasing time observed so far for a liquid medium. Recently, several authors reported an exceptionally long energy relaxation time of the fundamental vibrational mode of liquid N_2 (Calaway and Ewing, 1975; Brueck and Osgood, 1976). In this case, where $T_1/T_2 \sim 10^{11}$, the dephasing process is not affected by the depopulation of the first excited vibrational state. Careful measurements exist of the linewidth $\delta\tilde{\nu}$ of the fundamental vibration of liquid N_2 (Clements and Stoicheff, 1968; Scotto, 1968). From these data we calculate a time constant of $T_2/2 = 78$ psec, which agrees quite favorably with the relaxation time obtained from our time-resolved measurement. More recently, similar results were reported for liquid N_2:Ar mixtures (Hesp *et al.*, 1977).

We recall that the pure dephasing time τ_{ph} may be determined from experimental values of T_2 and T_1 [see Eq. (19)]. In the presently discussed liquids the population lifetime T_1 is considerably larger than the dephasing time T_2; as a result we find $\tau_{ph} \approx T_2/2$. The values of τ_{ph} calculated in the quasielastic collision model are indeed in fair agreement with our measured T_2 data (see Sec. II.A.5).

B. Vibrational modes with neighboring isotope components: Dephasing time and collective beating

Many liquids are composed of several isotopic species. The resulting multiplicity of the vibrational modes may or may not be resolved by spontaneous Raman (or infrared) spectroscopy. It will be shown here that coherent excitation and coherent probing allow us to determine the dephasing time of one isotope component. In addition, a new beating phenomenon is observed which gives values of the frequency difference of the vibrational isotope components.

Well-known molecules, the tetrahalides, were chosen to demonstrate our ideas and to test the theoretical calculations of Secs. II and III. The isotope effect of Cl and Br gives rise to vibrational multiplicity of the totally symmetric tetrahedron vibration. Stimulated Raman scattering of these vibrational modes is readily achieved on account of the large scattering cross sections. The isotopic line structure of the spontaneous Raman spectrum has been extensively studied for some of these compounds (Clark and Willis, 1971; Brandmüller *et al*, 1967; Eysel and Lucas, 1970). In Fig. 28(a) the Raman band of the tetrahedron A_{1g} vibration of CCl_4 around 459 cm^{-1} is depicted. The frequency difference between two neighboring lines is approximately 3 cm^{-1}. The molecular components $C^{35}Cl_4$ (1), $C^{37}Cl^{35}Cl_3$ (2), $C^{37}Cl_2{}^{35}Cl_2$ (3), and $C^{37}Cl_3{}^{35}Cl$ (4) have concentration ratios of 0.772 : 1 : 0.486 : 0.105, in agreement with the respective Raman line intensities in Fig. 28(a). The significant overlap of the lines does not allow an accurate measurement of the linewidth of a single isotope component.

Considerably different is the situation for liquid $SnBr_4$ at 305 K, where the tetrahedron mode around 221 cm^{-1} is shown in Fig. 28(b). A structure of the Raman band, on account of the natural abundance of the ^{79}Br and ^{81}Br isotopes, is not visible in the spontaneous Raman band. The isotope distribution is masked by the homogeneous broadening of the closely spaced isotope components. The wings of the observed band differ notably from a

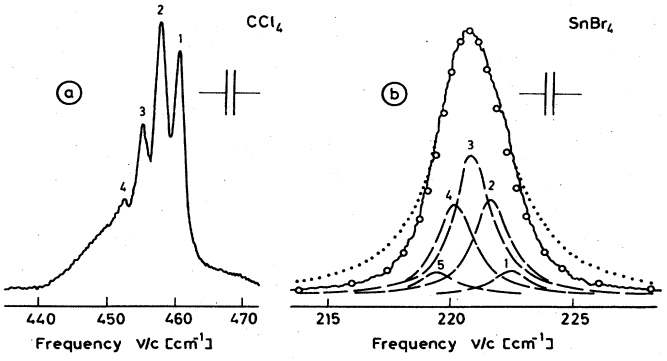

FIG. 28. Spontaneous Raman–Stokes spectra of (a) CCl_4 and (b) $SnBr_4$. The line splitting of CCl_4 is due to the natural abundance of ^{35}Cl and ^{37}Cl. The five Raman bands (broken curves in b) are calculated from the measured dephasing time and isotope splitting using the natural abundances of ^{79}Br and ^{81}Br. The sum of these lines (open circles) adds up to the spontaneous line shape. Dotted curve represents a Lorentzian line profile.

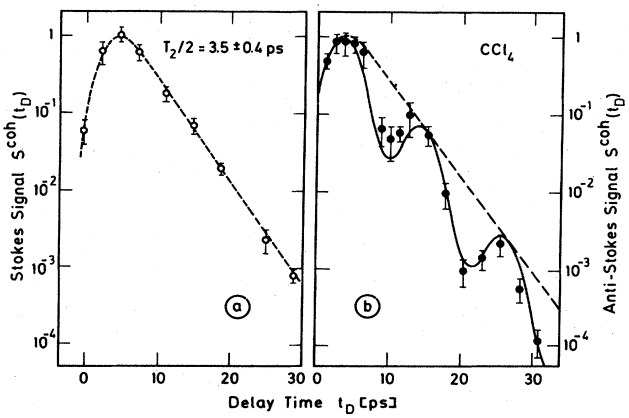

FIG. 29. (a) Coherent Stokes signals vs delay time measuring one isotope component [number 2 in Fig. 28(a)] of CCl_4 by a selective collinear phase-matching geometry. (b) Coherent anti-Stokes signals vs time observed in a nonselective off-axis geometry. The beating of the different isotope components of CCl_4 is clearly visible.

Lorentzian line (dotted curve). The broken lines and the open circles in the figure are calculated and will be explained below.

We now present our picosecond investigations on CCl_4 and $SnBr_4$ (Laubereau, Wochner, and Kaiser, 1976a and b). The results on CCl_4 are discussed first. The most abundant isotope component $C^{37}Cl^{35}Cl_3$ was investigated under two different selective phase-matching conditions: (i) Using the collinear geometry of Fig. 24, the Stokes shifted coherent scattering signal $S^{coh}(t_D)$ was measured as a function of delay time t_D [see Fig. 29(a)]. Discrimination against the strong Stokes signal of the pump pulse was achieved by carefully adjusting the polarization directions of pump and probe pulse. The small aperture in front of the spectrometer ensures a small acceptance angle around the forward direction. k matching and observation of the most abundant isotope component is straightforward under these conditions. From Fig. 29(a) we deduce a dephasing time of $T_2/2 = 3.5 \pm 0.4$ psec. (ii) k matching for a coherent anti-Stokes scattered signal requires an off-axis geometry. Wave-vector calculations indicate that the scattered probe emission of the different isotope components occurs in different cones of ~2 mrad under slightly different angles $\Delta\varphi \simeq 6$ mrad. Selective k matching was experimentally adjusted with a small aperture which selects a probe scattering beam of ~2 mrad. The coherent anti-Stokes signal S^{coh} was measured as a function of delay time t_D using an experimental system depicted in Fig. 23. The resulting dephasing time of 3.6 ± 0.4 psec is in excellent agreement with the data obtained by the collinear geometry (for experimental data see Fig. 7(a) in the paper by Laubereau *et al.*, 1976b).

Different results are observed when the aperture A in the off-axis geometry is removed (Fig. 23). Now, the solid angle of acceptance is considerably larger (~10 mrad); probe scattering components within this divergence are readily detected. The total signal is expected to be strongly modulated by the beating of the isotope components. In Fig. 29(b) the coherent probe scattering

S^{coh} is plotted versus delay time t_D. The decaying part of the signal curve differs drastically from the data of Fig. 29(a). Two minima and additional maxima of the signal curve are clearly indicated by the experimental data which monitor the relaxation process over four orders of 10. Collective beating of the isotope species of CCl_4 is readily seen in the figure. The solid curve is calculated from the theory outlined above for a nonselective k-matching geometry taking into account the scattering contributions of the four most abundant isotope species of CCl_4. Since the dephasing time is determined in an independent experiment [see Fig. 29(a)], the only fitting parameter in the calculation is the frequency difference $\Delta\omega$ between neighboring vibrational components, which is determined with considerable accuracy from the data of Fig. 29(b). A value of $\Delta\omega/2\pi c = 2.9 \pm 0.15$ cm^{-1} is found, which favorably compares with the spontaneous Raman data of Fig. 28(a). The good agreement of the theoretical curve (solid line) and the experimental points in Fig. 29(b) should be noted (see also Fig. 16).

We turn now to our investigations of the tetrabromides, where the isotopic effect is notably smaller on account of the lower vibrational frequencies and the smaller relative mass effect $\Delta m/m$ of the ^{79}Br and ^{81}Br isotopes. For $SnBr_4$ the line splitting is not resolved in the spontaneous Raman spectrum [see Fig. 28(b)]. According to Herzberg (1945), the frequency spacing $\Delta\omega \simeq \omega\Delta m/8(m + \Delta m)$ of the isotope components is estimated to be $\Delta\omega/2\pi c \simeq 0.67$ cm^{-1}. This value is considerably smaller than the width of the Raman band of $\delta\tilde{\nu}_{tot} \simeq 3.2$ cm^{-1} depicted in Fig. 28(b).

With selective k matching we were able to resolve and to study two single components of the five isotope species. The collinear wave-vector geometry of Fig. 24 was used and the tetrahedron vibrations around 221 cm^{-1} were excited. For a sample length of $l = 10$ cm, we estimated an effective interaction length for the probe scattering of $\Delta l \simeq 0.4$ cm. First we measured the scattered anti-Stokes signal and obtained the dephasing time of the isotope component $j = 4$ ($Sn^{81}Br_3{}^{78}Br$); then we observed the scattered Stokes signal and studied the most abundant isoisotope component $j = 3$ ($Sn^{81}Br_2{}^{78}Br_2$).

Coherent anti-Stokes scattering is well phase matched for the component $j = 4$, as discussed in connection with Fig. 19. In fact, for $j = 4$ one calculates $2\Delta k\Delta l = 0.24$, while for the neighboring isotope components $j = 3$ and $j = 5$ one obtains considerable mismatch with $2\Delta k\Delta l \simeq 6.8$. As a result, the components $j = 3$ and $j = 5$ contribute less than 3% to the anti-Stokes scattering signal [see Eq. (111)]. The measured probe scattering signal S^{coh} of the isolated isotope species $j = 4$ is plotted versus delay time t_D in Fig. 30(a). The exponential decay of S^{coh} extends over a factor of approximately 500. The dephasing time of the single isotope component of $T_2/2 = 3.0 \pm 0.3$ psec is deduced from the slope of the signal curve. This value corresponds to a homogeneous linewidth of 1.8 cm^{-1}, a number significantly smaller than the bandwidth of 3.2 cm^{-1} observed in the spontaneous spectrum [Fig. 28(b)].

Coherent Stokes scattering is phase matched for $j = 3$, which is located at the center of the spontaneous Raman band [see Fig. 28(b)]. We recall that the Stokes frequency of the excitation process occurs in the middle of the Raman band. As a result, a strong material excitation

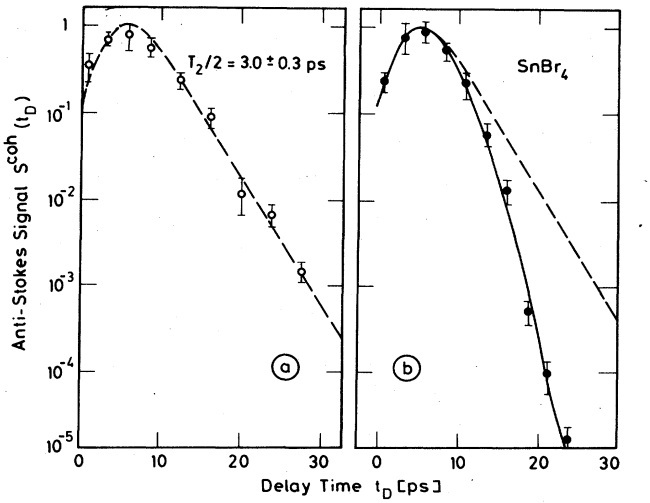

FIG. 30. (a) Coherent anti-Stokes signal measuring a single-isotope component [number 4 of Fig. 28(b)] in $SnBr_4$. A selective collinear phase-matching geometry was used. (b) Coherent anti-Stokes signals observed by a nonselective off-axis geometry. The rapid decay of the data points is due to the destructive interference of different isotope components of $SnBr_4$.

is generated for $j = 3$ in the forward direction. We have measured the Stokes signal S^{coh} versus delay time t_D using careful adjustment of the polarizers. The signal curve was found to be the same as for the anti-Stokes frequency [Fig. 30(a)]. This result demonstrates that the two neighboring isotope species have the same dephasing time $T_2/2 = 3.0$ psec within the experimental accuracy of 10%.

We have studied the same vibrational mode of $SnBr_4$ with the off-axis geometry of Fig. 23 under nonselective k-matching conditions. Coherent superposition of the different isotopic components is observed in this case. The picosecond probe data, S^{coh}, are presented in Fig. 30(b). The signal decays rapidly over five orders of 10 during a time interval of ~18 psec. For $SnBr_4$ we estimate a long beat period of 50 psec on account of the small isotope splitting. As a result, the signal does not reach the first minimum and subsequent maximum of the beating curve. In fact, the beating maximum around $t_D \simeq 50$ psec is expected nine orders of 10 below the peak scattering signal. The solid curve in Fig. 30(b) is calculated for the nonselective k-matching situation using the beat frequency $\Delta\omega$ as a fitting parameter and the measured value of the dephasing time $T_2/2 = 3$ psec which was determined in Fig. 30(a). Good agreement of the theoretical curve with the experimental data (full points) in the figure is obtained for a value of $\Delta\omega/2\pi c = 0.7 \pm 0.15$ cm^{-1}, which favorably compares with the theoretical estimates of 0.67 cm^{-1}.

The apparent decay time of the solid curve in Fig. 30(b) of 1.2 psec does not represent a relaxation time of the vibrational system. The observed time dependence results from the destructive interference of the coherently excited vibrational modes. A relaxation time of 1.2 psec would correspond to a spectral linewidth of 4.4

cm^{-1}, which is in contradiction to the observed spontaneous bandwidth of 3.2 cm^{-1}.

Knowing the dephasing time T_2, the frequency spacing $\Delta\omega$, and the abundance of the $SnBr_4$ species, we are able to evaluate the composed spontaneous Raman band. The natural abundance of the two Br isotopes leads to a relative concentration of the five components $Sn^{81}Br_x^{79}Br_{4-x}$ ($x = 0$–4) of 0.173, 0.685, 1.0, 0.653, and 0.160. In Fig. 28(b), five homogeneous bands with linewidth of 1.8 cm^{-1} corresponding to the five isotope components are depicted by broken curves. The sum of the five Raman lines gives the open circles which agree completely with the experimental Raman band of common $SnBr_4$. This result demonstrates that our picosecond data of T_2 and $\Delta\omega$ are fully consistent with the integral information supplied by spontaneous Raman spectroscopy. It is interesting to note that the investigations of Figs. 29 and 30 give evidence of the spatial phase correlation in liquids discussed in Sec. III.A.4.

To conclude this section, the following remarks should be made. The beating phenomenon originates from the coherent superposition of the vibrational amplitudes $\langle q\rangle_j$ of the excited quantum states. $\langle q\rangle_j$ denotes the expectation value of the displacement operator (Giordmaine and Kaiser, 1966). There are differences from the quantum beats previously observed in gases (Shoemaker and Brewer, 1972; Gornik *et al.*, 1972; Haroche *et al.*, 1973; and Heritage *et al.*, 1975): (i) The different excited states belong to various molecular species. (ii) The vibrational states have no optically allowed transitions, i.e., there is no emission to be observed. (iii) The beat frequency is very high, on the order of 10^{11} sec^{-1}, and the dephasing times are very short, on the order of several 10^{-12} sec. Ultrashort pump and probe pulses are required to study the beating process in the condensed phase.

C. Molecular vibrations with inhomogeneously broadened Raman lines

At present, there is limited information on inhomogeneous line broadening in liquids. The best known examples are liquids with strong hydrogen bonding and broad inhomogeneous OH bands (Pimentel and McClellan, 1960). Spontaneous spectroscopic techniques provide the total Raman or infrared band, but do not allow a separation between homogeneous and inhomogeneous contribution to the total line shape. As a result, it is not possible in most cases to decide to which extent a normal mode is inhomogeneously broadened. Our preliminary investigations indicate that even relatively narrow Raman lines of several cm^{-1}, which are generally believed to be homogeneously broadened, have inhomogeneous contributions not detected by presently existing experimental methods.

The investigations discussed now are aimed at tackling this problem (Laubereau, Wochner, and Kaiser, 1977). In Sec. V.B, where we derived a method to study Raman lines of well-known (isotopic) substructure, we measured the dephasing time of one molecular component. We now extend these investigations and apply our selective k-matching technique to vibrational bands of unknown inhomogeneous character. It will be shown below that we are able to study the dephasing time of a small group of molecules of narrow frequency width.

Two types of measurements are performed to study the coherent scattering of inhomogeneously broadened Raman lines. First, we investigate the spectra of different scattered light pulses, and second, we measure the time dependence of the relaxation process.

The following spectral data give direct information on the material excitation by transient stimulated Raman scattering. The CH_2 stretching mode of ethylene glycol at 2935 cm^{-1} was chosen to demonstrate the strong effect of the transient stimulated Raman excitation of a very broad (60 cm^{-1}) vibrational band. A large Stokes divergence, typical for nonselective k-matching geometry, was used in a short cell of 1 cm length. Under these conditions the probe pulse interacts with many excited vibrational components with good scattering efficiency. In Fig. 31, four different spectra are presented.

(a) The spectrum of the incident laser pulse at $\tilde{\nu}_L = 18\,910$ cm^{-1} shows a linewidth of $\delta\tilde{\nu}_L \simeq 5$ cm^{-1}, which is the Fourier transform of the pulse duration of 3–4 psec.

(b) The spectrum of the Stokes pulse has a bandwidth of $\delta\tilde{\nu}_S \simeq 8$ cm^{-1}. We know that the Stokes pulse is shorter than the pump pulse by approximately a factor of 2 since the transient buildup of the material excitation scatters the incoming laser pulse for approximately half of the pulse duration. The reduced pulse duration gives a Stokes spectrum of $\delta\tilde{\nu}_S \simeq 8$ cm^{-1}. Note: Theory predicts that the molecules of the vibrational distribution are driven with the frequency $\omega_L - \omega_S$ during the early part of the excitation process. As a result, the Stokes spectrum does not reflect the molecular distribution.

(c) The spectrum of the Stokes scattered probe light, $S^{coh}(t_D = 0)$, is taken at the same time as the previous spectrum (b), but with a perpendicular polarization direction. As expected from the isotropic Raman tensor of the normal mode investigated here, the spectrum of $S^{coh}(t_D = 0)$ has the same bandwidth as the previous one in (b).

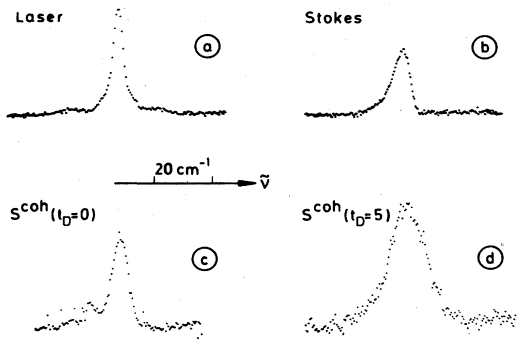

FIG. 31. Optical spectra of four different pulses: (a) incident laser pulse; (b) generated Stokes pulse; (c) Stokes scattered probe pulse $S^{coh}(t_D = 0)$ without delay time; (d) Stokes scattered probe pulse $S^{coh}(t_D = 5$ psec) taken 5 psec after the maximum of the exciting laser pulse. Note the broad spectrum of the freely relaxing molecular system. Measurements were made with the CH_3 stretching mode at $\tilde{\nu} = 2935$ cm^{-1} of ethylene glycol, cell length 1 cm.

(d) The Stokes scattered pulse $S^{coh}(t_D = 5$ psec) sees a completely different situation at the delay time $t_D = 5$ psec. For times $t \gtrsim t_p$ the molecules relax freely with their own resonance frequencies. A bandwidth of ~18 cm^{-1} is deduced from the spectrum of Fig. 31(d). This bandwidth will be discussed below after the time-resolved investigations.

As pointed out above, the interaction of the probe pulse with the material excitation depends strongly upon the k-matching condition. A greater interaction length Δl, resulting from a longer sample, gives a more selective phase-matching situation. High selectivity means interaction with a smaller frequency band of the distribution of excited molecules. We have measured the spectra of the Stokes scattered probe pulse for the same delay times of $t_D = 0$ and $t_D = 5$ psec, but with a longer sample of 10 cm (similar to Figs. 31(c) and 31(d), where $l = 1$ cm). The spectrum for $t_D = 0$ is found to be $\delta\tilde{\nu} = 8$ cm^{-1}, which, in analogy to Fig. 31(c), is the Fourier transform of the ultrashort Stokes pulse. The spectrum measured with a delay time of $t_D = 5$ psec showed a spectral width of 8 cm^{-1} in contrast to Fig. 31(d). This spectrum is considered to result from the interaction of the probe pulse of $t_p \sim 3$ psec with the fast-decaying material excitation (see below); but in this case we have adjusted a selective k-vector geometry and the probe pulse interacts with a molecular group of a small frequency spread of less than one cm^{-1}.

The six spectra discussed so far give the following information: (i) Selective k matching allows us to look at a small group of excited molecules. (ii) The broad spectrum of 18 cm^{-1} gives evidence that molecules are excited over a considerable fraction of the spontaneous bandwidth ($\delta\tilde{\nu}_{spon} = 60$ cm^{-1} for ethylene glycol). These observations suggest that the investigated vibrational mode is inhomogeneously broadened (homogeneous lines do not allow the excitation of a molecular subgroup).

We now discuss our investigations of the time evolution of the coherently excited vibrations. The following data are obtained on the CH_3 stretching mode of methanol at 2835 cm^{-1}. The spontaneous Raman band of this vibration gives a linewidth (FWHH) of $\delta\tilde{\nu}_{spon} = 20$ cm^{-1} (see Fig. 32). A series of measurements was carried out with different k-matching geometries varying the sample length (between 1 and 10 cm) and the divergence of the detected Stokes beam. We present experimental data of two different experimental situations. In Fig. 33(a), a highly selective k-matching situation is used with a sample length of $l = 10$ cm and with a small divergence of the Stokes beam of $\alpha = 3$ mrad. In Fig. 33(b), on the other hand, we devised a less selective k-vector geometry by using a shorter cell of $l = 1$ cm and a larger Stokes divergence of $\alpha = 10$ mrad.

The experimental results of Fig. 33(a) are of special importance for this section. The scattered probe signal extending over a factor of 500 is plotted as a function of delay time t_D. After the maximum of the material excitation we find an exponential decay of the scattered signal providing a time constant of 2.3 ± 0.5 psec. For an interpretation of this time constant, we estimate the frequency spread of the molecules monitored by the highly selective k-matching geometry. We recall that S^{coh} is produced predominantly by molecules with $\Delta k \Delta l < 1$ or

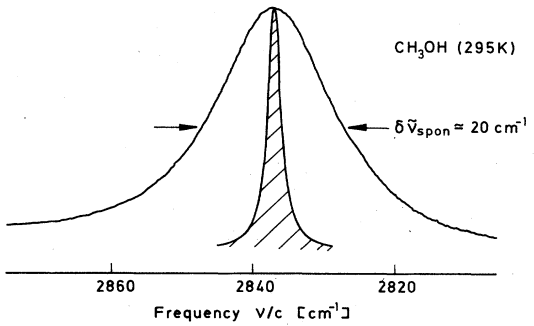

FIG. 32. Spontaneous Raman spectrum of a CH_3 stretching mode of methanol at 2835 cm^{-1}. The homogeneous line of the observed molecules at the center of the inhomogeneously broadened Raman band is indicated.

$\delta\tilde{\nu} < (2\pi\mu\Delta l)^{-1}$. For our geometry of sample length $l = 10$ cm and corresponding effective interaction length $\Delta l \sim 0.4$ cm and for an index of refraction of $\mu = 1.5$, we calculate $\delta\tilde{\nu} < 0.25$ cm^{-1}. This number indicates that molecules with vibrational frequencies around the center of the spontaneous line and with a very small frequency spread scatter predominantly the delayed probe pulse.

The following additional experimental information is of interest: The measurement was repeated with $l = 5$ cm, keeping all other parameters unchanged. We found a signal curve is similar to the one of Fig. 33(a), indicating the same time constant. Obviously, the increased bandwidth of the observed molecules did not affect the observed time constant. For $l = 1$ cm, however, the measured signal curve showed a noticeably steeper slope, intermediate to Fig. 33(b), where the k matching had even less selectivity.

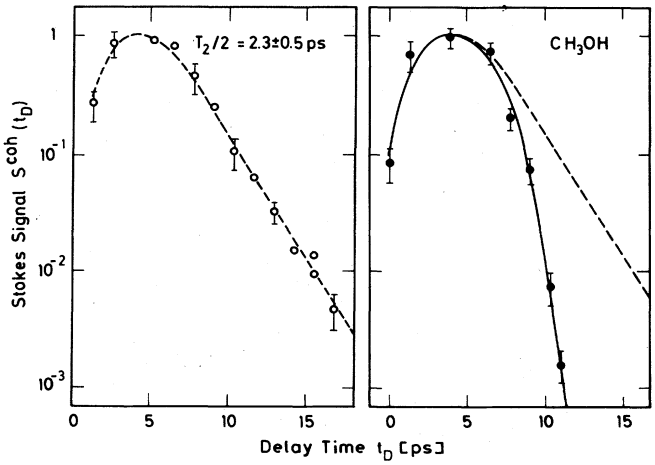

FIG. 33. (a) Coherent Stokes scattered probe signals vs delay time measured in a highly selective collinear k-matching geometry. The vibrational mode of CH_3OH of Fig. 32 is investigated. We observe a dephasing time $T_2/2 = 2.3$ psec corresponding to a homogeneous linewidth of 2.3 cm^{-1}. (b) Coherent Stokes signals for a less selective k-matching geometry. The signal decays rapidly on account of destructive interference of neighboring excited molecules.

We conclude from the results presented here that the observed time constant of 2.3 psec in Fig. 33(a) corresponds to the dephasing time $T_2/2$ of a small group of molecules, the frequency of which is close to the center frequency of the spontaneous inhomogeneously broadened Raman band. We note that $T_2/2 = 2.3 \pm 0.5$ psec corresponds to a linewidth of 2.3 cm^{-1}, which is smaller by a factor of approximately 8 than the spontaneous bandwidth. To illustrate the situation, this homogeneous narrow line is drawn in Fig. 32 into the center of the spontaneous Raman curve.

Completely different is the time dependence $S^{coh}(t_D)$ for less selective k matching [solid points full line in Fig. 33(b)]. Under these experimental conditions the coherent scattering signal disappears rapidly. The lower part of the curve gives an apparent decay time of ~0.6 psec. We know from the spectral investigation of the scattered signal (Fig. 31) that a wide frequency band of relaxing molecules exists in the medium. The fast signal decay of Fig. 33(b) is the consequence of the coherent superposition of the vibrating molecules. The measured time dependence does not correspond to a time constant of the excited molecules but represents the destructive interference of molecules which vibrate with a wide distribution of frequencies. We recall our findings of Figs. 29(b) and 30(b), where the interference of several equidistant isotope components gave rise to a collective beating with time periods of rapid decay of the scattered signal.

We have measured the scattered anti-Stokes signals for an off-axis geometry without selectivity of the k matching. The probe interacts with a broad spectrum of excited molecules. A very rapid decay with a time of ~0.3 psec is observed, which again does not represent a molecular time constant. This result demonstrates the good time resolution of our experimental system.

Similar time-resolved data were obtained for the CH_2 stretching mode in ethylene glycol, $(CH_2OH)_2$, at 2935 cm^{-1} with a spontaneous bandwidth (FWHH) of $\delta\nu_{spon} \simeq 60$ cm^{-1}. The results were similar to those of methanol. With highly selective k matching a dephasing time of $T_2/2 = 3.0 \pm 0.5$ psec was found. The corresponding linewidth of 1.8 cm^{-1} was smaller by a factor of 35 than the measured inhomogeneous Raman band. The larger value of T_2 in ethylene glycol appears to be reasonable since dynamic processes are reduced in this strongly associated liquid.

In Table II we have listed dephasing times T_2 for a number of vibrational modes and molecules.

D. Comments on the resolution of the wave-vector spectroscopy

It is well known that the spectral resolution of time-resolved spectroscopic investigations is limited by $\delta\omega_p$, the width of the Fourier transform of the applied pulses. For instance, the spontaneous Raman spectrum exhibits linewidths never sharper than the bandwidth of the incident short light pulses.

We wish to emphasize that the selective k-matching technique offers a high resolution not limited by $\delta\omega_p$. We recall that the first exciting pulse generates a collective material excitation with a well-defined spatial distribution of corresponding k vectors. The material excitation is strongest at the end part of the medium, where the second probe pulse is effectively scattered over an interaction length Δl. The finite length of the material excitation gives an uncertainty $\delta k_{instr} \cong (2\Delta l)^{-1}$ with a corresponding frequency value of $\delta\tilde{\nu}_{instr} = \delta k_{instr}/2\pi\mu$. For our highly selective collinear system with total length $l = 10$ cm and $\Delta l = 0.4$ cm we estimate $\delta k_{instr} \simeq 1.2$ cm^{-1} and $\delta\tilde{\nu}_{instr} \simeq 0.12$ cm^{-1}. In other words, in k space we probe molecules which belong to a small group of frequency spread (FWHH) $2\delta\tilde{\nu}_{instr}$. The time-resolved investigation of this group of molecules gives us directly the dephasing time T_2 when we select a frequency spread of $\delta\tilde{\nu}_{instr} \ll 1/T_2$. In this way it is possible to determine the linewidth $1/T_2$ within a vibrational distribution (an inhomogeneously broadened vibrational mode). The conditions discussed here are satisfied in our experiments. In $SnBr_4$, the isotropic components were well resolved since their frequency spacing was $\Delta\omega/2\pi c = 0.7$ cm^{-1}. Furthermore, the dephasing time $T_2 = 3.0$ psec suggests a homogeneous linewidth of one isotope component of 1.8 cm^{-1}, much larger than $\delta\tilde{\nu}_{instr}$ of the selective experimental arrangement.

In practical cases we have to consider additional factors which limit the k-vector selectivity: (i) beam divergence expressed by distribution of plane waves; (ii) effects due to diffraction resulting from finite beam diameters; and (iii) frequency modulation of the laser pulse.

(i) A certain beam divergence of the pumping and probing pulse leads to a distribution of k vectors which contribute to the observed scattered signal. For the collinear geometry ($\beta = 0$) it is possible to derive from Eq. (124) the following expression: $\delta\Delta k_S \simeq k_{L2}(\sin\alpha)\delta\beta$. With an accepted Stokes emission of $\alpha = 3 \times 10^{-3}$ and for a divergence of the probing beam of $\delta\beta = 10^{-3}$ we estimate $\delta\Delta k_S/2\pi\mu \simeq 0.06$ cm^{-1}. (ii) For a beam diameter d and a wavelength λ we have a diffraction angle of $\delta\alpha = 1.22\lambda/d$. This angle gives for a collinear geometry a deviation of the material excitation $\mathbf{k}_j$ by an amount $\delta k_j = (k_L k_S/2k_j)\delta\alpha^2$ [from Eq. (120)]. With $d \simeq 5 \times 10^{-2}$ cm and $\lambda \simeq 5 \times 10^{-5}$ cm we calculate $\delta\alpha \simeq 10^{-3}$ and $\delta k_j/2\pi\mu = 0.05$ cm^{-1}. (iii) Possible small contributions of frequency modulation to the total emission spectrum are difficult to assess. The product, bandwidth times pulse duration, $\delta\nu_p \times t_p$, is an important experimental criterion of the pulse quality. Small chirps and small random phase fluctuations contribute to an uncertainty of k_{L2} in the probing process.

In summary, factors (i)–(iii) point to the necessity of working with highly collimated beams of sufficient beam cross section and of paying special attention to the coherence of the ultrashort light pulses. From our experimental observation on $SnBr_4$ and $(CH_2OH)_2$ we conclude that our experimental system has an overall k resolution equivalent to $\delta\tilde{\nu} \lesssim 0.5$ cm^{-1}. Besides these experimental points we recall the effect of the spatial phase correlation of the physical system (Sec. III.A). Conservation of the k vectors generated by the excitation process is required for investigations with a selective k-vector geometry.

VI. RESULTS AND DISCUSSION OF VIBRATIONAL ENERGY TRANSFER AND POPULATION LIFETIMES IN LIQUIDS

Experimental data are now presented for the population (energy) lifetime T_1 of the first vibrational state (electronic ground state) of normal modes of vibrations of polyatomic molecules. We have devised several experimental techniques to study T_1 of a variety of vibrations in a number of molecules. Two excitation processes are discussed here: First, the vibrational excess population is generated by a first intense light pulse via stimulated Raman scattering (Sec. VI.A); and second, the vibrational mode is directly pumped by resonant infrared absorption (Sec. VI.B). After an excess population is established by the first ultrashort light pulse, the temporal change is monitored by subsequent interrogating pulses. It is now possible to observe energy decay routes, energy transfer processes, and redistribution between vibrational states.

A. Investigations with stimulated Raman excitation

The generation of excess population of the first excited vibrational state by transient stimulated Raman scattering was discussed in Sec. II.B.3 and illustrated in Fig. 5. We recall that the excess population n decays with the population lifetime T_1 after the excitation pulse has passed through the medium. In the experiments discussed now, the momentary degree of excitation is determined by incoherent Raman probe scattering (see Sec. III.B). In Fig. 21 the probe scattering signal S^{inc} was calculated as a function of delay time t_D between the excitation and probe pulse. The exponential decay of S^{inc} allows a direct determination of the population lifetime T_1.

The following numbers are of interest for the evaluation of the Raman excitation process. With 10^{17} pump photons (10^{-2} J) in the picosecond laser pulse we generate approximately 5×10^{15} Stokes photons and the same number of vibrationally excited molecules. For an excited volume of 10^{-3} cm^{-3} we calculate an occupation density (at $v=1$) of 5×10^{18} cm^{-3}. Since the total number of molecules per cm^3 in a liquid is approximately 5×10^{21} cm^{-3}, we estimate an occupation number of $n\simeq10^{-3}$. This number has to be compared with the thermal incoherent scattering signal. For vibrational modes of $\tilde{\nu}=3000$ cm^{-1} and 1000 cm^{-1} one estimates for 300 K values of $\bar{n}\simeq10^{-6}$ and 10^{-2}, respectively; i.e., using the stimulated Raman process, we are able to excite molecular vibrations with $\tilde{\nu}=3000$ cm^{-1} far above the thermal equilibrium value. This statement does not hold for low-lying vibrational modes ($\tilde{\nu}<1500$ cm^{-1}), where the thermal population is substantial at 300 K.

1. Determination of the population lifetime

The population lifetime T_1 of well-defined vibrational modes was measured in a number of neat liquids and mixed liquid systems (Laubereau *et al.*, 1972; Alfano and Shapiro, 1972; Monson *et al.*, 1974). An example is presented in Fig. 34, where the totally symmetric CH_3 valence bond vibration at $\tilde{\nu}=2939$ cm^{-1} of 1,1,1-trichlorethane is investigated (Laubereau *et al.*, 1973).

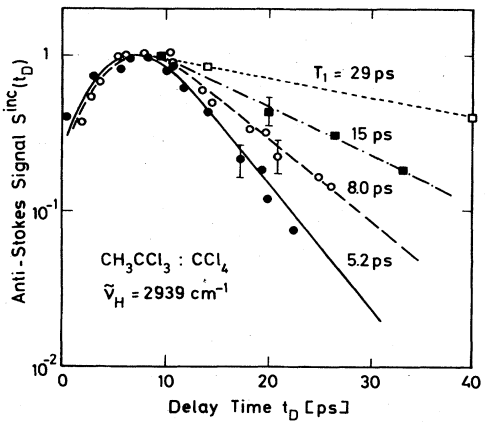

FIG. 34. Incoherent probe signals vs delay time t_D measured in pure (solid circles) CH_3CCl_3 and in $CH_3CCl_3:CCl_4$ mixtures; mole fractions of CH_3CCl_3 are 0.8 (○); 0.6(■); and 0.4 (□). The totally symmetric valence bond vibration at $\tilde{\nu}=2939$ cm^{-1} is investigated. The observed population lifetimes T_1 are listed.

The measured spontaneous anti-Stokes signal $S^{\text{inc}}(t_D)$ is directly proportional to the momentary excitation of the observed vibrational mode. The signals $S^{\text{inc}}(t_D)$ are plotted as a function of delay time t_D for various mixtures with CCl_4. The data points rise to a delayed maximum during the pumping process and decay exponentially providing the desired population lifetime T_1. For the neat liquid CH_3CCl_3 (full circles) we find a time constant of $T_1=5.2$ psec. This value should be compared with the dephasing time $T_2/2=1.2$ psec of the same molecule and vibrational mode which was discussed in connection with Fig. 26.

The question now arises of which physical processes determine the population lifetime T_1 in the liquid state. We shall demonstrate in a number of experiments that vibrational energy can decay via inter- and intramolecular processes. In several cases it was possible to see directly part of the decay routes of the excited mode.

A straightforward demonstration of the importance of intermolecular processes is given by the concentration dependence of the population lifetime of CH_3CCl_3 depicted in Fig. 34 (Laubereau *et al.*, 1973). It is readily seen from the figure that the population lifetime increases strongly from 5.2 psec to 29 psec when the mole fraction x of CH_3CCl_3 decreases from 1.0 to 0.4. Since CCl_4 has low-lying molecular vibrational levels ($\tilde{\nu}<800$ cm^{-1}) as compared to the excited ν_H vibration at 2939 cm^{-1}, the interaction between the two different types of molecules is expected to be small. We shall return to the population lifetime of the ν_H vibration of CH_3CCl_3 below. We note briefly that the spontaneous Raman linewidth of the ν_H vibration in $CH_3CCl_4:CCl_4$ mixtures shows a small concentration effect of the order of 10%; i.e., it is not possible to deduce population lifetimes from the spontaneous Raman linewidth.

2. Energy transfer and redistribution between vibrational states

We continue with the discussion of experimental investigations which provide direct information concern-

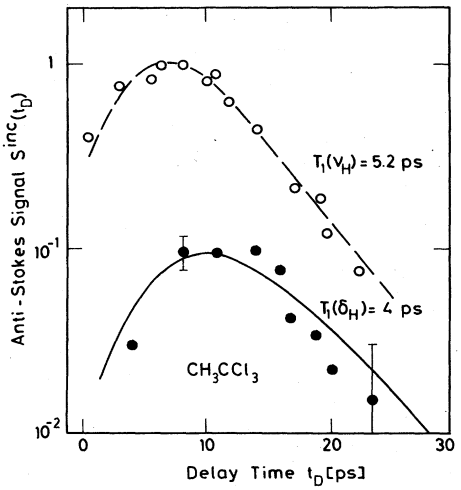

FIG. 35. Incoherently scattered probe signals measured in CH_3CCl_3. The upper curve (○) represents the temporal occupation of the laser-excited ν_H vibration at 2939 cm^{-1}. The lower curve (●) represents the occupation of the δ_H vibration at 1450 cm^{-1}. The curves through the experimental points are calculated.

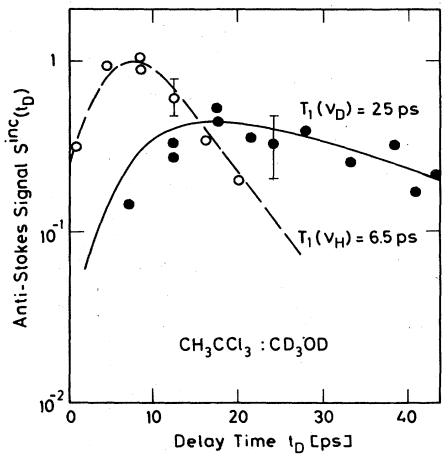

FIG. 36. Incoherent probe signals of $CH_3CCl_3 : CD_3OD$ (with mole fraction 0.6 of CH_3CCl_3). The open circles represent the occupation of the primary excited ν_H vibration (2939 cm^{-1}) of CH_3CCl_3. Vibrational energy transfer leads to subsequent occupation of the ν_D vibration (2200 cm^{-1}) of CD_3OD (closed circles).

ing vibrational energy relaxation processes in liquids.

Evidence for the decay of high-lying vibrational states to lower energy levels is presented next. It is well known that CH stretching modes correspond to a frequency of $\nu_H \sim 3000$ cm^{-1}, while the CH bending modes have approximately half the energy of $\delta_H \sim 1500$ cm^{-1}. As a result, a decay of a primarily excited stretching mode via bending modes is expected. This notion was confirmed experimentally for CH_3CCl_3 (Laubereau *et al.*, 1973) and for ethanol (Alfano and Shapiro, 1972; Laubereau *et al.*, 1974). In Fig. 35 we present data for pure CH_3CCl_3. The spontaneous anti-Stokes signal is plotted for two frequencies. The upper curve (open circles) corresponds to a frequency shift of $\nu_H = 2939$ cm^{-1}; it gives information on the degree of occupation of the primary excited vibrational mode. The value of $T_1 = 5.2$ psec has been discussed above. Of interest are the scattering data at a frequency shift of ~1450 cm^{-1} (full circles). These data points are a measure of the occupation density of the δ_H bending modes. It is seen from the figure that the bending modes are populated as a result of the decay of the higher-lying stretching modes. The ratio of the maxima of the initial and the lower mode indicates that one vibrational quantum at ν_H produces two quanta at δ_H with high efficiency.

The following experiment was designed to give direct evidence for intermolecular energy transfer in liquid systems (Laubereau *et al.*, 1973). The ν_H stretching mode at 2939 cm^{-1} was first excited in the mixture $CH_3CCl_3 : CD_3OD$ with $x = 0.6$ of CH_3CCl_3. The vibrational decay of this mode was monitored at the corresponding frequency and found to have a time constant of $T_1 = 6.5$ psec (open circles in Fig. 36). Then the occupation density of the stretching mode of the deuterated alcohol at $\nu_D = 2227$ cm^{-1} was measured. The full circles in Fig. 36 clearly show the rise and decay of the population of this lower-lying mode. Knowing the spontaneous scattering cross section of the higher and lower vibrational modes and taking the ratio of the corresponding maxima from the curves of Fig. 36, we are able to estimate the transfer rates of the vibrational decay processes. Our calculations indicate highly efficient vibrational transfer processes $\nu_H \rightarrow \nu_D$ and $\nu_H \rightarrow \delta_H$ in this liquid system.

In Fig. 37, the normal vibrational modes are depicted for four molecules, CH_3CCl_3, CD_3OD, CCl_4, and CH_3I. The decay of the excited ν_H stretching mode into two δ_H bending modes is marked by two arrows. The energy transfer from $\nu_H = 2939$ cm^{-1} of CH_3CCl_3 to $\nu_D = 2227$ cm^{-1} of CD_3OD and $\nu_{Cl} = 713$ cm^{-1} of CH_3CCl_3 is also indicated in the figure. We stress the near energy resonance of the energy transfer process in the mixed liquid system.

With increasing size of a molecule the density of vi-

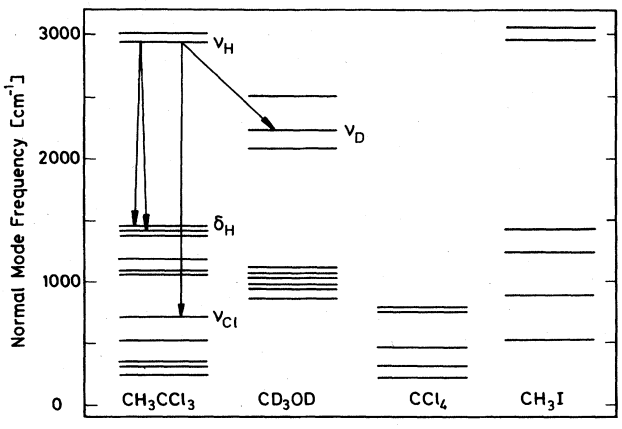

FIG. 37. Energy values of the normal modes of vibrations of CH_3CCl_3, CD_3OD, CCl_4, and CH_3I. Arrows indicate investigated or discussed transitions.

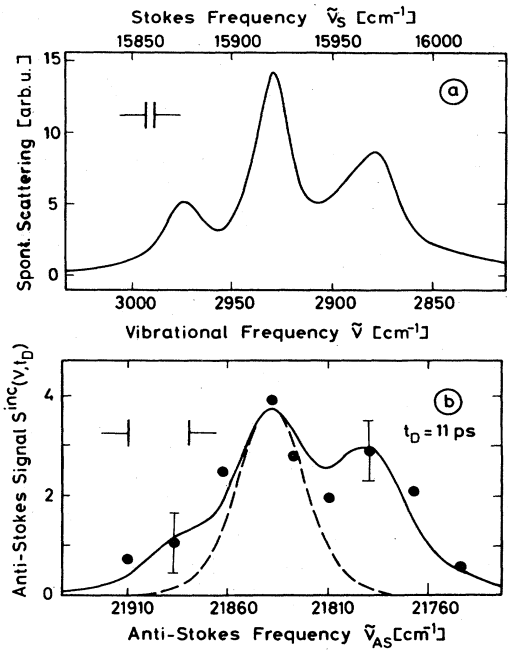

FIG. 38. *Top*: The spontaneous Raman–Stokes spectrum of the CH stretching vibrations of ethanol measured with a cw argon laser. *Bottom*: Incoherent anti-Stokes probe signals vs frequency taken with a delay time of 11 psec (●). Broken curve indicates the expected profile of the primarily excited vibrational mode at 2928 cm^{-1}. The solid curve is calculated assuming quasiequilibrium between vibrational states around 2900 cm^{-1}.

brational states rises very rapidly for higher energy. The rate of redistribution of vibrational energy between neighboring energy states is an important question in molecular physics. We have performed a number of experiments with different molecules which allow us to observe the rapid energy redistribution process.

As a first example we report on investigations of ethanol CH_3CH_2OH (Laubereau *et al.*, 1974). This molecule has five vibrational modes (one being degenerate) around 2900 cm^{-1}. The spontaneous Raman–Stokes spectrum in this frequency range (measured with a cw argon laser) is depicted in Fig. 38(a). Three resolved bands and one shoulder correspond to the four vibrational modes. In the stimulated Raman process, the most intense Raman band at 2928 cm^{-1} has the largest gain and, as a result, this vibrational mode is primarily excited. In Fig. 38(b), anti-Stokes signals of the delayed (11 psec) interrogating pulses are presented as a function of frequency. The data points clearly indicate that the observed spectrum is much broader (150 cm^{-1}) than expected from the occupation of just the primarily excited vibrational level at 2928 cm^{-1} (the broken line in Fig. 38(b) is calculated for an instrumental resolution of 30 cm^{-1}). The curve through our experimental point is calculated under the assumption that quasiequilibrium exists between the vibrational states around 2900 cm^{-1}. We conclude from these data that shortly after the excitation a vibrational redistribution has occurred, which is followed by energy decay to low-energy states. More detailed investigations suggest a redistribution time of approximately 1 psec (Laubereau *et al.*, 1974).

B. Investigations with infrared excitation

With tunable infrared pulses we are in a position to excite any vibrational mode which has a sufficiently large transition dipole moment. The occupation number n, which can be achieved in the medium, depends upon the absorption coefficient γ of the specific vibration. Typical numbers for the following investigations follow: Our infrared pulses around 3000 cm^{-1} have approximately 10^{15} photons. For absorption coefficients of several 100 cm^{-1} we obtain occupation numbers of several 10^{-3} in a focused beam. Spontaneous Raman probe scattering is possible with diluted liquid systems of several 10^{-2} concentration. Using the fluorescence probe technique, the sensitivity of the system is higher by three orders of magnitude (see below).

Let us return to the investigations of ethanol (Spanner *et al.*, 1976). In Fig. 39, the anti-Stokes probe signal with frequency shift of 2930 cm^{-1} (spectrometer bandwidth of 85 cm^{-1}) is plotted as a function of delay time t_D. The sample consisted of 4% of CH_3CH_2OH in CCl_4. An infrared pulse at $\tilde{\nu} = 2930$ cm^{-1} excites the CH_3 strectching mode of ethanol. The scattered probe signal shows two interesting features: a first rapid decay with a time constant of approximately 1 psec, and a considerably slower relaxation time of ~40 psec. Taking into consideration previous investigations of ethanol (Laubereau *et al.*, 1974), we interpret the results of Fig. 39 as follows: (i) During and immediately following the infrared excitation, rapid distribution of population occurs between 11 degrees of freedom, five neighboring CH stretching modes at $v = 1$, and six CH bending modes at $v = 2$. The total spontaneous scattering cross section of these modes is much smaller than that of the primary excited state. The reduced total scattering cross section leads to a de-

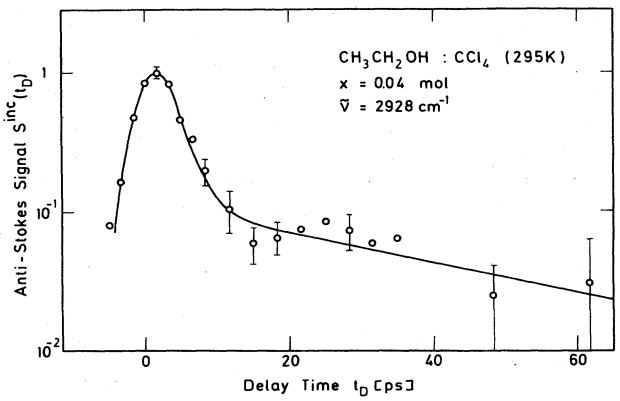

FIG. 39. Incoherent anti-Stokes probe signals with frequency shift of ~2900 cm^{-1} vs delay time. Sample: 4 mol % CH_3CH_2OH in CCl_4. The CH_3 stretching mode was excited by an infrared pulse. The first fast signal decay is related to rapid energy redistribution between neighboring energy states. The slower decay corresponds to energy relaxation to lower-lying bending modes.

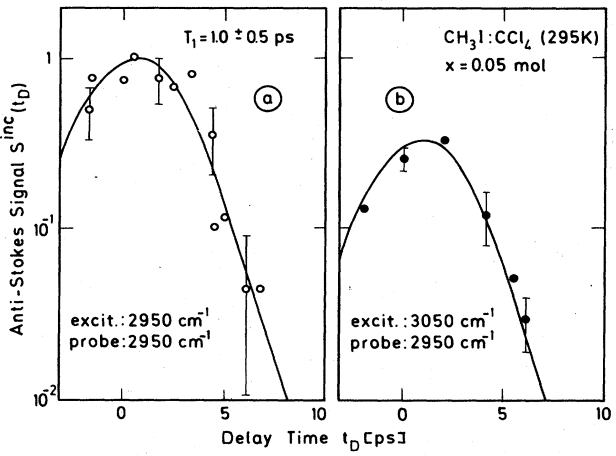

FIG. 40. Incoherent anti-Stokes signals of CH_3I measured at a frequency shift of 2950 cm^{-1}. (a) The molecule is excited by an infrared pulse of $\tilde{\nu} = 2950$ cm^{-1} (open circles). (b) The infrared pumping pulse has a frequency of $\tilde{\nu} = 3050$ cm^{-1}, exciting the highest vibrational mode of CH_3I. Note the small time delay necessary for energy exchange.

crease of the scattered probe signal. (ii) The slower vibrational energy relaxation results from decay to lower-lying bending modes. We recall that in pure ethanol the decay of ν_H was measured to have a time constant of $T_1 = 22$ psec. Obviously, the presence of intermolecular contributions in the pure liquid gives rise to the shorter population lifetime.

Next, we present investigations of CH_3I, a relatively small and well studied molecule (Spanner *et al.*, 1976). The high symmetry (C_{3v}) gives rise to six fundamental vibrations, three of which are totally symmetric and three of which are degenerate (see Fig. 37). All modes are Raman and infrared active (Herzberg, 1945). The highest vibrational modes at $\nu_4(e) = 3050$ cm^{-1} and $\nu_1(a_1) = 2950$ cm^{-1} correspond to the asymmetric and symmetric CH_3 stretching modes, respectively. The CH bending mode at $\nu_5(e) = 1440$ cm^{-1} is degenerate and in Fermi resonance with the ν_1 vibration. In Fig. 40, the anti-Stokes scattered probe signal with frequency shift of 2970 cm^{-1} is plotted versus delay time t_D. These data monitor the temporal development of the ν_1 mode, the lower of the two CH_3 vibrations. We have performed two experiments: First, we excited the ν_1 mode of the CH_3I molecule with an infrared pulse centered at frequency of 2950 cm^{-1}. The rapid rise and decay of the scattered probe signal (open circles) suggest a fast disappearance of the population of this excited vibration. Second, we tuned the frequency of the infrared pulse to 3050 cm^{-1} in order to excite the higher ν_4 vibration of CH_3I. The scattered probe signals are shifted by approximately 1 psec and decay again with the same slope of $T_1 = 1.0$ psec (closed circles). We feel that the shift of the maxima of the two curves gives direct evidence for the short time required to establish energy redistribution between the two neighboring CH_3 stretching modes. To interpret our data, we calculated a simple model with an energy transfer rate $1/T_r$ between the two CH_3 modes and two separate transfer rates $1/T(\nu)$ between the individual CH_3 modes and other energy states of the molecule. In this model the observed decay rate of the lower ν_1 mode has the form $1/T_1 = 1/T_r + 1/T(\nu_1)$. We emphasize that the calculated time constants have to be compatible with a number of experimental observations: the position and relative height of the maxima in Figs. 40(a) and 40(b), the slopes of the curves in Fig. 40, and the limits given by the spontaneous Raman linewidths. Under these conditions, our model gives the following values: $T_r \simeq 1.5$ psec, $T(\nu_1) \simeq 3$ psec, and $T(\nu_4) \simeq 0.5$ psec. The calculated curves in Figs. 40(a) and 40(b) are based on these three time constants. The agreement with the data points is quite satisfactory. Our observations indicate that vibrational energy of the CH_3 stretching modes relaxes very rapidly in CH_3I. Overtones and combination modes are expected to provide the primary transfer and decay channels. Theoretical results indicate that interaction with rotation and neighboring vibrational levels is effective on account of coriolis coupling and strong Fermi resonance (Laubereau *et al.*, 1978).

A final remark should be made concerning the spontaneous Raman band of the ν_1 mode of CH_3I. Experimentally, we find a linewidth of $\delta\nu = 5$ cm^{-1}, which, assuming a homogeneously broadened Lorentzian line, corresponds to a time constant of 1.0 psec. Comparing this number with the short T_1 value obtained in the preceding experiment, we see readily that the energy relaxation provides a considerable contribution to the spontaneous Raman linewidth.

The third investigation in this section introduces a new two-pulse fluorescence technique to monitor the momentary vibrational excitation (Laubereau, Seilmeier, and Kaiser, 1975). The theory of this probing process was discussed in Sec. III.C. We briefly repeat. A first ultrafast infrared pulse (~3 psec) of frequency ν_1 pumps vibrational modes and a second delayed interrogating pulse of frequency ν_2 promotes the vibrationally excited molecules to the first excited singlet state S_1. The observed fluorescence originating from the S_1 state is a direct measure of the instantaneous degree of excitation. The frequencies ν_1 and ν_2 have to be adjusted to the energy states of the molecules under investigation. In particular, the frequency ν_2 is selected in such a way that thermally occupied energy states of $E < h\nu_1$ lead to a small fluorescence signal.

Our first measurements using the resonance probing technique were made with coumarin 6, a relatively large molecule with 43 atoms (see Fig. 41 top). This molecule was selected for a number of reasons: The quantum efficiency is high; the solubility in CCl_4 (no vibrations > 800 cm^{-1}) is good; the molecule is available in high purity; and with ν_1 around 3000 cm^{-1} we are able to work with $\tilde{\nu}_2 = 18\,910$ cm^{-1}, the second harmonic frequency of our Nd-glass laser. In these experiments the molecule was excited with infrared pulses of $\tilde{\nu}_1 = 2970$ cm^{-1}. The normalized fluorescence signal $F(t_D)$ is plotted versus delay time between infrared pump and green probe pulse in Fig. 42. We point to the small concentration of $4 \times 10^{-4} M$. The observed fluorescence rises to a maximum during the infrared excitation and decays first rapidly with a time constant of 1.3 psec and later with a longer time value of 8 psec. Tentatively

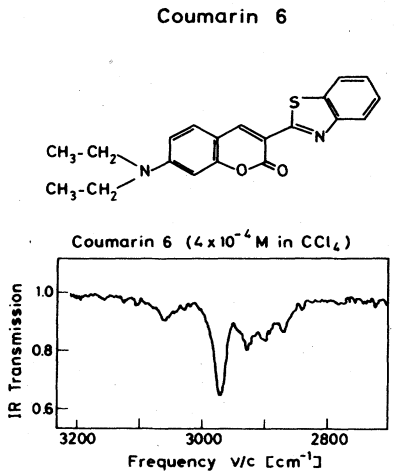

FIG. 41. *Top*: The coumarin 6 molecule. *Bottom*: Infrared absorption spectrum around 3000 cm^{-1} of coumarin 6 in CCl_4.

the short time constant corresponds to a redistribution process to the many neighboring vibrational energy states and/or to a decay to lower energy levels. The longer time value appears to be connected with a not yet identified long-lived energy state. This picture is supported by the fact that we observe a considerably smaller effective transition probability to the S_1 state (smaller Franck-Condon factor) during the early fast decay than during the later slow relaxation. In this context some recent experimental observations on nile-blue-*A*-oxazone are of interest. Seilmeier *et al* (1978) tuned the frequency ν_1 of the infrared pulse between 2700 and

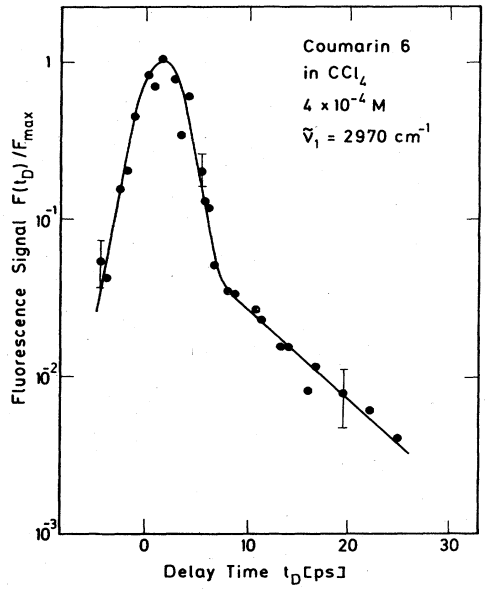

FIG. 42. Normalized fluorescence signal vs delay time t_D between infrared pump pulse and green probe pulse. The molecule is excited by an infrared pulse at 2970 cm^{-1}. The fluorescence signal is a measure of the instantaneous vibrational excitation in the electronic ground state.

3400 cm^{-1} and correspondingly the frequency ν_2 holding the sum $\nu_1 + \nu_2$ constant at 18910 cm^{-1}. In this way, more than 10 distinct peaks in the fluorescence signal were found. Tentatively, these modes are assigned to mixed states of low lying bending modes with overtones of the skeletal vibrations of the chromophore. The good coupling of the latter modes to the π electrons gives rise to large Franck-Condon factors and large matrix elements for the transition to the S_1 state.

A final word concerning the time resolution of the two-pulse technique of Fig. 42 appears to be appropriate. Replacing the cell containing the coumarin molecules by a nonlinear crystal (e.g., $LiNbO_3$), we have measured the parametrically generated sum frequency $\nu_1 + \nu_2$ at the intersection of the two pulses. The energy of this sum signal was determined as a function of delay time between the two incident pulses of frequency ν_1 and ν_2. The signal curve gave two important data: the time zero, where the peaks of the two pulses coincide, and the time resolution resulting from the overlap of the wings of the two pulses. Experimentally we found a time resolution of better than 0.5 psec (Spanner *et al.*, 1977). This result suggests that the two time constants observed above are true parameters of the coumarin molecule.

A different approach to learning more about relaxation times in the electronic ground state was reported by Ricard and Ducuing (1975). Rhodamin 6G in alcohols was strongly excited by a first intense pump pulse at 18 800 cm^{-1}. The specimen was partially bleached by transitions to the first singlet state S_1. After a time delay of 200 psec, a second preparing pulse at 17 800 cm^{-1} forced, by stimulated emission, the molecules to return to the vibrational manifold of the electronic ground state. A third weak pulse at 18 800 cm^{-1} monitored the recovery of the ground-state absorption. Relaxation times of 4 and 3 psec were estimated for rhodamin 6G in ethanol and 1-butanol, respectively. We note that this experiment reports on the ground-state recovery via a higher-lying vibrational manifold. Our experiments with ultrafast infrared pulses are concerned with the time development of vibrational modes which were excited within a (narrow) known frequency range.

VII. VIBRATIONAL RELAXATION TIMES IN SOLIDS

In solids, it is possible to excite optical phonons by the stimulated Raman process. The phonon dispersion branches $\omega(k)$ are known for many crystals and the excited phonons are well defined. With our pump pulse of $\lambda \sim 1$ μm or $k = 2\pi/\lambda \sim 10^5$ cm^{-1} we excite phonons very near to the center of the Brillouin zone. In the experiments discussed here, optical phonons are excited by a first pump pulse and the decay of the excitation is monitored with delayed probe pulses using coherent probe scattering in a properly calculated phase-matched geometry. There are two physical processes which give rise to a decay of the probe signal: (i) The generated phonons decay into phonons of lower energy via anharmonic terms of the lattice potential. For instance, one TO phonon decays into one TA and one LA phonon of approximately half the energy. Conservation of crystal mo-

mentum and selection rules restrict the decay routes to well-defined terminal states. This three-phonon process has been discussed in the literature and is believed to be the dominant phonon decay mechanism (Orbach and Vredevoe, 1964; Orbach, 1966 and 1967). (ii) The collimated pump beam generates phonons within a very small volume of k space. Only phonons with these k vectors are monitored by the phase-matched probing technique. The probe signal decays when the phonons change their wave vectors, for instance, by scattering on lattice imperfections in a diffusive process or by interaction with acoustic phonons of very small energy in a four-phonon process. Since the dispersion of optical phonons is small over a considerable part of k space, the excited phonons might change their k vector along the phonon branch without significant loss of energy. Such phonon processes have been very rarely discussed previously, and to our knowledge there is no experimental evidence for this phenomenon. The coherent probing technique does not distinguish between the two processes (i) and (ii).

One difference between liquids and solids should be noted. In liquids, we start with individual molecules which are characterized by a two-level system. The excitation leads to a moderate excess population of the first vibrational state with occupation number n. Some small intermolecular coupling is introduced later in this paper (Sec. III.A.5). In solids, we study optical phonons, a collective excitation of the crystal lattice with harmonic oscillator levels. The optical pump beam excites a small number of lattice modes with very large phonon occupation. Numerical examples of phonon occupation numbers are given in Sec. VII.A.

The differential equations for the vibrational excitation e.g., Eqs. (31) to (33), and the probing technique, e.g., Eq. (105) with $s_1 = 1$, are also valid for solids as has been confirmed experimentally.

We have investigated three types of lattice vibrations: the fundamental TO phonon of diamond; the internal vibration (A_{1g}) of CO_3^{--} in $CaCO_3$; and a polariton mode of GaP.

A. Fundamental TO phonon in diamond

The phonon dispersion of diamond is well established from inelastic neutron scattering (Warren *et al.*, 1965 and 1967). There is one TO phonon branch in the diamond lattice. By stimulated Raman scattering, one excites TO phonons at $\tilde{\nu}_P = 1332\ \mathrm{cm}^{-1}$ very near to the center of the Brillouin zone. It is interesting to estimate the number of strongly excited modes and the phonon occupation number n_0. Our highly collimated and monochromatic pump beam generates phonons within a beam divergence of 2×10^{-2} rad and within $\Delta k \simeq 20\ \mathrm{cm}^{-1}$. From the equation $N_m = k^2 \Delta k \Delta\Omega (2\pi)^{-3}$ we estimate a density of optical modes of $N_m = 10^7$ modes/cm^3. Considering the small excitation volume of high phonon density ($\sim 10^{-5}$ cm^3), the number of modes participating in the excitation process is of the order of 100. Our pump pulse produces a phonon density of $N_0 \sim 10^{17}\ \mathrm{cm}^{-3}$, which gives a phonon occupation number of $n_0 = N_0/N_m = 10^{10}$; i.e., 10^{10} quanta are generated per mode via the stimulated scattering process. A comparison with the thermal equilibrium value $n_0^T \simeq 10^{-3}$ (at 300 K) indicates a high degree of excitation exceeding the thermal value by a factor of 10^{13}. Experiments have been performed to study the relaxation process of these hot phonons (Colles and Giordmaine, 1971).

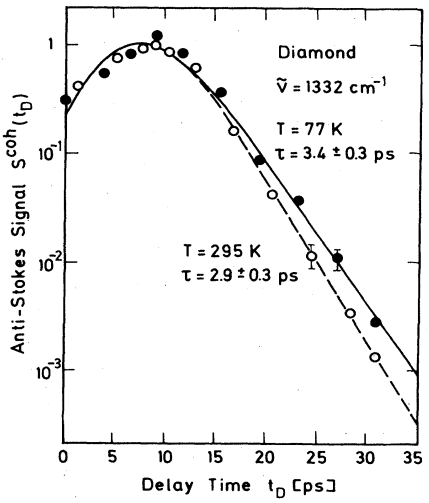

FIG. 43. Coherent anti-Stokes scattering signal of the *TO* phonon of diamond vs delay time t_D for two crystal temperatures, 77 K (full circles) and 295 K (open circles).

In Fig. 43 the coherent anti-Stokes probe signal is plotted versus delay time t_D for 300 and 77 K (Laubereau *et al.*, 1971). The delayed maximum of the excitation and the exponential decay (over three orders of 10) allow a direct determination of the vibrational lifetime. Time constants of 2.9 ± 0.3 psec and 3.4 ± 0.3 psec are found for 295 and 77 K, respectively. A comparison with time constants deduced from the linewidths of spontaneous Raman scattering gives very good agreement with our directly measured lifetimes. This result suggests that our hot phonons decay with the same time constant as phonons excited at the low power level of spontaneous Raman experiments. To understand this finding, one has to consider the large number of 8.8×10^{22} modes/cm^3 in one phonon branch which participates in the thermal vibration. The total rms amplitude of the C atoms at 77 K is approximately 0.2 A (James, 1959), while the vibrational amplitude of our small number of modes is estimated to be 10^{-4} Å, i.e., less than 10^{-3} of the thermal amplitude. It is not surprising that our hot phonons decay via the same anharmonic terms as the thermal TO phonons.

Detailed calculations exist on the lattice dynamics of the diamond lattice (Bilz, 1978). These calculations suggest that the relaxation times measured here correspond to the energy decay of the TO phonon into two acoustic phonons.

B. Internal A_{1g} vibrational relaxation of CO_3^{--} in $CaCo_3$

Calcite has a complicated phonon spectrum with 27 phonon branches (Plihal, 1973). The intense pump pulse excites via stimulated Raman scattering the internal A_{1g} mode of the CO_3^{--} islands with $\nu_L = 1086\ \mathrm{cm}^{-1}$ and

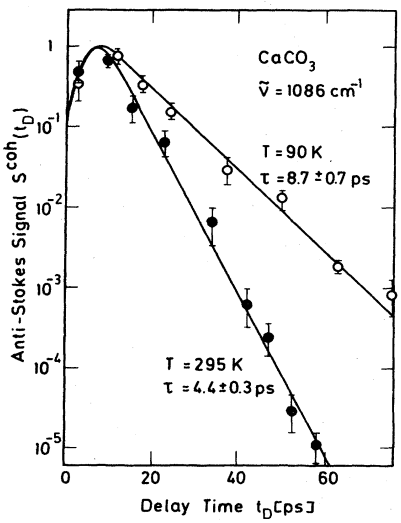

FIG. 44. Coherent anti-Stokes probe signal of a $CaCO_3$ crystal vs time t_D for two crystal temperatures, 90 K (open circles) and 295 K (full circles). The internal A_{1g} mode of the CO_3^{--} group at $\tilde{\nu} = 1086$ cm^{-1} is investigated.

wave vector $k_L = 1.1 \times 10^4$ cm^{-1}. The coherent probe scattering technique takes advantage of the optical birefringence of the trigonal $CaCO_3$ crystal (Giordmaine and Kaiser, 1966). When the pump pulse at ν_L propagates as an ordinary beam through the specimen, an extraordinary probe pulse at $2\nu_L$ gives excellent phase matching for probe scattering. Details of the experimental system and the scattering geometry are discussed by Laubereau, Wochner, and Kaiser (1975). In Fig. 44, the probe scattering signal is presented as a function of delay time between pump and probe pulse. The signal curve rises to a maximum shortly after the peak of the pump pulse, since time is required to build up the lattice excitation to its maximum value. For larger values of t_D the excitation process rapidly terminates and we measure the free relaxation of the internal vibration. We wish to emphasize the large range of experimental data. We are able to measure the exponential decay of the signal over five orders of 10 and follow in this way the vibrational relaxation with good accuracy over a period of 60 psec. From the slopes of the signal curves we obtain time constants of 4.4 ± 0.3 psec and 8.7 ± 0.7 psec at 295 and 90 K, respectively. The curves in the figure are calculated according to the theory outlined above; the experimental parameters of the pump and probe pulse are used together with values of the time constants deduced from the exponential slopes.

Experimental data are available for the spontaneous Raman linewidth of the same vibrational mode investigated here (Park, 1966, 1967; Kiefer and Laubereau, 1978). Assuming a Lorentzian line profile, the corresponding time constants are calculated to be 4.4 ± 0.2 psec and 7.8 ± 0.9 psec at 295 and 90 K, respectively. The good agreement with our experimental relaxation times should be noted. In earlier work by Alfano and Shapiro (1971) larger time constants were reported.

The physical processes responsible for the observed phonon decay time are not certain at present. The excited optical mode at 1086 cm^{-1} is far above the acoustic branches which have energies $\lesssim 100$ cm^{-1}. This fact rules out a decay process similar to the situation in diamond. Three-phonon decay processes to lower optical branches are possible according to symmetry selection rules and conservation laws. One example is $1086\ (A_{1g}) \rightarrow 712\ (E_u) + 376\ (E_u)$. A different vibrational process, the change in phase relation between individual CO_3^{--} complexes, leads also to a decay of the observed coherent scattering signal. This relaxation process has some analogy to the case of polyatomic liquids. Measurement of the energy relaxation, i.e., of the incoherent probe signal, would be of great value in learning more about the relaxation process of internal molecular modes in crystals.

C. Polariton mode in GaP

GaP has the simple zinc blende structure with one TO phonon branch. The single lattice resonance is both Raman and infrared active. In recent years, the polariton mode (a mixed phonon–photon state) of GaP has received considerable attention. The energy dispersion $E(\omega)$ is well established for this compound (Henry and Hopfield, 1965). Very little is known about the lifetime of the polariton along its dispersion curve. In a first investigation we measured the relaxation time of one definite polariton which is still close to the pure TO lattice mode (Laubereau, von der Linde, and Kaiser, 1973).

The polariton mode was coherently excited by two intense picosecond light pulses. One pulse was generated by a mode-locked Nd-glass laser and the second one was obtained by a Raman–Stokes process in $SnCl_4$. The frequency difference between the pump pulses determines the frequency ω_0 and the beam geometry selects the wave vector k_0 of the polariton. The insert of Fig. 45 shows part of the polariton dispersion curve of GaP indicating the position of the investigated polariton. The material excitation was monitored by a third probe pulse of variable time delay with respect to the two pump pulses. The phase-matched anti-Stokes scattering of the probe pulse is presented as a function of delay time t_D in Fig. 45. The delayed maximum of the scattered signal is due to the transient nature of the pumping process. Of interest is the later part of the scattering curve which corresponds to the free decay of the excited mode. Our experimental data show directly an exponential decay over two orders of magnitude. A time constant of 5.5 ± 0.5 psec is inferred from the figure.

The spontaneous Raman line of the TO phonon of GaP shows a complex line shape of a width of approximately 4 cm^{-1} (Barker 1968; Ushioda and McCullen, 1972; Hon and Faust, 1972). This Raman line is not fully understood at the present time. Infrared reflection data and measurements of surface polaritons in GaP suggest a lifetime of the TO phonon of 4.8 psec (Kleinmann and Spitzer, 1960; Marschall and Fischer, 1972). With this time constant we estimate for a simple polariton model that the polariton investigated here has a relaxation

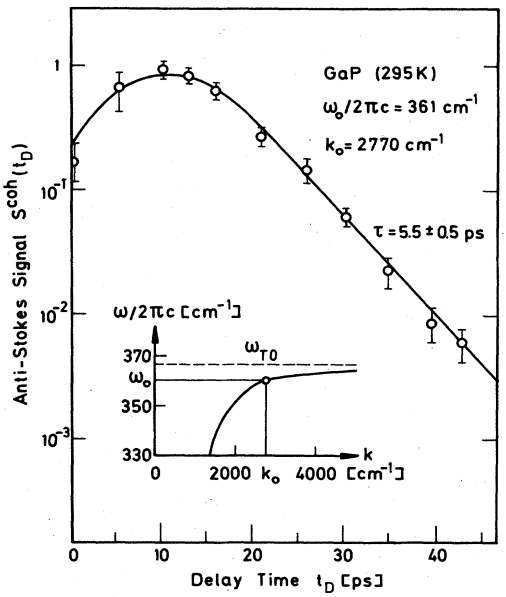

FIG. 45. Anti-Stokes scattering signal of a GaP crystal vs time t_D. The insert shows part of the polariton dispersion curve and indicates the observed mode by an open circle.

time of ~5 psec. The good agreement with our experimental time constant of 5.5 psec indicates that we measured indeed the lifetime of a polariton mode with our time-resolved probing technique.

VIII. CONCLUDING REMARKS

In this paper we have reported on a series of independent experiments concerning ultrafast vibrational processes in condensed matter. To achieve these data we had to develop new experimental tools which were discussed in the first part of this article. The brief excitation of the vibrational system is the first step in our investigations. The coherent excitation via stimulated Raman scattering plays an important role in various experiments. Stimulated Raman scattering prepares the vibrational system in such a way that subsequent probing with a second ultrashort light pulse allows a detailed study of the spatial distribution and the temporal development of the material excitation. The time evolution of the excitation has received special consideration in this paper since it enables us to learn directly about the dynamic behavior of the molecular system. One important time constant, the dephasing time T_2, was studied for a variety of vibrations and molecules. It was shown that the temporal decay of the coherently prepared vibrational system gives direct information of the value of T_2. We have demonstrated in a number of examples that care has to be taken in performing these experiments. Vibrational modes which have a substructure of isotope components or which are inhomogeneously broadened require special attention in the interpretation of the temporal behavior of the measured scattered probe signal. The destructive interference of neighboring vibrational components is able to obscure the true value of the dephasing time. We have developed a technique which allows us to isolate a small group of excited molecules with small frequency spread and to study their time behavior. Highly selective k-matching geometries have proved to be a useful tool for these measurements. We have started to investigate rather complicated vibrational modes and to determine directly the dephasing time of the molecules close to the center of the vibrational distribution. These investigations allow us for the first time to separate homogeneous and inhomogeneous contributions to the measured spontaneous Raman line. In most of these cases, the value of T_2 is the major line broadening factor; i.e., the Raman lines are predominantly homogeneously broadened. We wish to note that we are not allowed to make the reverse statement; the spontaneous Raman linewidth is not a measure of the dephasing time. Without additional information, the isotropic part of a spontaneous Raman line should not be related to a single time constant.

Investigations of the vibrational energy relaxation are believed to be an important contribution to the understanding of dynamical processes in condensed phases. We have developed two excitation processes, stimulated Raman scattering and direct resonant infrared pumping. It is now possible to study a variety of ultrafast vibrational phenomena. Experiments are presented on the population lifetime T_1, on the decay routes of excited vibrational states, on the energy transfer between different molecules, and on the energy redistribution within the same molecules. At the present time, a very limited number of vibrations and molecules has been investigated. The vibrational systems were selected to get a first understanding of different fundamental processes. The population lifetime of several polyatomic molecules was found to be between one and 100 psec. The report of the population lifetime in liquid N_2 of T_1 ~10 sec was certainly a surprise after the dephasing time was established to be $T_2/2 = 75$ psec. It is very difficult for a molecule without dipole moment and without lower energy states to dissipate its high vibrational energy of 2350 cm^{-1}. Of considerable interest is the experimental observation that energy transfer between different molecules occurs very rapidly and very efficiently under near-resonance conditions. Transfer rates of 10^{13} sec^{-1} have been observed. Similarly, the energy redistribution between neighboring vibrational states appears to proceed very fast, with time constants of the order of 1 psec. This observation is of interest for larger molecules or for the higher excited vibrational states where the mode densities become quite large. We were able to observe rapid changes of vibrational population in relatively large dye molecules (~50 atoms per molecule) working under well-defined excitation and probing conditions.

The combined knowledge of dephasing time T_2 and population lifetime T_1 allows us to estimate the pure dephasing time τ_{ph}. We are now able to state which dynamic process determines the homogeneous linewidth. For several molecules (e.g., N_2, CH_3CCl_3) we found $T_2/2 \sim \tau_{ph}$; i.e., the population lifetime plays a negligible or minor role in the dephasing process. The situation is different for the CH_3 stretching vibration of CH_3I,

where the rapid energy decay gives a major contribution to the value of T_2 and, as a result, to the measured spontaneous linewidth.

The various experimental techniques discussed here are applicable to solids as well. Our first results on three crystals are quite limited at present. Coherent probe scattering was used in all cases. It is generally believed that for the TO mode of diamond we have $T_2/2 = T_1$. More dynamic measurements should be made in other crystals.

In summary we wish to say that the investigations presented here have provided a variety of new information on ultrafast molecular processes. We are still at an early stage. Many experiments have to be done which promise to answer still open questions. We consider the field a challenging and intriguing topic of molecular physics.

ACKNOWLEDGMENTS

The authors are indebted to Professor S. Fischer for numerous discussions on molecular relaxation processes. We wish to acknowledge the expert work of A. Seilmeier, K. Spanner, and G. Wochner; their recent experimental results made valuable contributions to different subjects reviewed in this paper.

APPENDIX A: DERIVATION OF THE EQUATIONS OF MOTION

We derive the equations of motions of the vibrational system in terms of a two-level model. A weakly coupled ensemble is considered. The wave function for an individual molecule i may be written

$$\psi_i(t) = a_i(t)\psi_a + b_i(t)\psi_b . \tag{A1}$$

ψ_a and ψ_b denote the first excited vibrational state and the ground state corresponding to eigenvalues of the Hamiltonian of energies $\hbar\omega_0/2$ and $-\hbar\omega_0/2$, respectively. The energy of the system connected to other degrees of freedom (which remain unchanged) is taken as the zero of energy. ω_0 is the transition frequency. Interaction of the vibrational system with an external perperturbation is described by the Hamiltonian

$$H = H_0 + H' , \tag{A2}$$

where H_0 refers to the unperturbed system and H' represents the interaction. The time evolution of the ensemble of two-level systems may be described by a vector r (Feynman, Vernon, and Hellwarth, 1957), the components of which are connected to the elements of the density matrix ρ as follows:

$$\begin{aligned} r_1 &= \rho_{ab} + \rho_{ba} = \overline{a^* b} + \overline{b^* a} , \\ r_2 &= i(\rho_{ba} - \rho_{ab}) = i\,(\overline{b^* a} - \overline{a^* b}) , \\ r_3 &= \rho_{aa} - \rho_{bb} = \overline{a^* a} - \overline{b^* b} . \end{aligned} \tag{A3}$$

The rhs of Eq. (A3) indicates that the elements of the density matrix are readily expressed in terms of the coefficients $a(t)$ and $b(t)$ of the wave function [Eq. (A1)]. The bar indicates that an ensemble average has to be taken. It should be noted that r_1 and r_2 are real quantities whereas ρ_{ab} and ρ_{ba} are complex in general.

The molecular system develops as a function of time according to Eq. (A4):

$$\frac{d\rho}{dt} = \frac{i}{\hbar}[\rho, H] = \frac{i}{\hbar}[\rho H - H\rho] . \tag{A4}$$

Equations (A2)–(A4) give the following equations of motion:

$$\begin{aligned} \frac{dr_1}{dt} &= -\omega_0 r_2 + \frac{i}{\hbar}(H'_{ab} - H'_{ba})r_3 , \\ \frac{dr_2}{dt} &= \omega_0 r_1 - \frac{i}{\hbar}(H'_{ab} + H'_{ba})r_3 , \\ \frac{dr_3}{dt} &= -\frac{i}{\hbar}(H'_{ab} - H'_{ba})r_1 + \frac{1}{\hbar}(H'_{ab} + H'_{ba})r_2 . \end{aligned} \tag{A5}$$

The quantities H'_{ab} and H'_{ba} denote the matrix elements of the perturbation H', e.g., $H'_{ab} = \langle \psi_a | H' | \psi_b \rangle$. Equations (A5) are valid for a perturbation H'_{ab} of arbitrary magnitude. It is assumed that the diagonal elements H'_{aa} and H'_{bb} may be neglected as compared to $\hbar\omega_0/2$. In many practical applications we have $H'_{aa} = H'_{bb} = 0$. In cases where $H'_{aa}, H'_{bb} \neq 0$, these terms produce a shift of the transition frequency ω_0. Redefining H_0 and H', the shift (averaged over time) may be included in H_0.

The physical meaning of the vector r is readily seen from its definition. Equations (A3) indicate that the component r_3 is a measure of the excited-state population and of the energy stored in the two-level system. It will be shown below that the interesting observables of the system are closely connected with the component r_1 and r_3. Defining a vector ω, the components of which are connected to the interaction elements H'_{ab}, H'_{ba} and the transition frequency ω_0, Eqs. (A5) can be written as a vector equation. This equation leads to the well-known spin vector model for magnetic dipole transitions or to the pseudospin vector model for electric dipole transitions.

Equations (A5) represent the response of the two-level systems to an external perturbation. Relaxation processes due to the interaction between the molecules have to be included. This problem has been extensively studied for systems with magnetic dipole interaction (Wangsness and Bloch, 1953; Redfield 1957; Slichter, 1963). It has been shown that Eq. (A4) may be generalized in the following way in order to account for relaxation processes:

$$\frac{d\rho_{\alpha\alpha'}}{dt} = \frac{i}{\hbar}[\rho, H]_{\alpha,\alpha'} + \sum_{\beta,\beta'} R_{\alpha,\alpha',\beta,\beta'}(\rho_{\beta\beta'} - \overline{\rho_{\beta\beta'}}) , \tag{A6}$$

where $\overline{\rho_{\beta\beta'}}$ denotes the equilibrium value of the element $\rho_{\beta\beta'}$. It is important to note that the relaxation terms $R_{\alpha\alpha',\beta\beta'}$ in Eq. (A6) are constant factors. The important terms of the tensor R involve $\alpha - \alpha' = \beta - \beta'$. The symmetry properties reduce R to two parameters:

$$\begin{aligned} R_{aa,bb} &= R_{bb,aa} \equiv -1/T_1 , \\ R_{ab,ab} &= R_{ba,ba} \equiv -1/T_2 . \end{aligned} \tag{A7}$$

T_1 and T_2 are the two relaxation times of interest. Equations (A6) are valid for sufficiently large time constants $T_1, T_2 \gg \tau_C$, where τ_C is a correlation time (see Sec. II.A). The equations of motion which include relaxation processes are

$$\frac{dr_1}{dt}+\frac{r_1}{T_2}=-\omega_0 r_2+\frac{i}{\hbar}(H'_{ab}-H'_{ba})r_3,$$
$$\frac{dr_2}{dt}+\frac{r_2}{T_2}=\omega_0 r_2-\frac{1}{\hbar}(H'_{ab}+H'_{ba})r_3, \tag{A8}$$
$$\frac{dr_3}{dt}+\frac{r_3-\bar{r}_3}{T_1}=-\frac{i}{\hbar}(H'_{ab}-H'_{ba})r_1+\frac{1}{\hbar}(H'_{ab}+H'_{ba})r_2.$$

$\bar{r}_3$ denotes the equilibrium value of the population difference r_3. It is interesting to note that the components r_1 and r_2 which are related to the off-diagonal elements ρ_{ab} are governed by the dephasing time T_2. The component r_3 is connected to the population lifetime T_1. Equations (A8) are quite general with respect to the perturbation H' and will be applied to two specific interaction processes.

1. Raman interaction

We wish to treat a situation where the external electromagnetic field does not contain resonant components of frequency ω_0; i.e., electric dipole transitions are negligible. The interaction occurs via the Raman polarizability $\partial\alpha/\partial q$ leading to the perturbation Hamiltonian of Eq. (A9) [Eq. (4) of Sec. II.A.]:

$$H'=-\tfrac{1}{2}q\sum_{h,i}\left(\frac{\partial\alpha}{\partial q}\right)_{hi}E_hE_i \tag{A9}$$

so that

$$H'_{ab}=-\tfrac{1}{2}\sum_{h,i}\left(\frac{\partial\alpha}{\partial q}\right)_{hi}E_hE_iq_{ab}, \tag{A10}$$

where q_{ab} denotes the transition element $\langle\psi_a|q|\psi_b\rangle$ of the normal mode operator q. To simplify the discussion we choose the phases of the eigenfunctions ψ_a and ψ_b in such a way that q_{ab} is real, i.e., $q_{ab}=q_{ba}$. Using the properties of the density matrix we see that the expectation value of $\langle q\rangle$ is given by

$$\langle q\rangle=\mathrm{Tr}(\rho q)=r_1q_{ab}. \tag{A11}$$

We introduce the excess population of the upper vibrational state n and relate it to the component r_3 of the vector r (which represents the instantaneous state of the vibrational system):

$$r_3=2(n+\bar{n})-1. \tag{A12}$$

Substituting the quantities r_1 and r_3 in Eqs. (A8) and eliminating r_2, we get the following results for small damping, $\omega_0T_2\ll 1$:

$$\left(\frac{d}{dt^2}+\frac{2}{T_2}\frac{d}{dt}+\omega_0^2\right)\langle q\rangle=\frac{\omega_0}{\hbar}q_{ab}^2\sum_{h,i}\left(\frac{\partial\alpha}{\partial q}\right)_{hi}E_hE_i[1-2(n+\bar{n})], \tag{A13}$$

$$\frac{dn}{dt}+\frac{n}{T_1}=\frac{1}{2\hbar\omega_0}\sum\left(\frac{\partial\alpha}{\partial q}\right)_{hi}E_hE_i\frac{d\langle q\rangle}{dt}. \tag{A14}$$

Equations (A13) and (A14) correspond to Eqs. (5) and (7) of Sec. II.A. For the transition element q_{ab} the expression

$$q_{ab}\simeq(\hbar/2m\omega_0)^{1/2} \tag{A15}$$

was introduced for a harmonic vibration. Partial derivatives are used in Eqs. (5) and (7) on account of the spatial dependence of the physical variables $\langle q\rangle$ and n.

2. Electric dipole transition

The resonant interaction of an external electromagnetic field E with the vibrational system via dipole coupling is described by the Hamiltonian [see Eq. (67), Sec. II.E]

$$H'=-\tilde{p}E_{\mathrm{loc}}\cos\theta. \tag{A16}$$

The interaction matrix element of interest is given by

$$H'_{ab}=-p_{ab}E_{\mathrm{loc}}\cos\theta, \tag{A17}$$

where p_{ab} denotes the electric dipole matrix element $p_{ab}=\langle\psi_a|\tilde{p}|\psi_b\rangle$. p_{ab} is assumed to be real, which can be achieved by a proper choice of the phases of the basis ψ_a and ψ_b. The expectation value of the transition dipole moment is connected with the component r_1 of the pseudospin vector [compare (A11)]:

$$\langle\tilde{p}\rangle=\mathrm{Tr}(\rho\tilde{p})=r_1p_{ab}. \tag{A18}$$

The excess population n of the upper vibrational state is related to the vector component r_3 as in the case of the Raman interaction [see Eq. (A12)]. Substitution of Eqs. (A18) and (A12) in Eqs. (A8) and elimination of r_2 yield an equation for $\langle\tilde{p}\rangle$. We use the local field:

$$E_{\mathrm{loc}}=\tfrac{1}{3}(\bar{\mu}^2+2)E \tag{A19}$$

and the ansatz of Eq. (68) (Sec. II.E). Neglecting second-order derivatives yields Eqs. (69) and (70) for the amplitude $\langle p\rangle$ of the electric dipole moment.

APPENDIX B: SPONTANEOUS RAMAN SCATTERING

For the reader who is not familiar with Raman scattering, several definitions and relationships are summarized in this appendix.

Measurements of the spontaneous Raman effect are conveniently done with a linearly polarized laser (intensity I_L and frequency ω_L). The scattered light is observed at 90° scattering angle in a plane perpendicular to the electric vector of the incident light. With the help of a polarizer, two components of the scattered light are recorded within a small solid angle of acceptance: (i) scattered light of intensity $I_\parallel$ being polarized parallel with respect to the laser, and (ii) scattered light of intensity $I_\perp$ with perpendicular polarization. $I_\parallel+I_\perp$ is the total scattered intensity of the Raman line centered at frequency $\omega_L-\omega_0$. The ratio of the scattered to the incident light intensity per molecule, per unit solid angle and length, determines the total differential scattering cross section of Raman scattering,

$$\partial\sigma/\partial\Omega=(I_\perp+I_\parallel)/(I_LNx\Delta\Omega), \tag{B1}$$

where N denotes the number density of the molecules. x is the length of the scattering volume seen by the detector.

According to the theory of Placzek (1934), the scattered light is determined by the polarizability tensor $(\partial\alpha/\partial q)$ of the observed vibrational mode [see Eqs.

(3) and (8)]. The isotropic and anisotropic components a and γ of the polarizability tensor are related to the scattering components $I_{\parallel}$ and $I_{\perp}$ as follows:

$$I_{\parallel} \propto 45a^2 + 4\gamma^2,$$
$$I_{\perp} \propto 3\gamma^2. \tag{B2}$$

The two scattering components add up to the total scattering cross section. From scattering theory we obtain

$$\partial\sigma/\partial\Omega = \tfrac{1}{135} f(45a^2 + 7\gamma^2), \tag{B3}$$

where f combines several factors:

$$f = \bar{g}\,\frac{\hbar(\omega_L - \omega_0)^4}{cm^4\omega_0[1 - \exp(-\hbar\omega_0/kT)]}. \tag{B4}$$

$\bar{g}$ denotes the degree of degeneracy and m the reduced mass of the vibrational mode of frequency ω_0. The scattering cross section is seen from Eqs. (B3) and (B4) to depend strongly on the frequency ω_L of the incident laser. The polarizability constants a and γ, on the other hand, are frequency independent and characteristic of the molecules and the specific vibrational mode. For liquids a local field correction L is incorporated in the parameters a and γ:

$$a = La' \text{ and } \gamma = L\gamma'. \tag{B5}$$

a' and γ' are the corresponding constants of the isolated molecules. L denotes the correction factor. In simple cases one uses the Lorentz field correction $L = (\mu^2 + 2)^2/9$ (Schrötter, 1960; Nestor and Lippincott, 1973).

The scattering cross section $\partial\sigma/\partial\Omega$ is of the order of 10^{-29} cm^2 (per steradian and molecule) for strong Raman lines. The absolute magnitude of $\partial\sigma/\partial\Omega$ may be determined with good accuracy using modern laser techniques (Kato and Takuma, 1971).

The depolarization ratio for linear polarized light ρ_s is defined by the intensity ratio:

$$\rho_s = I_{\perp}/I_{\parallel}. \tag{B6}$$

This ratio is found from Eqs. (B2) and (B6) to be

$$\rho_s = 3\gamma^2/(45a^2 + 4\gamma^2). \tag{B7}$$

Equation (B7) indicates that $0 \leq \rho_s \leq 0.75$. Values of $\rho_s < 0.1$ are often found for highly symmetric, strong Raman lines. Values of $\partial\sigma/\partial\Omega$ and ρ_s have been listed in the literature for numerous liquids (see, for example, Nestor and Lippincott, 1973). Knowing these two parameters, one may readily calculate the constants a and γ with the help of Eqs. (B3) and (B7):

$$a = \left[\frac{3 - 4\rho_s}{f(1+\rho_s)}\,\frac{\partial\sigma}{\partial\Omega}\right]^{1/2},$$
$$\gamma = \left[\frac{45\rho_s}{f(1+\rho_s)}\,\frac{\partial\sigma}{\partial\Omega}\right]^{1/2}. \tag{B8}$$

For an incident plane wave the scattered intensity I_S within a solid angle of $\Delta\Omega$ is, according to Eq. (B1),

$$I_S = N\frac{\partial\sigma}{\partial\Omega}\,xI_L\Delta\Omega. \tag{B9}$$

Using Eqs. (B3) and (B4), we rewrite Eq. (B9) for the case of an isotropic scattering tensor ($\gamma = 0$), a non-degenerate vibrational transition ($\bar{g} = 1$), and for $\hbar\omega_0 \gg kT$,

$$I_S = \frac{N\hbar\omega_S^4 a^2}{3c^4 m\omega_0}\,xI_L\Delta\Omega, \tag{B10}$$

where $\omega_S = \omega_L - \omega_0$. Introducing the electric field E_L ($I_L = c\mu|E_L|^2/8\pi$) we obtain

$$I_S = \frac{N\hbar\omega_S^4\mu a^2}{24\pi c^3 m\omega_0}\,x|E_L|^2\Delta\Omega. \tag{B11}$$

This equation will be used in Appendix C for the calculation of the initial Stokes intensity.

The spectral intensity distribution of the spontaneous Raman lines gives information on vibrational and rotational processes. This point is briefly discussed in Sec. II.A.6.

APPENDIX C: INITIAL CONDITION FOR STIMULATED SCATTERING

In Sec. II.B analytic expressions for the stimulated Stokes pulse and the coherent material excitation are presented which include an initial Stokes field $E_S(0, t')$. The initial vibrational amplitude $Q(0, t')$ was neglected in Eqs. (34) and (35). In the high gain situation of interest the stimulated emission builds up over many orders of 10. Our calculations for the conversion of laser to Stokes light depend only weakly on the absolute magnitude of the initial Stokes field. The following derivation of the effective initial Stokes field is adequate for most practical cases.

The theory of stimulated Raman scattering includes spontaneous scattering as a limiting case for very weak incident laser light. A comparison with results of spontaneous Raman scattering yields the desired initial condition for the stimulated Stokes amplification process. As discussed in Appendix B, an incident laser pulse $E_L(t')$ generates a spontaneous Stokes scattered intensity (in the forward direction) within a solid angle $\Delta\Omega$ of

$$I_{\text{spon}} = \frac{N\hbar\omega_S^4\mu}{24\pi c^3 m\omega_0}\,x\left(\frac{\partial\alpha}{\partial q}\right)^2|E_L(t')|^2\Delta\Omega. \tag{C1}$$

x denotes the sample length.

Our result for the stimulated process is presented by Eq. (34) in Sec. II.B for the case of a homogeneously broadened vibrational system with isotropic scattering tensor. We are concerned here with very weak laser pulses. Expanding the Bessel function I_1 in Eq. (34) to first order we obtain the following expression for the scattered Stokes field:

$$E_S(x, t') = E_S(0, t') + \kappa_1\kappa_2 xE_L(t') \times \int_{-\infty}^{t'} dt''\exp\left(\frac{t'' - t'}{T_2}\right) E_L(t'')E_S(0, t'') + \cdots. \tag{C2}$$

Going to intensities, we set $I_{S0} = c\mu E_S^2(0, t')/8\pi$:

$$I_S(x, t') = I_{S0}[1 + 2\kappa_1\kappa_2 x E_L(t') \times \int_{-\infty}^{t'} dt'' \exp\left(\frac{t'' - t'}{T_2}\right) E_L(t'') \times \langle E_S(0, t') E_S(0, t'')\rangle / E_S^2(0, t') + \text{higher terms.} \quad \text{(C3)}$$

In Eq. (C3) we introduced the first-order autocorrelation function of the initial Stokes field where the brackets $\langle\ \rangle$ denote an average over a finite acceptance angle $\Delta\Omega$ (number of electromagnetic modes which participate in the Raman scattering process). This function deviates from zero during a short correlation time t_C which is related to the frequency width $\Delta\omega_S$ of the initial Stokes field: $t_C \simeq 1/\Delta\omega_S$. Assuming exponential time behavior we write

$$\frac{\langle E_S(0, t') E_S(0, t'')\rangle}{E_S(0, t')^2} \simeq \exp[-\Delta\omega_S |t' - t''|]. \quad \text{(C4)}$$

Substitution of Eq. (C4) in Eq. (C3) yields

$$I_S(x, t') = I_{S0}[1 + 2\kappa_1\kappa_2 x E_L(t') \times \int_{-\infty}^{t'} dt'' \exp[(t'' - t')\Delta\omega] E_L(t'') + \cdots, \quad \text{(C5)}$$

where we introduced the effective bandwidth

$$\Delta\omega = \Delta\omega_S + 1/T_2, \quad \text{(C6)}$$

which will be discussed below. The second term in Eq. (C5) is proportional to the incident peak laser intensity and to the sample length x', as is expected for the spontaneous scattering signal. On the other hand, Eq. (C5) depends on the shape and duration of the incident laser pulse as well as on the frequency width $\Delta\omega$ or dephasing time T_2 [note Eq. (C6)]. This point was discussed by Akhmanov *et al.* (1971) and Bloembergen and co-workers (1971). For steady-state conditions we have $\Delta\omega_S \simeq 1/T_2$ or $\Delta\omega \simeq 2/T_2$, and the integral in Eq. (C5) is readily solved to give

$$I_S(t', x) \simeq I_{S0}[1 + 2\kappa_1\kappa_2 x E_L^2/\Delta\omega]. \quad \text{(C7)}$$

Using the definitions of κ_1 and κ_2 [Eq. (15)], comparison of Eqs. (C1) and (C7) yields the desired initial Stokes intensity:

$$I_{S0} = \frac{\hbar\,\mu^2}{12\pi^2 c^2}\omega_S^3 \Delta\omega\Delta\Omega. \quad \text{(C8)}$$

The result of Eq. (C8) is equivalent (except for a factor close to unity) to the zero-point energy flux of the number of Stokes modes contained in the solid angle $\Delta\Omega$ and the frequency interval $\Delta\omega = 2/T_2$ (equal to the spontaneous Raman linewidth). In other words, the initial condition I_{S0} represents the equivalent noise input of the Raman generator.

In the transient case the frequency width of the stimulated Stokes emission is larger than the incident laser pulse by a factor of approximately 2, due to a corresponding reduction in pulse duration: $\Delta\omega_S \simeq 2\Delta\omega_L$. As a result, the exponential term in Eq. (C5) varies considerably more rapidly in time than $E_L(t'')$. Equations (C7) and (C8) remain approximately valid and are used in the computations of Sec. II.B.[3]

The equivalent noise input I_{S0} of Eq. (C7) is estimated in the following example: For a sample length of $x' = 2$ cm and a beam diameter 2×10^{-2} cm the stimulated Raman process occurs in a solid angle of $\Delta\Omega \simeq 10^{-4}$ sr. For a Stokes emission at frequency $\omega_S/2\pi c \simeq 2 \times 10^4$ cm^{-1} within a bandwidth of $\Delta\omega/2\pi c \simeq 10$ cm^{-1} we find an initial Stokes intensity of 10^{-2} W/cm^2. This equivalent input level should be compared with the incident laser intensity of the order of 10^{10} W/cm^2; i.e., amplification of the Stokes light over many orders of 10 is required in the stimulated Stokes process to achieve the conversion efficiencies (e.g., $\eta = 10^{-2}$) discussed in Sec. II.B (see Fig. 2).

APPENDIX D: STIMULATED RAMAN SCATTERING FOR AN ANISOTROPIC SCATTERING TENSOR

In this appendix, the differential equations of transient stimulated Raman scattering for the anisotropic case are derived; they are solved and discussed in Sec. II.C. Inspection of the general equations (12)–(14) shows that rotational motion influences the scattering process, and averages over the orientational distribution have to be carried out. For a homogeneous vibrational system ($\omega_j = \omega_0$) these equations have the following form (the subscript j may be omitted):

$$\frac{\partial}{\partial x'} E_{Sz} = \kappa_1 E_L \langle Q^* s_1\rangle, \quad \text{(D1a)}$$

$$\frac{\partial}{\partial x'} E_{Sy} = \kappa_1 E_L \langle Q^* s_2\rangle, \quad \text{(D1b)}$$

$$\left(\frac{\partial}{\partial t'} + \frac{1}{T_2}\right) Q = \kappa_2 E_L (E_{Sz}^* s_1 + E_{Sy}^* s_2), \quad \text{(D2)}$$

$$\left(\frac{\partial}{\partial t'} + \frac{1}{T_1}\right) n = \frac{a}{8\hbar} E_L (E_{Sz}^* \langle Q^* s_1\rangle + E_{Sy}^* \langle Q^* s_2\rangle) + \text{c.c.} \quad \text{(D3)}$$

Equations (D1)–(D3) refer to a retarded time frame $t' = t - x/v$ with $x' = x$. The factors s_1 and s_2 contain direction cosines and are defined by Eq. (16) in Sec. II.A. The brackets $\langle\ \rangle$ denote the orientational average. The subscript "or" has been dropped for simplicity.

Integration of Eq. (D2), multiplication with the factor s_1 or s_2, and taking the orientational average, yield

$$\langle Q(t') s_l(t')\rangle = \kappa_2 \int_{-\infty}^{t'} dt'' \exp\left(\frac{t'' - t'}{T_2}\right) E_L(t'') \times \{[E_{Sz}^*(t'')\langle s_l(t') s_1(t'')\rangle + E_{Sy}^*(t'')\langle s_l(t') s_2(t'')\rangle\} \quad \text{(D4)}$$

where $l = 1, 2$.

---

[3] A different approach was taken by Akhmanov *et al.* (1971). These authors introduced a random force term in the material equation (32) to account for the spontaneous fluctuations of the vibrational amplitude and used the conditions $E_S(0, t') = 0$ and $Q(0, t') = 0$.

The molecular reorientation produced by the incident laser field and the generated Stokes field via the anisotropy γ of the Raman scattering is small. Even for high-intensity light pulses of $\sim 10^{10}$ W/cm^2, the torque exerted by the electromagnetic fields is negligible due to the smallness of the Raman polarizability $\partial\alpha/\partial q$. Consequently the orientational averages may be carried out to a good approximation for a random orientational distribution.

Using the definitions of the factors s_1 and s_2 [Eq. (16)], we find:

$$\begin{aligned}\langle s_1(t')s_1(t'')\rangle &= 1 + \tfrac{4}{45}\gamma^2/a^2\phi_{2R}(t'-t''),\\ \langle s_2(t')s_2(t'')\rangle &= \tfrac{1}{15}\gamma^2/a^2\phi_{3R}(t'-t''),\\ \langle s_1(t')s_2(t'')\rangle &= 0.\end{aligned} \tag{D5}$$

ϕ_{2R} and ϕ_{3R} represent rotational correlation functions for the molecular motion around different axes (Frenkel, 1955):

$$\begin{aligned}\phi_{2R} &\equiv \frac{45}{4}\langle\cos^2\theta_3(t')\cos^2\theta_3(t'') - \tfrac{1}{9}\rangle,\\ \phi_{3R} &\equiv 15\langle\cos\theta_2(t')\cos\theta_2(t'')\cos\theta_3(t')\cos\theta_3(t'')\rangle.\end{aligned} \tag{D6}$$

Rotational relaxation has been extensively studied in a number of theoretical and experimental papers (Gordone, 1965 and 1966; McClung, 1969 and 1971; Bratos *et al.*, 1970 and 1971; Bartoli and Litovitz, 1972; Kivelson and Keyes, 1972; Fixman and Rider, 1969; for a review, see Bailey, 1974).

We are not interested here in details of the rotational motion but wish to discuss the basic features of rotational–vibrational coupling in the stimulated scattering process. For simplicity we assume an exponential form of the first correlation function [Eq. (D6)]:

$$\phi_{2R} \simeq \exp(-|t'-t''|/\tau_{2R}). \tag{D7}$$

The time dependence of Eq. (D7) holds for the special case of small-step rotational diffusion (Debye, 1929). It should be noted that the orientational correlation time τ_{2R} introduced in Eq. (D7) may be determined from the anisotropic scattering component of spontaneous Raman spectroscopy. On account of the simple form of Eq. (D7) the following discussion of the influence of rotational motion is expected to be of a semiquantitative nature for cases where the rotational diffusion model is not adequate.

Substitution of Eqs. (D5) and (D7) in Eq. (D4) leads to an expression which may be written as follows:

$$\langle Qs_1\rangle = \langle Qs_1\rangle_{\rm is} + \langle Qs_1\rangle_{\rm an}. \tag{D8}$$

The first component $\langle Qs_1\rangle_{\rm is}$ is connected to the isotropic polarizability a (through factor κ_2) and the vibrational dephasing time T_2:

$$\langle Qs_1\rangle_{\rm is} = \kappa_2\int_{-\infty}^{t'} dt''\exp\left(\frac{t''-t'}{T_2}\right) \times E_L(t'')E^*_{Sz}(t''). \tag{D9}$$

The second part depends on the anisotropy of the Raman tensor and the relaxation time τ_{2R}:

$$\langle Qs_1\rangle_{\rm an} = \frac{4}{45}\frac{\gamma}{a}\kappa_2\int_{-\infty}^{t'} dt''\exp\left(\frac{t''-t'}{\tau_{\rm an}}\right) \times E_L(t'')E_{Sz}(t'')^*, \tag{D10}$$

where an effective relaxation time $\tau_{\rm an}$ is used:

$$\frac{1}{\tau_{\rm an}} = \frac{1}{T_2} + \frac{1}{\tau_{2R}}. \tag{D11}$$

It is interesting to note that the total material excitation $\langle Qs_1\rangle$ is determined by the "polarized" Stokes field E_{Sz} in Eqs. (D9) and (D10). The influence of rotational motion is contained in the component $\langle Qs_1\rangle_{\rm an}$ of Eq. (D10) and disappears for small anisotropy γ/a of the scattering tensor.

Differentiation of the integrals of Eqs. (D9) and (D10) gives, together with Eqs. (D1a) and (D3), the complete set of differential equations (38)–(40) of Sec. II.C describing the transient stimulated Raman process for an anisotropic scattering tensor. For a "depolarized" Stokes field E_{Sy} (of perpendicular polarization) and for the material excitation $\langle Qs_2\rangle$ a corresponding set of equations is obtained which is completely independent of E_{Sz} and $\langle Qs_1\rangle$. As discussed in Sec. II.C, the gain of E_{Sy} is considerably smaller than that of E_{Sz} in the Raman generator setup. For this reason, the contribution of E_{Sy} and $\langle Qs_2\rangle$ to the excess population n in Eq. (40) has been omitted.

APPENDIX E: COHERENT GENERATED STOKES FIELD

In our ansatz Eq. (2) we assumed a coherent incident laser pulse and a coherent generated Stokes field. A coherent electromagnetic signal is represented by a well-defined frequency ω and wave vector k together with an amplitude function (which contains a constant phase factor). While our experimental bandwidth-limited laser pulses are coherent pulses, the generated Stokes pulses require some consideration.

The following general remark should be made at this point. In this paper the light fields are described in real time and local space. As a result, we are dealing with a small number of coherent pulses of well-defined phases. Incoherent signals may be approximated by distributions of coherent pulses with random phases. The time picture should be distinguished from treatments in frequency space. Fourier transformation shows that a short coherent signal corresponds to a spectrum of Fourier components with a distribution of frequencies and wave vectors. The frequency picture is not used in the present discussion.

We are interested here in a Raman generator system. The intense Stokes light builds up from quantum noise: i.e., a rather complex initial condition leads to a high power stimulated Stokes field. It is shown in Appendix C that the stimulated amplification process for the Stokes field develops from the spontaneous Raman process. In fact, during the very early initial stages of the stimulated process the Stokes emission is essentially incoherent and broadband.

In order to include incoherent Stokes components in our calculations we generalize the discussion of Sec.

II.D [Eqs. (52)–(55)] to a Stokes field of complex amplitude E_S:

$$E_S = |E_S| \exp(i\Psi), \tag{E1}$$

where $\Psi(x, t)$ denotes a phase factor of E_S. A time-dependent fluctuating phase $\Psi(x, t)$ represents an incoherent Stokes field. With Eq. (E1), our ansatz of Eq. (2) for the electromagnetic field is still valid (where E_S is complex):

$$E = \tfrac{1}{2} e_z [E_L \exp(ik_L x - i\omega_L t) + E_S \exp(ik_S x - i\omega_S t) + \text{c.c.}]. \tag{E2}$$

ω_S denotes the carrier frequency of the Stokes pulse; the value of ω_S is determined by the vibrational system [see Eq. (55)]. As in Sec. II we consider E_L to be real; i.e., a coherent incident laser pulse of well-defined, constant phase is assumed. For the coherent material excitation it is convenient here to make an ansatz different from that in Sec. II.D. We write

$$\langle q_j \rangle = \tfrac{1}{2} i Q_j' \exp[i(k_L - k_S)x - i(\omega_L - \omega_S)t] + \text{c.c.} \tag{E3}$$

with the frequency and wave-vector difference $\omega_L - \omega_S$ and $k_L - k_S$, respectively. The rapidly oscillating factor of (E3) is the consequence of the driving force $E_L E_S^*$, which excites the molecular vibration. Phase differences due to the individual resonance frequencies ω_j of the inhomogeneous molecular system are contained in the complex amplitude factors Q_j' of Eq. (E3). Introducing Eqs. (E2) and (E3) in the wave equation [Eq. (1)] and the material equation [Eq. (5)] yields, with the help of Eqs. (8) and (9), in a way similar to that in Sec. II.A, the expressions

$$\left(\frac{\partial}{\partial x} + \frac{1}{v_S}\frac{\partial}{\partial t}\right) E_S = \kappa_1 E_L \sum_j f_j Q_j'^*, \tag{E4}$$

$$\left(\frac{\partial}{\partial t} + \frac{1}{T_2} - i\Delta\omega_j\right) Q_j' = \kappa_2 E_L E_S^*, \tag{E5}$$

where we use the abbreviation $\Delta\omega_j = \omega_L - \omega_S - \omega_j$. The coupling parameters of κ_1 and κ_2 are defined by Eq. (15). Equations (E4) and (E5) are derived for approximations similar to those of Eqs. (46) and (47) and refer to the case of an isotropic scattering tensor ($\gamma = 0$). Since derivatives of the field E_S and the amplitudes Q_j' are retained in the calculation to first order only, the present discussion is restricted to phase factors (contained in E_S or Q_j) varying not too rapidly in time; i.e., narrow Raman bands $\delta\omega \ll \omega_0$ and not too short pulses $t_p \gtrsim \delta\omega^{-1}$ are considered.

The driving term on the rhs of Eq. (E4) should be noted; it contains the sum over the vibrational components. This term would vanish for random phases of the amplitudes Q_j'; obviously, phase correlation has to build up between the vibrating molecules in order to produce an intense stimulated Stokes field. In Eq. (E6) we present a solution of the total vibrational excitation $\sum f_j Q_j'$ obtained from Eq. (E5):

$$\sum_j f_j Q_j = \kappa_2 \int_{-\infty}^{t'} dt'' E_L E_S^* \exp\frac{(t'' - t')}{T_2} \times \sum f_j \exp[-i\Delta\omega_j (t'' - t')]. \tag{E6}$$

The material excitation averages over fluctuations of the Stokes field which are present during an early stage of the stimulated amplification process. This fact is accounted for in Eq. (E6) by the exponential factor containing the lifetime T_2 of the physical system. As a result, a smooth time dependence of the vibrational excitation and of the stimulated Stokes emission may be expected after amplification over several orders of magnitude.

These ideas are substantiated by numerical results for the stimulated Stokes field obtained from Eqs. (E4) and (E6). The calculations indicate that the stimulated Stokes field quickly approaches a constant phase, although the initial Stokes field displays rapid fluctuations. Comparison with the situation of an incident coherent Stokes field shows that the amplitude $|E_S|$ of the Stokes radiation (E1) grows approximately at the same rate and develops to the same pulse shape.

These results are obtained for homogeneous ($\Delta\omega_j = 0$) and inhomogeneous ($\Delta\omega_j \neq 0$) systems in the high amplification regime and for small group velocity dispersion between the laser pulse and Stokes field. (For the homogeneous case see also Carman *et al.*, 1970.)

The theoretical data fully support the notion of a coherent Stokes field which is used in our calculations of Sec. II.

REFERENCES

Aartsma, T. J., and D. A. Wiersma, 1976, Chem. Phys. Lett. 42, 520.

Abragam, A., 1961, *The Principles of Nuclear Magnetism* (Oxford University, New York).

Akhmanov, S. A., 1969, Mater. Res. Bull. 4, 455.

Akhmanov, S. A., K. N. Drabovich, A. P. Sukhorukov, and A. S. Chirkin, 1971, Sov. Phys.-JETP 32, 266.

Akhmanov, S. A., K. N. Drabovich, A. P. Sukhorukov, and A. K. Shchednova, 1972, Sov. Phys.-JETP 35, 279.

Akhmanov, S. A., Yu. E. Dyakov, and L. I. Pavlov, 1974, Sov. Phys.-JETP 39, 249.

Alfano, R. R., and S. L. Shapiro, 1971, Phys. Rev. Lett. 26, 1247.

Alfano, R. R., and S. L. Shapiro, 1972, Phys. Rev. Lett. 29, 1655.

Allamandola, L. J., Jr., and J. W. Nibler, 1974, Chem. Phys. Lett. 28, 335.

Amme, R. C., 1975, Adv. Chem. Phys. 28, 171.

Bailey, R. T., 1974, in *Molecular Spectroscopy* (The Chemical Society, London), Vol. 2.

Barker, A. S., 1968, Phys. Rev. 165, 917.

Bartoli, F. J., and T. A. Litovitz, 1972, J. Chem. Phys. 56, 404 and 413.

Bauer, D. R., J. I. Brauman, and R. Pecora, 1976, Annu. Rev. Phys. Chem. 27, 443.

Berry, M. J., 1975, Annu. Rev. Phys. Chem. 26, 259.

Bilz, H., 1978, Handbook of Physics (Springer, Heidelberg), Vol. 25 (to be published).

Bloembergen, N., and P. Lallemand, 1966, in *Physics of Quantum Electronics*, edited by P. L. Kelley, B. Lax, and N. P. Tannenwald (McGraw-Hill, New York).

Bloembergen, N., 1967, Am. J. Phys. 35, 989.

Bloembergen, N., M. J. Colles, J. Reintjes, and C. S. Wang, 1971, Indian J. Pure Appl. Phys. 9, 874.

Bradley, D. J., B. Liddy, and W. E. Sleat, 1971, Opt. Commun. 2, 391.

Bradley, D. J., G. H. New, and S. J. Caughey, 1969, Phys.

Lett. A 30, 78.
Brandmüller, J., K. Buchardi, H. Hacker, and H. W. Schrötter, 1967, Z. Angew. Phys. 22, 177.
Brandmüller, J., and H. Moser, 1962, *Einführung in die Ramanspektroskopie* (Steinkopff, Darmstadt).
Bratos, S., and E. Maréchal, 1971, Phys. Rev. A 4, 1078.
Bratos, S., J. Rios, and Y. Guissany, 1970, J. Chem. Phys. 52, 439.
Brewer, R. G., 1975, in *Very High Resolution Spectroscopy*, edited by P. A. Smith (Academic, New York), p. 127.
Brewer, R. G., and R. C. Shoemaker, 1971, Phys. Rev. Lett. 27, 631.
Brueck, S. R., and R. M. Osgood, Jr., 1976, Chem. Phys. Lett. 39, 568.
Buckingham, A. D., 1958, Proc. R. Soc. A 248, 169.
Buckingham, A. D., 1960a, Proc. R. Soc. A 255, 32.
Buckingham, A. D., 1960b, Trans. Faraday Soc. 56, 753.
Byer, R. L., 1975, in *Quantum Electronics*, edited by H. Rabin and C. L. Tang (Academic, New York), Vol. 1B.
Calaway, W. F., and G. E. Ewing, 1975a, Chem. Phys. Lett. 30, 485.
Calaway, W. F., and G. E. Ewing, 1975b, J. Chem. Phys. 63, 2842.
Carman, R. L., F. Shimizu, C. S. Wang, and N. Bloembergen, 1970, Phys. Rev. A 2, 60.
Clark, R. J. H., and C. J. Willis, 1971, Inorg. Chem. 10, 1118.
Clarke, J. F., and M. McChesney, 1976, *Dynamics of Relaxing Gases* (Butterworths, London).
Clements, W. R. L., and B. P. Stoicheff, 1968, Appl. Phys. Lett. 12, 246.
Colles, M. J., 1969, Opt. Commun. 1, 169.
Colles, M. J., and J. A. Giordmaine, 1971, Phys. Rev. Lett. 27, 670.
Colles, M. J., and J. E. Griffiths, 1972, J. Chem. Phys. 56, 3384.
Courtens, E., 1972, in *Laser Handbook*, edited by F. T. Arecchi and E. D. Schulz-Dubois (North-Holland, Amsterdam), Vol. 2, p. 1259
Crisp, M. D., 1970, Phys. Rev. A 1, 1604; 2, 2172(E).
Debye, P., 1929, *Polar Molecules* (Reinhold, New York).
DeMartini, F., and J. Ducuing, 1966, Phys. Rev. Lett. 17, 117.
Duguay, M. A., J. W. Hansen, and S. L. Shapiro, 1970, IEEE J. Quantum Electron. QE-6, 725.
Eckardt, R. C., C. H. Lee, and J. N. Bradford, 1971, Appl. Phys. Lett. 19, 420.
Eysel, H. H., and K. Lucas, 1970, Z. Naturforsch. 25a, 316.
Feynman, R. P., F. C. Vernon, and R. W. Hellwarth, 1957, J. Appl. Phys. 28, 49.
Fischer, S. F., and A. Laubereau, 1975, Chem. Phys. Lett. 35, 6.
Fixman, M., and K. Rider, 1969, J. Chem. Phys. 51, 2425.
Frenkel, J., 1955, *Kinetic Theory of Liquids* (Dover, New York).
Gibbs, H. M., and R. E. Slusher, 1970, Phys. Rev. Lett. 24, 638.
Giordmaine, J. A., and W. Kaiser, 1966, Phys. Rev. 144, 676.
Giordmaine, J. A., and R. C. Miller, 1965, Phys. Rev. Lett. 14, 973.
Giordmaine, J. A., P. M. Rentzepis, S. L. Shapiro, and K. W. Wecht, 1967, Appl. Phys. Lett. 11, 216.
Gmelin, L., 1972, *Handbuch der Anorganischen Chemie* (Chemie, Weinheim), Vol. 46, p. 405.
Gordon, R. G., 1964, J. Chem. Phys. 40, 1973.
Gordon, R. G., 1965a, J. Chem. Phys. 42, 3658.
Gordon, R. G., 1965b, J. Chem. Phys. 43, 1307.
Gordon, R. G., 1966, J. Chem. Phys. 44, 1830.
Görner, H., M. Maier, and W. Kaiser, 1974, J. Raman Spectr. 2, 363.
Gornik, W., D. Kaiser, W. Lange, J. Luther, and J. H. Shuk, 1972, Opt. Commun. 6, 327.
Grasyuk, A. Z., 1974, Sov. J. Quantum. Electron. 4, 269.
Grieneisen, H. P., J. Goldhar, N. A. Kurnit, A. Javan, and H. R. Schlossberg, 1972, Appl. Phys. Lett. 21, 559.
Grischkowsky, D., 1973, Phys. Rev. A 7, 2096.
Grun, J. B., A. K. McQuillan, and B. P. Stoicheff, 1969, Phys. Rev. 180, 61.
Hamadani, S. M., J. Goldhar, N. A. Kurnit, and A. Javan, 1974, Appl. Phys. Lett. 25, 160.
Haroche, S., F. A. Paisner, and W. L. Schawlow, 1973, Phys. Rev. Lett. 30, 948.
Henry, C. H., and J. J. Hopfield, 1965, Phys. Rev. Lett. 15, 964.
Heritage, J. P., R. K. Gustafson, and C. H. Lin, 1975, Phys. Rev. Lett. 34, 1299.
Herzberg, G., 1945, *Molecular Spectra and Molecular Structure* (Van Nostrand, Princeton).
Herzfeld, K. F., and T. A. Litovitz, 1959, *Absorption and Dispersion of Ultrasonic Waves* (Academic, New York).
Hesp, H. M. M., J. Langelaar, B. Bebelaar, and J. D. W. van Voorst, 1977, Phys. Rev. Lett. 39, 1376.
Hon, D. T., and W. L. Faust, 1972, Appl. Phys. 1, 241.
James, R. W., 1959, *The Optical Properties of the Diffraction of X-Rays* (Bell, London).
Kaiser, W., and M. Maier, 1972, in *Laser Handbook*, edited by F. T. Arecchi and E. O. Schulz-Dubois (North-Holland, Amsterdam), Vol. 2, p. 1077.
Kato, Y., and H. Takuma, 1971, J. Opt. Soc. Am. 61, 347.
Kiefer, W., and A. Laubereau, 1978 (unpublished).
Kivelson, D., and T. Keyes, 1972, J. Chem. Phys. 57, 4599.
Kleinman, D. A., and W. G. Spitzer, 1960, Phys. Rev. 118, 110.
Knaap, H. F. P., and P. Lallemand, 1975, Annu. Rev. Phys. Chem. 26, 59.
Koningstein, J. A., 1972, *Introduction to the Theory of the Raman Effect* (Reidel, Dordrecht).
Kroll, N. M., and P. L. Kelley, 1971, Phys. Rev. A 4, 763.
Kryukov, P. G., and V. S. Letokhov, 1969, Usp. Fiz. Nauk 99, 169 [Sov. Phys.-Usp. 12, 641 (1970)].
Kurnit, N. A., I. D. Abella, and S. R. Hartmann, 1964, Phys. Rev. Lett. 13, 567.
Lascombe, J., 1974, *Molecular Motions in Liquids* (Reidel, Dordrecht).
Laubereau, A., 1974, Chem. Phys. Lett. 27, 600.
Laubereau, A., S. I. Fischer, K. Spanner, and W. Kaiser, 1978, Chem. Phys. (to be published).
Laubereau, A., L. Greiter, and W. Kaiser, 1974, Appl. Phys. Lett. 25, 87.
Laubereau, A., G. Kehl, and W. Kaiser, 1974, Opt. Commun. 11, 74.
Laubereau, A., L. Kirschner, and W. Kaiser, 1973, Opt. Commun. 9, 182.
Laubereau, A., A. Seilmeier, and W. Kaiser, 1975, Chem. Phys. Lett. 36, 232.
Laubereau, A., D. von der Linde, and W. Kaiser, 1971, Phys. Rev. Lett. 27, 802.
Laubereau, A., D. von der Linde, and W. Kaiser, 1972, Phys. Rev. Lett. 28, 1162.
Laubereau, A., D. von der Linde, and W. Kaiser, 1973, Opt. Commun. 7, 173.
Laubereau, A., G. Wochner, and W. Kaiser, 1975, Opt. Commun. 14, 75.
Laubereau, A., G. Wochner, and W. Kaiser, 1976a, Opt. Commun. 17, 91.
Laubereau, A., G. Wochner, and W. Kaiser, 1976b, Phys. Rev. A 13, 2212.
Laubereau, A., G. Wochner, and W. Kaiser, 1978, Chem. Phys. 28, 363.
Legay, F., 1977, in *Chemical and Biochemical Applications of Lasers*, edited by C. B. Moore (Academic, New York).
Letokhov, V. S., and C. B. Moore, 1976, Sov. J. Quantum Electron. 3, 129 and 259.

Levenson, M. D., 1974, IEEE J. Quantum Electron. QE-10, 110.
Levenson, M. D., and N. Bloembergen, 1974, Phys. Rev. B 10, 4447.
Madden, P. A., and R. M. Lynden-Bell, 1976, Chem. Phys. Lett. 38, 163.
Maier, J. P., A. Seilmeier, A. Laubereau, and W. Kaiser, 1977, Chem. Phys. Lett. 46, 527.
Maier, M., W. Kaiser, and J. A. Giordmaine, 1969, Phys. Rev. 177, 580.
Malyutin, A. A., and M. Ya. Shchelev, 1969, JETP Lett. 9, 266.
Marshall, N., and B. Fischer, 1972, Phys. Rev. Lett. 28, 811.
Martin, P. C., 1968, *Measurements and Correlation Functions* (Gordon and Breach, New York).
McCall, S. L., and E. L. Hahn, 1967, Phys. Rev. Lett. 18, 908.
McClung, R. E. D., 1969, J. Chem. Phys. 51, 3842.
McClung, R. E. D., 1971, J. Chem. Phys. 54, 3248.
Monson, P. R., Jr., H. L. Chen, and G. E. Ewing, 1968, J. Mol. Spectrosc. 25, 501.
Monson, P. R., L. Patumtevapibal, K. J. Kaufmann, P. W. Robinson, 1974, Chem. Phys. Lett. 28, 312.
Moore, C. B., 1971, Annu. Rev. Phys. Chem. 22, 387.
Murphy, W. F., M. V. Evans, and P. Bender, 1967, J. Chem. Phys. 47, 1836.
Nafie, L. A., and W. L. Peticolas, 1972, J. Chem. Phys. 57, 3145.
Nestor, J. R., and E. R. Lippincott, 1973, J. Raman Spectr. 1, 305.
Orbach, R., 1966, Phys. Rev. Lett. 16, 15.
Orbach, R., 1967, IEEE Trans. SU-14, 140.
Orbach, R., and L. A. Vredevoe, 1968, Physics 1, 91.
Ormonde, S., 1975, Rev. Mod. Phys. 47, 193.
Oxtoby, D. W., and S. A. Rice, 1976, Chem. Phys. Lett. 42, 1.
Pantell, R. H., and H. E. Puthoff, 1969, *Fundamentals of Quantum Electronics* (Wiley, New York).
Park, K., 1966, Phys. Lett. 22, 39.
Park, K., 1967, Phys. Lett. A 25, 490.
Patel, C. K. N., and R. E. Slusher, 1967a, Phys. Rev. Lett. 19, 1019.
Patel, C. K. N., and R. E. Slusher, 1967b, Phys. Rev. Lett. 20, 1087.
Penzkofer, A., and W. Kaiser, 1977, Optical and Quant. Electr. 9, 315.
Penzkofer, A., A. Laubereau, and W. Kaiser, 1973, Phys. Rev. Lett. 31, 863.
Penzkofer, A., D. von der Linde, A. Laubereau, and W. Kaiser, 1972, Appl. Phys. Lett. 20, 351.
Pimentel, G. C., and A. L. McClellan, 1960, *The Hydrogen Bond* (Freeman, San Francisco).
Placzek, G., 1934, in *Handbuch der Radiologie*, edited by E. Marx (Akademische Verlagsgesellschaft, Leipzig).
Plihal, M., 1973, Phys. Status Solidi B 56, 495.
Redfield, A. G., 1957, IBM J. Res. Dev. 1, 19.
Ricard, D., and J. Ducuing, 1975, J. Chem. Phys. 62, 3616.
Rothschild, W. G., 1976, J. Chem. Phys. 65, 2958.
Sargent, M., III, M. O. Scully, and W. E. Lamb, Jr., 1974, *Laser Physics* (Addison-Wesley, London).
Schrötter, H. W., 1960, Z. Elektrochem. 64, 853.
Schubert, M., and B. Wilhelmi, 1974, Sov. J. Quantum Electron. 4, 575.
Scotto, M., 1968, J. Chem. Phys. 49, 5362.
Seilmeier, A., A. Laubereau, and W. Kaiser, 1978, Opt. Commun. (to be published).
Seilmeier, A., K. Spanner, A. Laubereau, and W. Kaiser, 1978 Opt. Commun. 24, 237.
Sette, D., 1968, in *Physics of Simple Liquids*, edited by H. N. V. Temperley, J. S. Rowlinson, and G. S. Rushbrooke (North-Holland, Amsterdam), p. 325.
Shen, Y. R., 1975, in *Topics in Applied Physics*, "Light Scattering in Solids," edited by M. Cardona (Springer, Berlin), Vol. 8, p. 278.
Shoemaker, R. L., and R. Brewer, 1972, Phys. Rev. Lett. 28, 1430.
Slichter, C. P., 1963, *Principles of Magnetic Resonance* (Harper and Row, New York).
Smith, R. G., 1972, in *Laser Handbook*, edited by F. T. Arecchi and E. O. Schulz-Dubois (North-Holland, Amsterdam).
Spanner, K., A. Laubereau, and W. Kaiser, 1976, Chem. Phys. Lett. 44, 88.
Streudel, H., 1972, Exp. Tech. Phys. 20, 409.
Tang, C. L., and B. D. Silverman, 1966, in *Physics of Quantum Electronics*, edited by P. L. Kelley, B. Lax, and P. E. Tannenwald (McGraw-Hill, New York), p. 280.
Ushioda, S., and J. D. McCullen, 1972, Solid State Commun. 11, 299.
von der Linde, D., 1972, IEEE J. Quantum Electron. QE-8, 328.
von der Linde, D., O. Bernecker, and W. Kaiser, 1970, Opt. Commun. 2, 149.
von der Linde, D., O. Bernecker, and A. Laubereau, 1970, Opt. Commun. 2, 215.
von der Linde, D., and A. Laubereau, 1971, Opt. Commun. 3, 279.
von der Linde, D., A. Laubereau, and W. Kaiser, 1971, Phys. Rev. Lett. 26, 954.
Wang, C. S., 1975, in *Quantum Electronics*, edited by H. Rabin and C. L. Tang (Academic, New York), Vol. 1.
Wangsness, R. K., and F. Bloch, 1953, Phys. Rev. 89, 728.
Warren, J. L., R. G. Wenzel, and J. L. Yarnell, 1965, *Inelastic Scattering of Neutrons* (IAEA, Vienna).
Warren, J. L., J. L. Yarnell, G. Dolling, and R. A. Cowley, 1967, Phys. Rev. 158, 805.
Weitz, E., and G. Flynn, 1974, Annu. Rev. Phys. Chem. 25, 275.
Wilson, E. B., Jr., J. C. Decius, and P. C. Cross, 1955, *Molecular Vibrations* (McGraw-Hill, New York).
Zinth, W., A. Laubereau, and W. Kaiser, 1977, Opt. Commun. 22, 161.
Zinth, W., A. Laubereau, and W. Kaiser, 1978, Opt. Commun. (to be published).